Partial Oxidation of Methane over CeO_2 Loaded Hydrotalcite (MgNiAl) Catalyst for the Production of Hydrogen Rich Syngas (H_2, CO)

By
Muhammad Anees Ul Hasnain
Reg # 00000275972
Session 2018-2020

Supervised by
Dr. Asif Hussain Khoja

MASTERS of SCIENCE in
THERMAL ENERGY ENGINEERING

U.S-Pakistan Centre for Advanced Studies in Energy (USPCAS-E)
National University of Sciences and Technology (NUST)
H-12, Islamabad 44000, Pakistan
December 2021

Partial Oxidation of Methane over CeO_2 Loaded Hydrotalcite (MgNiAl) Catalyst for the Production of Hydrogen Rich Syngas (H_2, CO)

By
Muhammad Anees Ul Hasnain
Reg # 00000275972
Session 2018-2020

Supervised by
Dr. Asif Hussain Khoja

A Thesis Submitted to US Pakistan Centre for Advanced Studies in Energy in partial fulfilment of the requirements for the degree of MASTERS of SCIENCE in THERMAL ENERGY ENGINEERING

U.S-Pakistan Centre for Advanced Studies in Energy (USPCAS-E)
National University of Sciences and Technology (NUST)
H-12, Islamabad 44000, Pakistan
December 2021

THESIS ACCEPTANCE CERTIFICATE

Certified that final copy of MS/MPhil thesis written by Mr. Muhammad Anees Ul Hasnain, (Registration No. 00000275972), of U.S.-Pakistan Centre for Advanced Studies in Energy (USPCASE), NUST has been vetted by undersigned, found complete in all respects as per NUST Statues/Regulations, is in the allowable limits of plagiarism, errors, and mistakes and is accepted as partial fulfilment for award of MS/MPhil degree. It is further certified that necessary amendments as pointed out by GEC members of the scholar have also been incorporated in the said thesis.

Signature: _____

Supervisor: Dr. Asif Hussain Khoja

Date: _____

Signature: _____

HOD-TEE: Dr. Majid Ali

Date: _____

Signature: _____

Principal: Prof. Dr. Adeel Waqas

Date: _____

Certificate

This is to certify that work in this thesis has been carried out by **Mr. Muhammad Anees Ul Hasnain** and completed under my supervision in Fossil Fuels laboratory, USPCASE, National University of Sciences and Technology, H-12, Islamabad, Pakistan.

Supervisor: _____

Dr. Asif Hussain Khoja
U.S.-Pak Center for Advance Studies in Energy
NUST, Islamabad

GEC member 1: _____

Prof. Dr. Adeel Waqas
U.S.-Pak Center for Advance Studies in Energy
NUST, Islamabad

GEC member 2: _____

Dr. Muhammad Bilal Sajid
U.S.-Pak Center for Advance Studies in Energy
NUST, Islamabad

GEC member 3: _____

Dr. Mustafa Anwar
U.S.-Pak Center for Advance Studies in Energy
NUST, Islamabad

HoD-TEE: _____

Dr. Majid Ali
U.S.-Pak Center for Advance Studies in Energy
NUST, Islamabad

Principal: _____

Prof. Dr. Adeel Waqas
U.S.-Pak Center for Advance Studies in Energy
NUST, Islamabad

Acknowledgements

All praise to Allah Almighty who gave me the strength and knowledge to do the work presented in this thesis.

I would like to express my sincere gratitude to my research supervisor Dr. Asif Hussain Khoja for letting me be part of the research group at Fossil Fuels Lab, USPCAS-E, NUST, Islamabad. I feel privileged to have worked under his kind supervision. It's the blend of his patience, determination, guidance and inspiration that made me accomplish my research aims in due time. He refined my research skills and I have learned a lot under his supervision and guidance.

I would also like to thank the members of my GEC committee, Dr. Adeel Waqas, Dr. Muhammad Bilal Sajid and Dr. Mustafa Anwar who honoured my committee's presence. I would like to sincerely thank my fellows and specially, I pay gratitude to Lab Engineer Mr. Ali Abdullah for his unmatchable support during the whole research work.

Abstract

Syngas production from CH_4 is the most economical route for CH_4 effective utilization. Partial oxidation of methane (POM) is one of the best methane activation process for syngas production. Catalytic materials employed in POM requires a better catalytic performance in terms of activity and stability to make this process commercially applicable. Hydrotalcites, owing to their strong basic properties and uniform distribution of metallic particles inside their structure are suitable for POM applications. CeO_2 with strong redox properties due to its high oxygen storage capacity is an effective promoter for POM reaction.

In this work, partial oxidation of methane (POM) was investigated using Mg-Ni-Al (MNA) hydrotalcite promoted CeO_2 catalyst in a fixed bed reactor. MNA hydrotalcite was synthesized using the co-precipitation process, while CeO_2 was incorporated via the wetness impregnation technique. The CeO_2@MNA samples were characterized by X-ray diffraction (XRD), scanning electron microscopy (SEM), energy dispersive X-ray analysis (EDS), thermal gravimetric analysis (TGA), Fourier transform infrared spectroscopy (FTIR), and Brunauer-Emmett-Teller (BET) technique. The catalytic activity of CeO_2 promoted MNA (CeO_2@MNA) for POM reaction was evaluated for various CeO_2 loading kept the feed ratio CH_4/O_2=2 at 850 °C. The catalyst containing 10 wt.% cerium loading (10%CeO_2@MNA) showed 94% CH_4 conversion with H_2/CO ratio above 2.0, that is more suitable for FT synthesis. The performance of catalyst is attributed to highly crystalline stable CeO_2@MNA with better Ce-MNA interactions withstand for 35 h time on stream. Furthermore, the spent catalyst was examined by TGA, SEM-EDS, and XRD to evaluate the carbon formation and structural changes during the span of reaction time.

Keywords: *CeO_2; Partial oxidation of methane; Hydrogen production; Syngas; hydrotalcite;*

Table of Contents

List of Figures

List of Tables

List of Abbreviations

GC:	Gas chromatograph
FBR:	Fixed bed reactor
GTL:	Gas to liquid
FTS:	Fischer-tropsch synthesis
GHGs:	Greenhouse gases
DRM:	Dry reforming of methane
POM:	Partial oxidation of methane
SRM:	Steam reforming of methane
XRD:	X-ray diffraction
IEA:	International Energy Agency
SEM:	Scanning electron microscopy
EDS:	Energy dispersive X-ray spectroscopy
TGA:	Thermogravimetric analysis
FTIR:	Fourier transform infrared spectroscopy
WGS:	Water gas shift
RWGS:	Reverse water gas shift
CTAB:	Cetyl-trimethyl-ammonium-bromide
PVP:	Poly-vinyl-pyrrolidone
HTs:	Hydrotalcites
GHSV:	Gas hourly space velocity
TCD:	Thermal conductivity detector
TOS:	Time on stream

List of Publications

1. **Muhammad Anees Ul Hasnain**, Asif Hussain Khoja, Faaz Ahmed Butt, Mariam Ayesha, Faisal Saleem, Muhammad Taqi Mehran, Rabia Liaquat, Majid Ali, and Zaki Ismail Zaki. "*Partial oxidation of methane over CeO_2 loaded hydrotalcite (MgNiAl) catalyst for the production of hydrogen rich syngas (H_2, CO)*." International Journal of Hydrogen Energy, 2021. 46(74): p. 36663-36677. (IF=5.8, Q1).

Chapter 1: Introduction

1.1 Background

Due to increase in population and industrialization energy demand has been increased [1, 2]. Different types of energy resources are being utilized worldwide. The goal is to achieve such resources which are more efficient, economical and have minimum environmental footprint. Natural gas is one of the major source of energy whose demand is increasing and according to International Energy Agency (IEA) the demand for natural gas could increase by 50% in 2035 from 2010 level [3]. Natural gas is clean fuel having low environmental footprint whose deposits in the world are approximately 5000 trillion cubic feet which are equal to almost 47% of petroleum deposits but not widely used as petroleum [4]. The reason is that these huge deposits of natural gas available are expensive to transport to market place due to their location in far distance remote areas [5]. Methane, is the principal component of natural gas and major energy source used worldwide whose future demand is increasing. About 70% to 90% volume of natural gas consists of methane [6-8]. CH_4 is also a greenhouse gas whose green house potential is higher than CO_2 [9].This is highly desirable to obtain such processes which convert CH_4 to efficient and economical fuel.

Methane is burned for heating and power generation purposes but this usage causes high carbon emissions [10]. It can also be converted directly into ethylene through oxidative coupling of methane or into olefins and aromatics through non oxidative coupling of methane, but high temperature is required for satisfactory level of products synthesis [11, 12]. Another direct conversion applications is methanol synthesis from methane oxidation but in this reaction prevention from methane over oxidation is kinetically difficult to achieve [13]. Syngas (a mixture of H_2 and CO) synthesis, a very economical and commercially adopted route for CH_4 conversion along with co-reactants such as oxygen (O_2) and water via reforming techniques [14-16]. Syngas can be utilized directly as fuel or as a primary feedstock in the manufacture of important chemicals such as methanol synthesis, ammonia, synthetic oils and fuel cells [17-19]. Syngas has vast application i.e in gas turbine, internal combustion engine, aerospace power production, refineries, hydrogen production, alcohol

production and many other valuable chemical production [20-25]. Hydrogen which is the major component of syngas is a clean fuel.

About 60% of investment in syngas production is required for natural gas conversion plants[26] so conversion technology is very important aspect to be considered. Steam reforming of methane (SRM), dry reforming of methane (DRM), partial oxidation of methane (POM) and their combinations are generally employed techniques for production of syngas from CH_4 [27]. SRM and POM are most commonly employed methane activation process [28]. SRM process utilizes water and methane for syngas production. SRM is highly developed and most utilized technique for syngas production[29, 30]. But endothermic nature of reaction makes SRM an energy intensive technique and its reactor design is complicated [31, 32]. DRM process has certain advantages i.e clean usage of CO_2 and CH_4 which are also greenhouse gases (GHGs) [33]. However, catalyst stability is major issue associated with DRM process, deactivation of catalyst occurs at temperature above 640 °C due to deposition of inactive carbon and metal sintering [34]. POM process, owing to some advantages is promising technique for syngas production. In POM process syngas is produced from CH_4 and O_2. Simple reactor design, exothermic nature of reaction which makes POM energy saving and H_2/CO ratio of two suitable for Fischer-Tropsch synthesis attracts researchers [35, 36]. So, POM is a promising process for syngas production that provides clean energy from CH_4. Two types of catalyst systems are generally employed for POM (1) noble metal catalysts (2) Non noble metal (Ni, Co) catalysts. Noble metal catalysts have high activity and stability but these are much expensive [37]. Among non-noble metal catalysts, Ni based catalysts have comparable activity with noble metals and economical to use. Ni catalysts are used with different supports or promoters to enhance catalytic activity and stability [38]. Developments are being done to make POM process commercially applicable for economical syngas production.

1.2 Problem Statement

Among syngas production processes, partial oxidation of methane (POM) has gained great prominence due to the higher potential for syngas, with enhance H_2 production and their feasibility to conduct the processes in simple reactors. However, at higher temperatures of POM hotspot formation, carbon deposition and sintering of catalyst takes place. The deposited carbon on catalyst surface deactivates the active sites of catalyst.

The use of hydrotalcite of Mg, Ni and Al (MNA) for POM reaction has certain advantages owing to their properties such as uniform distribution of metal particles, high basicity, large surface area and porous structure which allows promoter atoms uniform distribution inside their structure. NiO, $MgAl_2O_4$, $MgNiO_2$, MgO like compounds formed in MNA are considered coke resistant and stable at high temperatures. The use of promoter with suitable characteristics improves the catalytic performance. CeO_2 promoter due to its excellent redox properties and high thermal stability, is suitable for oxidation reactions and have high activity and resistance to carbon formation. It can store and release different levels of bulk and surface oxygen vacancies which makes it suitable for carbon removal in POM reaction. Such properties associated with this catalyst system are effective for high activity and carbon removal from catalyst surface resulting in improved catalytic performance.

1.3 Objectives of Study

The focus of this research work is to synthesize a highly active and stable catalyst for POM reaction for that cause following are the main objectives:

- To synthesize and characterize CeO_2@MNA catalyst for POM process.
- To run the POM reaction in fixed bed reactor to investigate the catalytic activity of CeO_2@MNA with different CeO_2 loadings.
- To analyse stability of nano-composite with CeO_2 loading for best catalytic activity.

1.4 Scope and Limitations of Study

Three interacting phases are followed in this research work consisting of catalyst synthesis, characterization, and activity tests for process optimization. In first phase MNA hydrotalcite material was prepared from magnesium nitrate hexahydrate ($Mg(NO_3)_2.6H_2O$), aluminium nitrate nonahydrate ($Al(NO_3)_3.9H_2O$) and nickel nitrate hexahydrate ($Ni(NO_3)_2.6H_2O$) through wetness impregnation method. The second phase comprises nano-composite formation from CeO_2 promoter and MNA hydrotalcite followed by the characterization techniques X-ray diffraction (XRD), Scanning electron microscopy (SEM), Thermogravimetric analysis (TGA), Fourier transform infrared spectroscopy (FTIR) and Burnauer-Emmett-Teller (BET). In the third phase activity tests were performed for POM process optimization in fixed bed reactor. The nano-composite was tested for varying promoter loading to get better catalytic performance. The scope of this work is shown in **Fig 1.1**.

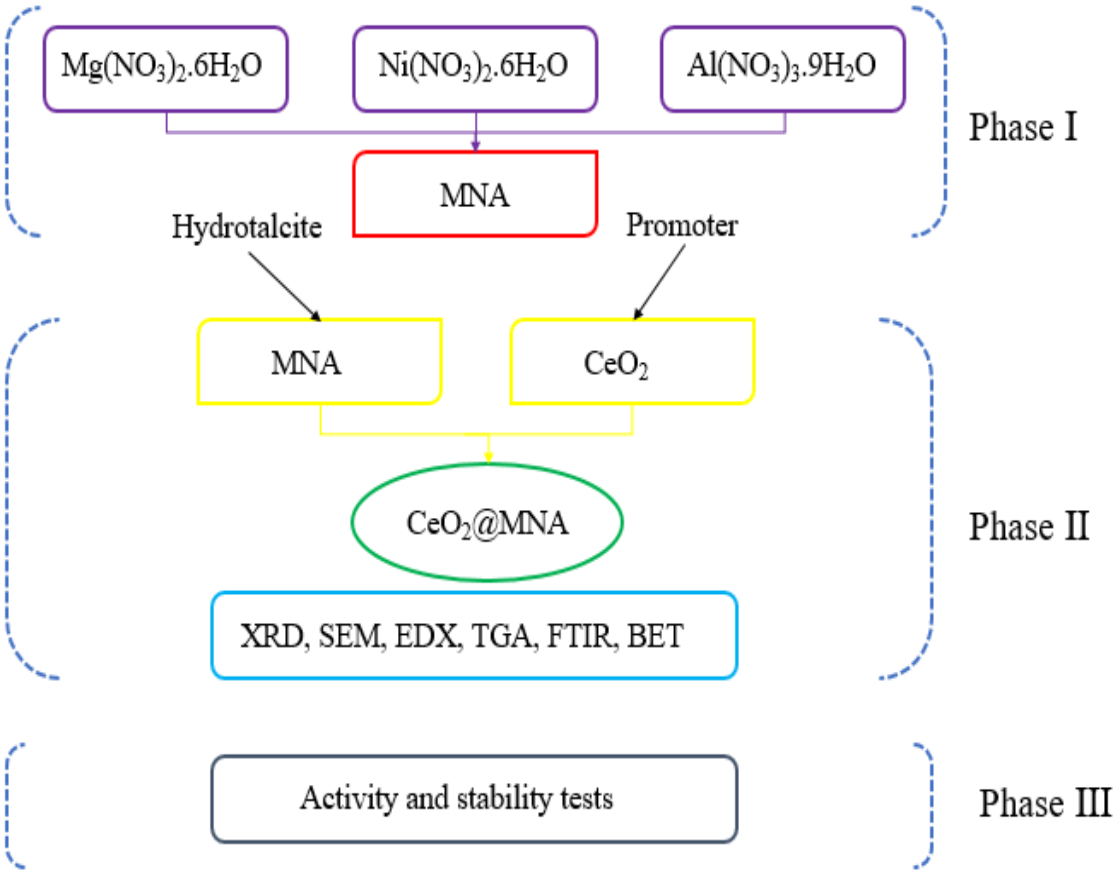

Figure 1.1 Scope of study

Process optimization, reactor design and POM intended catalyst are some of limitations that are beyond the scope of this study.

1.4 Flow Chart of Thesis

The literary review was initially done to find out the suitable metal and promoter selection for POM process and the effect of different parameters on the process. In the material preparation and characterisations section, catalyst was prepared and characterized through multiple characterizations techniques. In the experimentation section, the prepared catalyst samples were tested in fixed bed reactor for activity and stability performance. In results and discussion section, detailed analysis of results on basis of characterizations and literature was discussed. Conclusive section dealt with the associated benefits of the catalyst used in POM process and the application of the process on high scale production of syngas keeping in mind the environment friendly nature of the process.

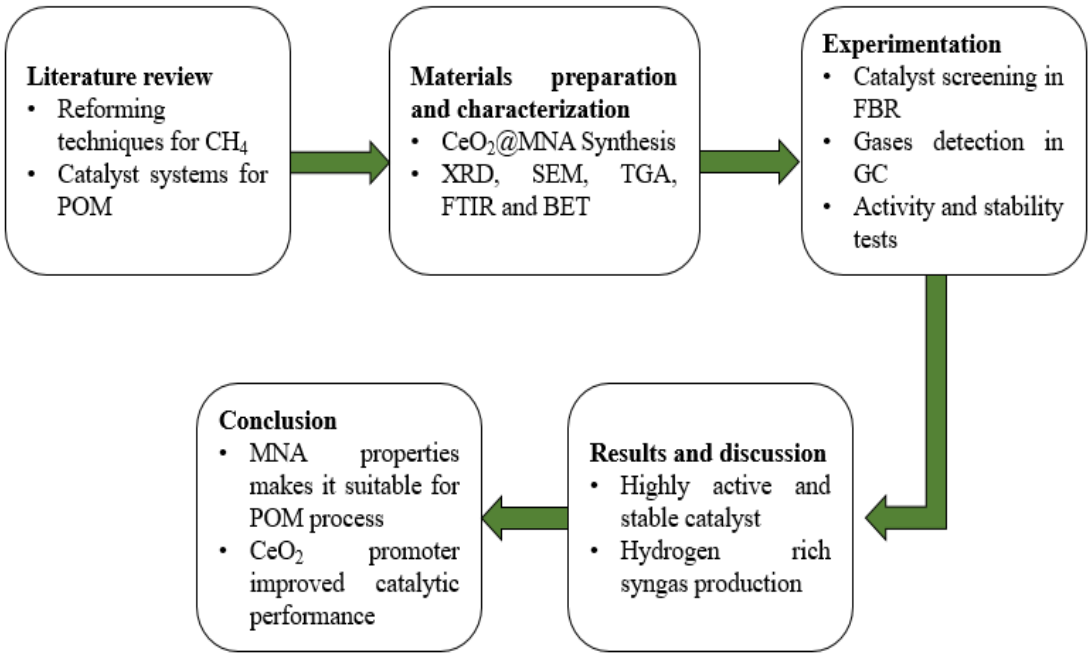

Figure 1.2 Flow chart of thesis

References

1. Abdullah, B., N.A. Abd Ghani, and D.-V.N. Vo, Recent advances in dry reforming of methane over Ni-based catalysts. Journal of Cleaner Production, 2017. 162: p. 170-185.

2. Li, X., Diversification and localization of energy systems for sustainable development and energy security. Energy Policy, 2005. 33(17): p. 2237-2243.

3. Wood, D.A., C. Nwaoha, and B.F. Towler, Gas-to-liquids (GTL): A review of an industry offering several routes for monetizing natural gas. Journal of Natural Gas Science and Engineering, 2012. 9: p. 196-208.

4. Khirsariya, P. and R.K. Mewada, Single Step Oxidation of Methane to Methanol–Towards Better Understanding. Procedia Engineering, 2013. 51: p. 409-415.

5. Christian Enger, B., R. Lødeng, and A. Holmen, A review of catalytic partial oxidation of methane to synthesis gas with emphasis on reaction mechanisms over transition metal catalysts. Applied Catalysis A: General, 2008. 346(1-2): p. 1-27.

6. Allen, D.T., et al., Methane emissions from process equipment at natural gas production sites in the United States: pneumatic controllers. Environ Sci Technol, 2015. 49(1): p. 633-40.

7. Abdulrasheed, A., et al., A review on catalyst development for dry reforming of methane to syngas: Recent advances. Renewable and Sustainable Energy Reviews, 2019. 108: p. 175-193.

8. Horn, R. and R. Schlögl, Methane Activation by Heterogeneous Catalysis. Catalysis Letters, 2014. 145(1): p. 23-39.

9. Singha, R.K., et al., Synthesis of highly coke resistant Ni nanoparticles supported MgO/ZnO catalyst for reforming of methane with carbon dioxide. Applied Catalysis B: Environmental, 2016. 191: p. 165-178.

10. McFarland, E., Chemistry. Unconventional chemistry for unconventional natural gas. Science, 2012. 338(6105): p. 340-2.

11. Galadima, A. and O. Muraza, Revisiting the oxidative coupling of methane to ethylene in the golden period of shale gas: A review. Journal of Industrial and Engineering Chemistry, 2016. 37: p. 1-13.

12. Guo, X., et al., Direct, nonoxidative conversion of methane to ethylene, aromatics, and hydrogen. Science, 2014. 344(6184): p. 616-9.

13. Hammond, C., S. Conrad, and I. Hermans, Oxidative methane upgrading. ChemSusChem, 2012. 5(9): p. 1668-86.

14. York, A.P., T. Xiao, and M.L. Green, Brief overview of the partial oxidation of methane to synthesis gas. Topics in Catalysis, 2003. 22(3-4): p. 345-358.

15. Khoja, A.H., et al., Thermal dry reforming of methane over La_2O_3 co-supported $Ni/MgAl_2O_4$ catalyst for hydrogen-rich syngas production. Research on Chemical Intermediates, 2020.

16. Mazhar, A., et al., Performance Analysis of TiO_2-Modified $Co/MgAl_2O_4$ Catalyst for Dry Reforming of Methane in a Fixed Bed Reactor for Syngas (H_2, CO) Production. Energies, 2021. 14(11): p. 3347.

17. Zhang, M., et al., Effect of Ni(111) surface alloying by Pt on partial oxidation of methane to syngas: A DFT study. Surface Science, 2014. 630: p. 236-243.

18. Krenzke, P.T., et al., Synthesis gas production via the solar partial oxidation of methane-ceria redox cycle: Conversion, selectivity, and efficiency. International Journal of Hydrogen Energy, 2016. 41(30): p. 12799-12811.

19. Song, L., Y. Kong, and X. Li, Hydrogen production from partial oxidation of methane over dielectric barrier discharge plasma and NiO/γ-Al2O3 catalyst. International Journal of Hydrogen Energy, 2017. 42(31): p. 19869-19876.

20. Cecere, D., E. Giacomazzi, and A. Ingenito, A review on hydrogen industrial aerospace applications. International Journal of Hydrogen Energy, 2014. 39(20): p. 10731-10747.

21. Bailera, M., et al., Future applications of hydrogen production and CO_2 utilization for energy storage: Hybrid Power to Gas-Oxycombustion power plants. International Journal of Hydrogen Energy, 2017. 42(19): p. 13625-13632.

22. Abdul Mujeebu, M., Hydrogen and syngas production by superadiabatic combustion – A review. Applied Energy, 2016. 173: p. 210-224.

23. Dedov, A.G., et al., High-selectivity partial oxidation of methane into synthesis gas: the role of the red-ox transformations of rare earth — alkali earth cobaltate-based catalyst components. Fuel Processing Technology, 2016. 148: p. 128-137.

24. Roslan, N.A., et al., A review on glycerol reforming processes over Ni-based catalyst for hydrogen and syngas productions. International Journal of Hydrogen Energy, 2020. 45(36): p. 18466-18489.

25. Xie, Y., et al., A comprehensive review on laminar spherically premixed flame propagation of syngas. Fuel Processing Technology, 2018. 181: p. 97-114.

26. Rostrup-Nielsen, J. and L.J. Christiansen, Concepts in syngas manufacture. Vol. 10. 2011: World Scientific.

27. Baltrusaitis, J. and W.L. Luyben, Methane Conversion to Syngas for Gas-to-Liquids (GTL): Is Sustainable CO_2 Reuse via Dry Methane Reforming (DMR) Cost Competitive with SMR and ATR Processes? ACS Sustainable Chemistry & Engineering, 2015. 3(9): p. 2100-2111.

28. Jahangiri, H., et al., A review of advanced catalyst development for Fischer–Tropsch synthesis of hydrocarbons from biomass derived syn-gas. Catalysis Science & Technology, 2014. 4(8): p. 2210-2229.

29. Yang, X., et al., Characterization and performance evaluation of Ni-based catalysts with Ce promoter for methane and hydrocarbons steam reforming process. Fuel, 2016. 179: p. 353-361.

30. Zhai, X., et al., Catalytic performance of Ni catalysts for steam reforming of methane at high space velocity. International Journal of Hydrogen Energy, 2011. 36(1): p. 482-489.

31. Katheria, S., G. Deo, and D. Kunzru, Washcoating of Ni/$MgAl_2O_4$ Catalyst on FeCralloy Monoliths for Steam Reforming of Methane. Energy & Fuels, 2017. 31(3): p. 3143-3153.

32. Zhu, L., L. Li, and J. Fan, A modified process for overcoming the drawbacks of conventional steam methane reforming for hydrogen production: Thermodynamic investigation. Chemical Engineering Research and Design, 2015. 104: p. 792-806.

33. Serrano-Lotina, A. and L. Daza, Influence of the operating parameters over dry reforming of methane to syngas. International Journal of Hydrogen Energy, 2014. 39(8): p. 4089-4094.

34. Serrano-Lotina, A., et al., Dry reforming of methane to syngas over La-promoted hydrotalcite clay-derived catalysts. International Journal of Hydrogen Energy, 2012. 37(17): p. 12342-12350.

35. Zhao, K., et al., La1-xSrxFeO_3 perovskites as oxygen carriers for the partial oxidation of methane to syngas. Chinese Journal of Catalysis, 2014. 35(7): p. 1196-1205.

36. Kobayashi, Y., et al., Effect of NiO content in mesoporous NiO–Al_2O_3 catalysts for high pressure partial oxidation of methane to syngas. Applied Catalysis A: General, 2011. 395(1-2): p. 129-137.

37. Bepari, S., et al., Steam reforming of ethanol over cerium-promoted Ni-Mg-Al hydrotalcite catalysts. Catalysis Today, 2017. 291: p. 47-57.

38. Ibrahim, A.A., et al., Study of Partial Oxidation of Methane by Ni/Al_2O_3 Catalyst: Effect of Support Oxides of Mg, Mo, Ti and Y as Promoters. Molecules, 2020. 25(21): p. 5029.

Chapter 2: Literature Review

2.1 Natural Gas Overview

Natural gas is a gaseous fossil fuel with hydrocarbon rich gas which is found in natural gas fields, oil fields and coal beds [1]. Natural gas is one of the major source of energy whose demand is increasing and according to International Energy Agency (IEA) the demand for natural gas could increase by 50% in 2035 from 2010 level [2]. Natural gas is clean fuel having low environmental footprint whose deposits in the world are approximately 5000 trillion cubic feet which are equal to almost 47% of petroleum deposits but not widely used as petroleum [3]. The reason is that these huge deposits of natural gas available with high volume are expensive to transport to market place due to their location in far distance remote areas [4]. This problem led to an increased interest for gas to liquid technology (GTL) for economical use of natural gas. Methane, is the principal component of natural gas and major energy source used worldwide whose future demand is increasing [5]. About 70% to 90% volume of natural gas consists of methane [6-8]. This motive attracted researchers for developments of methane utilization technologies for clean and economical use of methane.

2.2 Methane Utilization Routes and Syngas Importance

Major CH_4 utilization routes are shown in **Fig. 2.1** with applications. CH_4 is burned for heating and power generation purposes but this usage causes high carbon emissions [9]. It can also be converted directly into ethylene through oxidative coupling of methane or into olefins and aromatics through non oxidative coupling of methane, but high temperature is required for satisfactory level of products synthesis [10, 11]. Another direct conversion applications is methanol synthesis from methane oxidation but in this reaction prevention from methane over oxidation is kinetically difficult to achieve [12]. Syngas (a mixture of H_2 and CO) synthesis, is an economical route for effective utilization of methane and this is commercially adopted route for CH_4 conversion along with co-reactants such as oxygen (O_2) and water via reforming techniques [13-15]. Methane conversion to synthesis gas is competitive route for clean utilization of methane [16]. Syngas has multiple application for synthesis of fuels and

valuable chemicals such as methanol, hydrogen, alcohol, ammonia , synthetic oils and in fuel cells [17-19]. Syngas has vast power production applications in gas turbine, internal combustion engine, aerospace, refineries [20-25].

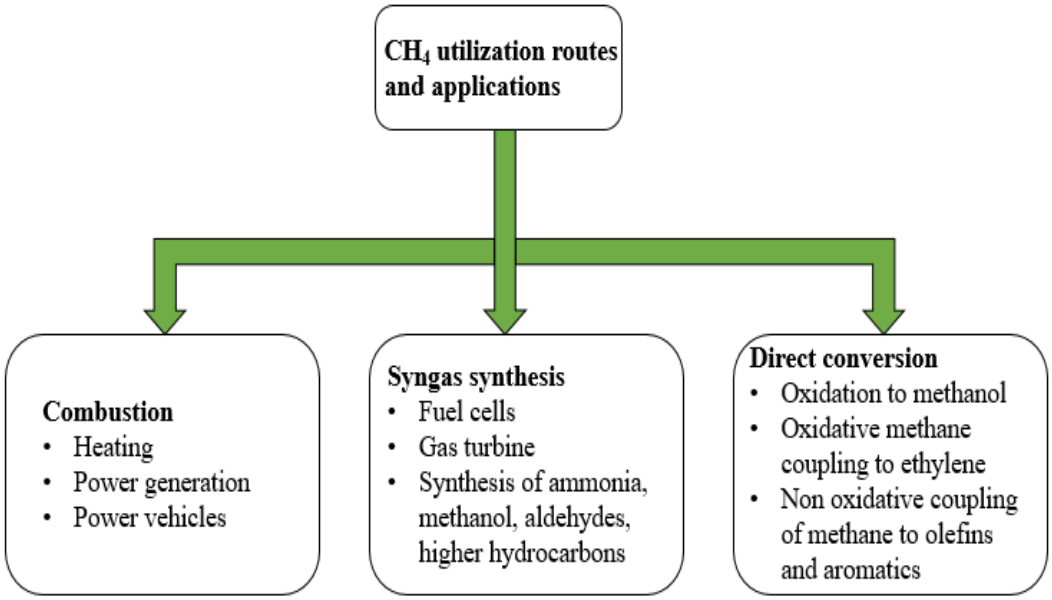

Figure 2.1 CH_4 utilization routes

2.3 Overview of Methane Reforming Technologies for Syngas Production

Due to increased energy demand with increasing population it is inevitable to move towards sustainable methane reforming technologies. Steam reforming, dry reforming, auto-thermal reforming, tri reforming and partial oxidation of methane are the main process for syngas production from methane. Overview of methane reforming technologies is shown in **Fig 2.2**. These catalytic processes producing hydrogen or syngas are basic processes for supply of fuel, food and valuable chemicals [26]. The developments are being done in these areas. The reforming processes are shown in the below reactions:

Steam reforming of methane

$$CH_4 + H_2O \rightarrow CO + 3H_2 \qquad \Delta H°_{298K} = 206\ KJ/mol \qquad (R1)$$

Dry reforming of methane

$$CH_4 + CO_2 \rightarrow 2CO + 2H_2 \qquad \Delta H°_{298K} = 247 \text{ KJ/mol} \qquad (R2)$$

Partial oxidation of methane

$$CH_4 + 0.5O_2 \rightarrow CO + 2H_2 \qquad \Delta H°_{298K} = -36 \text{ KJ/mol} \qquad (R3)$$

Auto-thermal reforming

$$CH_4 + H_2O \rightarrow CO + 3H_2 \qquad \Delta H°_{298K} = 206 \text{ KJ/mol} \qquad (R1)$$

$$CH_4 + 0.5O_2 \rightarrow CO + 2H_2 \qquad \Delta H°_{298K} = -36 \text{ KJ/mol} \qquad (R3)$$

Tri reforming of methane

$$CH_4 + H_2O \rightarrow CO + 3H_2 \qquad \Delta H°_{298K} = 206 \text{ KJ/mol} \qquad (R1)$$

$$CH_4 + CO_2 \rightarrow 2CO + 2H_2 \qquad \Delta H°_{298K} = 247 \text{ KJ/mol} \qquad (R2)$$

$$CH_4 + 0.5O_2 \rightarrow CO + 2H_2 \qquad \Delta H°_{298K} = -36 \text{ KJ/mol} \qquad (R3)$$

As shown in the above reactions, both DRM and SRM are endothermic reactions and require energy input but partial oxidation of methane (POM) is exothermic and don't require heat supply while the auto-thermal is self-sustaining type of reforming which has both exothermic and endothermic reactions. SRM is used mostly for CH_4 reforming but it also requires steam production. For POM, hot spot formation, catalyst deactivation are major issues. The developments are being done to optimize POM process for better performance

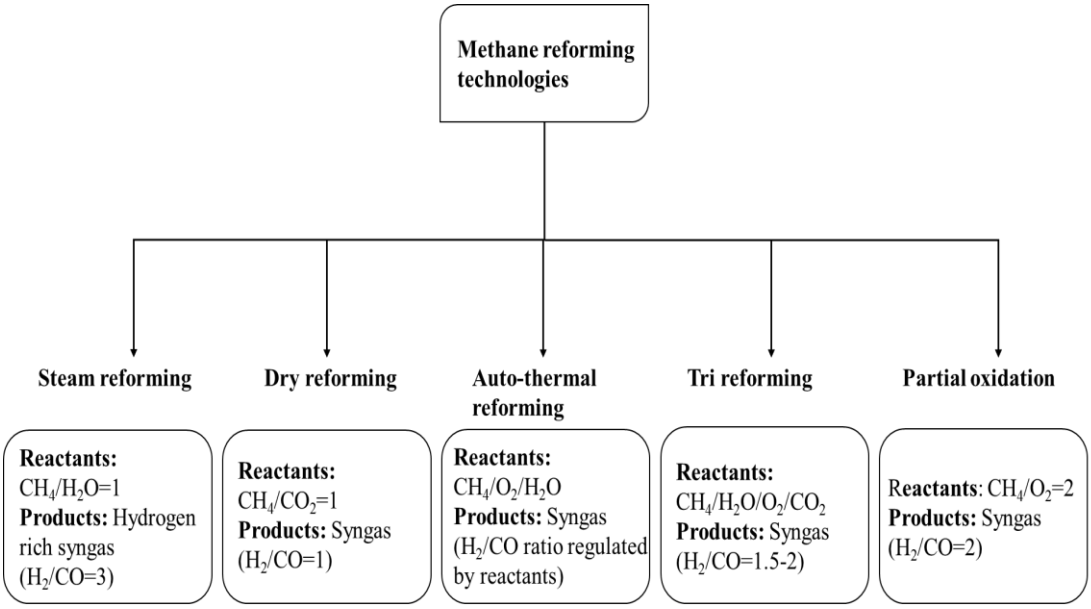

Figure 2.2 Overview of methane reforming technologies for syngas production

2.3.1 Steam Reforming of Methane

Steam Reforming of Methane (SRM) is the process which is being employed for industrial scale production of syngas from methane. Steam reforming reaction involves reaction between natural gas and steam which are steam reforming, water gas shift reaction and removal of CO_2 in conventional SMR process, that are accompanied by the reactions given below.

Steam reforming of methane

$$CH_4 + H_2O \rightarrow CO + 3H_2 \qquad \Delta H°_{298K} = 206 \text{ KJ/mol} \qquad \text{(R1)}$$

Steam reforming of methane

$$CH_4 + 2H_2O \rightarrow CO_2 + 4H_2 \qquad \Delta H°_{298K} = 163 \text{ KJ/mol} \qquad \text{(R4)}$$

Water gas shift reaction

$$CO + H_2O \rightarrow CO_2 + H_2 \qquad \Delta H°_{298K} = -41 \text{ KJ/mol} \qquad \text{(R5)}$$

Steam reforming of methane reaction (R1) and (R2) are reforming process in furnace to produce syngas where water gas shift reaction leads to complete oxidation and resulting high production of hydrogen. Supplementary CH_4 is supplied to furnace

as heat input owing to endothermic nature of steam reforming reaction. CO is reduced in the product to achieve the required syngas ratio by water gas shift reaction, while CO_2 is removed by adsorption technology [27]. Compared to other reforming processes, SRM is the most operational process on industrial scale in syngas and hydrogen production owing to being most economic and developed process. The disadvantages associated with SRM are higher syngas ratio of about 3 which is not favourable for FT synthesis, highly endothermic reaction demanding higher energy input with high operational cost [28].

2.3.2 Dry Reforming of Methane

DRM utilizes two abundantly occurring greenhouse gases, CH_4 and CO_2, having great potential by converting into green energy source and many other valuable chemicals[7, 29-34] but at high temperature catalyst deactivates due to coke formation and reaction is highly energy consuming[31, 35-38]. Syngas is produced in unity proportion as shown in reaction (R2). DRM reaction usually have three side reactions shown reactions (R6-R8). Methane cracking is the decomposition of methane which usually occurs at low temperature resulting in carbon deposition which cause catalyst deactivation. Boudouard reaction is the decomposition of carbon monoxide into carbon dioxide and coke which occurs at high temperature and this reaction also causes deactivation[39].

Dry reforming of methane

$$CH_4 + CO_2 \rightarrow 2CO + 2H_2 \qquad \Delta H°_{298K} = 247\ KJ/mol \qquad (R2)$$

Methane cracking

$$CH_4 \rightarrow C + 2H_2 \qquad \Delta H°_{298K} = 75KJ/mol \qquad (R6)$$

Boudouard reaction

$$2CO \rightarrow CO_2 + C \qquad \Delta H°_{298K} = -171KJ/mol \qquad (R7)$$

Reverse water gas shift

$$CO_2 + H_2 \rightarrow CO + H_2O \qquad \Delta H°_{298K} = 41KJ/mol \qquad (R8)$$

Reverse water gas shift (RWGS) reaction is another side reaction of DRM which affects the syngas ratio as more CO is produced with the reaction of hydrogen and carbon dioxide. This technique is not applied on industrial scale yet and is under investigation to achieve stable catalysts with good activity.

2.3.3 Auto-Thermal Reforming of Methane

Auto-thermal reforming is the combination of SRM and the POM process [16] shown in reactions (R1) and (R3) respectively. This process use both endothermic and exothermic reactions hence leaving the heat input requirement to least possible by bringing balance of the heat from exothermic POM process and heat supply to endothermic SRM process. Additionally this is more promising technique with better control in syngas production which is easily regulated by reactant input [40].

The process takes place in two steps: firstly, the reaction of CH_4 with oxygen to produce CO_2 and H_2O and in the second step the reaction of unconverted CH_4 with CO_2 or H_2O to produce syngas [41]. The disadvantages linked with auto-thermal reforming are the extensive control system for fuel processing system operation and sintering and deactivation of catalyst as a result of high temperature stream [42, 43].

2.3.4 Tri Reforming of Methane

Tri reforming is the synergetic combination of SRM (R1), DRM (R2) and POM (R3) reactions for syngas production. This process has some unique advantages than other reforming processes such as, it helps in achieving desirous syngas ratio regulated by feed gases composition [44]. Tri reforming have multiple advantages like inhibiting carbon formation, no feed lost and two endothermic reactions would avoid hot spot formation in presence of oxidative environment [45, 46]. Despite several advantages of this process, its implementation on large scale is difficult due to complex reaction environment, activation of reforming catalyst becomes more challenging [47].

2.3.5 Partial Oxidation of Methane

Among methane reforming technologies, POM process attracts researchers owing to its certain advantages over other reforming technologies. The very first paper for POM was published in 1929 by Liander [48]. POM H_2/CO molar ratio is 2 and this value is ideal for Fischer-Tropsch synthesis for liquid fuel production and other downstream applications, mildly exothermic nature of reaction makes POM an energy saving process which avoids energy usage for superheated steam as in SRM, compact

reactor sizes, low CO_2 contents in products, short contact time are some additional advantages [49] [50]. Exothermic nature of reaction is a thermodynamic advantage, heat released in this reaction can be utilized by combining with endothermic process to develop a more energy efficient process [41].

POM process syngas is formed through methane conversion in presence of stoichiometric supply of oxygen at high temperature heating (R3). If supply of oxygen is in excess amount i.e more than stoichiometric value, then it will lead to combustion reaction (R9), which is a huge waste and the products will be H_2O and CO_2.

Partial oxidation

$$CH_4 + 0.5O_2 \rightarrow CO + 2H_2 \qquad \Delta H°_{298K} = -36\ KJ/mol \qquad (R3)$$

POM reaction is a single step reaction which does not require any external energy source [51, 52]. However, two reaction mechanisms are reported for this process shown in **Fig. 2.3**. In the first one, CH_4 and O_2 are directly converted into H_2 and CO (R3). While, in the second mechanism, CH_4 and O_2 first form H_2O and CO_2 (R9) followed by SRM (R1) and DRM (R2) process to synthesize H_2 and CO, this is also called combustion reforming mechanism [53].

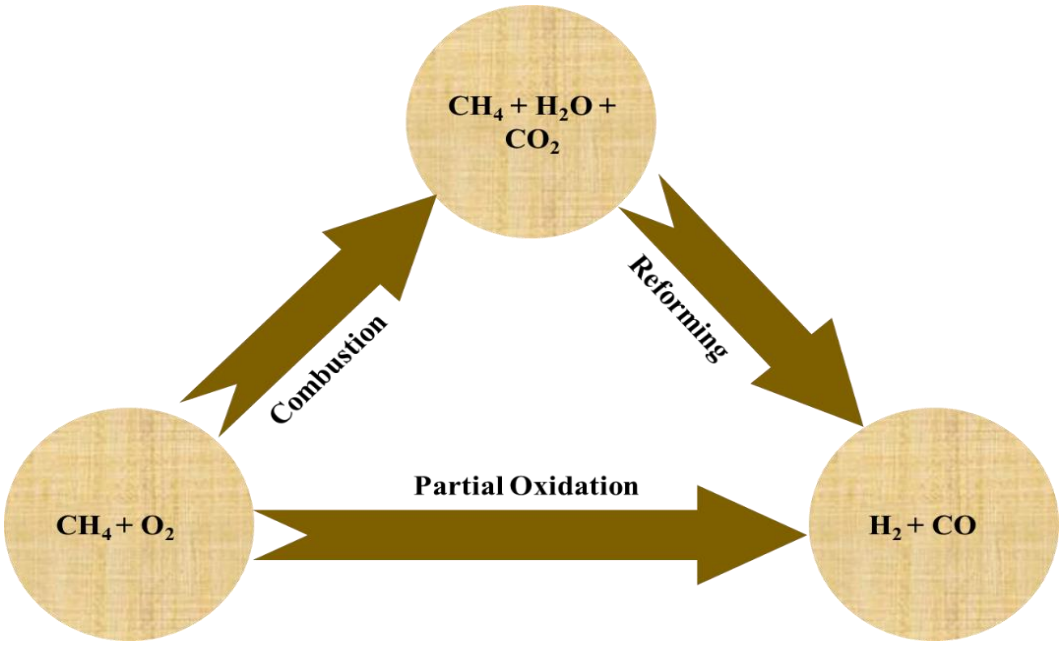

Figure 2.3 POM to syngas reaction pathways for two possible mechanisms

Some side reactions that occur parallel with POM process are CO_2 reforming, water gas shift reaction (R5), Boudouard reaction (R7) and combustion reaction (R9), methane cracking (R6) [54]. Presence of these reaction is mainly temperature dependant and they occur at specific temperature range.

CO_2 reforming

$$CH_4 + CO_2 \rightarrow 2CO + 2H_2 \qquad \Delta H°_{298K} = 247 \text{ KJ/mol}$$

(R2)

Water gas shift reaction

$$CO + H_2O \rightarrow CO_2 + H_2 \qquad \Delta H°_{298K} = -41 \text{ KJ/mol} \qquad \text{(R5)}$$

Boudouard reaction

$$2CO \rightarrow CO_2 + C \qquad \Delta H°_{298K} = -171 \text{KJ/mol} \qquad \text{(R7)}$$

Combustion

$$CH_4 + 2O_2 \rightarrow CO_2 + 2H_2O \qquad \Delta H°_{298K} = -801 \text{ KJ/mol} \qquad \text{(R9)}$$

Methane cracking

$$CH_4 \rightarrow C + 2H_2 \qquad \Delta H°_{298K} = 75 \text{KJ/mol} \qquad \text{(R6)}$$

At temperature above 750 ℃ presence of CO_2 reforming is possible that might decrease the H_2/CO ratio less than 2. Presence of water gas shift reaction results in higher hydrogen production from CO and H_2O consequently increased H_2/CO ratio is obtained. Its presence depends upon employed catalyst type, normally it occurs around 500 ℃ [54]. Boudouard reaction is responsible for carbon formation around 500 ℃. Combustion reaction is involved in process when sufficient supply of O_2 is provided. Methane decomposition also called methane cracking reaction occurs at high temperature [55].

The main challenge associated with POM is deposition of carbon on catalyst surface, it may come from Boudouard reaction, combustion reaction or methane

cracking [56, 57]. The deposited carbon deactivates the catalyst hence, an economical catalytic system is desirable with enhanced stability at higher temperature of POM with capability to remove surface carbon and better catalytic activity for syngas production [58-60].

POM performance for syngas is strongly influenced by various reactors configurations and catalytic systems. These effective parameters will be discussed in the next section.

2.4 Role of Reactor Configurations and Catalytic Systems in POM

Reactor configuration and catalytic systems are very important parameters that strongly influence catalytic activity, stability and carbon formation in POM process. These two important parameters are explained below.

2.4.1 Reactor Technology for POM

Catalytic bed optimization is an influential aspect to improve catalytic performance in POM. Aiming to discover a competitive reactor system, POM is investigated on multiple reactor systems such as fixed bed reactor, fluidized bed reactor, fixed bed/fluidized bed membrane reactors, hollow fibre membrane reactor, flow reactor, monolith reactor, porous reactor, flow tube reactor, catalytic membrane reactor, solid membrane reactor PEMFC type, swiss role reactor etc. These different reactors performance has been investigated with simulation work or experimentally.

Fixed bed reactors are the most common and simplest type of reactors employed in POM [61]. These reactor systems can perform reaction efficiently by employing a suitable catalyst. However, due to mildly exothermic POM reaction and high reaction rate a temperature gradient can be observed which can cause hot spot at catalyst bed [62]. Fluidized bed reactors resolves the issue of hot spot formation as the fluidized catalytic bed can act as a heat carrier, constructing a uniform temperature profile due to better heat transfer [63].

Ostrowski and co-workers conducted simulation study for POM performance investigation over fixed bed, fluidized bed and fixed bed/fluidized bed membrane reactors at industrial conditions (P=5 and 30 bar, T=1023-1073 K) [64]. It was observed that in fixed bed reactor process syngas yield was lower than fluidized bed reactor due to intra-particle mass transport limitations. Furthermore, simulation results revealed that in integrated reactors configuration with separation membrane the

performance of fixed bed reactor was more sensitive to separation selectivity than fluidized bed reactor. In another simulation study, fixed bed reactor for different parameters influence on POM performance was investigated by Bizzi and co-workers [65]. It was found in their work that at lower values of GHSV, increase in space velocity enhanced the performance of reactor that is associated with better mass diffusion. However, at higher GHSV values reactor blowout occurs. While investigating on various geometric configurations for different length to diameter ratios, it was found that performance of deeper reactors was better than the wider ones, at the cost of greater pressure loss.

A small reactor system known as micro reactor system is composed of submillimetre size channels which allow fast heating or cooling of reaction mixture, high syngas conversion due to large surface area to volume ratio [66]. A micro reactor was tested for POM using Rh catalyst and resulted in high CH_4 conversion of about 88% while hot spot formation was reported at inlet of fuel due to non-uniform axial temperature profile[67].

Another important reactor technology is modified type reactors known as monolith reactors, these are applied with porous washcoat of catalytically active material on honeycomb like structure having constant thickness [68]. Their fabrication cost is low, surface area to volume ratio is high and pressure drop is comparatively lower [69]. Halit Eren Figen investigated POM performance of molybdenum containing catalyst added with ruthenium in ceramic material based monolith reactor [26]. MoRu-3 (Ru-Mo-Co-Ni) catalyst showed the best performance with 98.5% CH_4 conversion, 94% H_2 selectivity, 93% CO selectivity, H_2/CO ratio of about 2 at 850 °C.

High cost of pure oxygen unit and hot spot formation due to temperature gradient are considered as main challenges associated with POM process [70]. Membrane reactors use air which reduce cost and their uniform temperature profile avoids hot spot formation [71]. Membrane reactors having an advantage of oxygen separation and POM chemical reaction in one unit reduced the cost of separate oxygen separation unit [72]. However, main challenge in these type of reactors is presence of reducing gases (H_2, CO, CH_4, O_2, CO_2, H_2O) involved in POM process those might decrease stability [73]. Disk type and tubular type reactors are two common types of membrane reactors. Disk type membrane reactors have low fabrication cost but they have lower stability

[74] while tubular type membrane reactors have high stability but their fabrication is costly [75].

An advanced reactor technology known as hollow fibre membrane reactor (HFMR), that unifies reaction and separation unit into a single unit which is expected to play a decisive role for sustainable energy technologies without the need of costly oxygen separation unit [76]. Its additional advantage to disc or tubular membranes is larger area per unit volume and stronger sealing which avoids decomposition of perovskite structure due to reducing gases H_2 and CO ability to cause a loss of lattice oxygen from the oxide phase [77] [78]. Zhigang Wang and co-workers conducted efficient POM process at low temperature (650-750 °C) and high CH_4 feeding rate of 25 ml/min using hollow fibre membrane reactor based on BBCN ($BaBi_{0.05}Co_{0.8}Nb_{0.15}O_{3-\delta}$) perovskite structure integrated with nickel phyllosilicate catalyst structure [79]. The good performance is strongly influenced by high oxygen permeation flux which is improved by roughness of membrane surface with syngas which is composed of reducing gases (H_2 & CO) produced from POM. This high oxygen permeation rate avoids breakage of perovskite structure to an optimum value controlled by oxygen permeation flux and CH_4 feed ratio for high H_2 yield (H_2 yield 33 ml/min and O_2 flux 15 ml/min at 730 °C for this reaction). Otherwise, for oxygen permeation flux higher than optimum value the excess oxygen will cause over oxidation of CH_4 consequently decreasing H_2 selectivity.

Multiple reactor systems are employed in POM to analyse catalytic performance for a better reactor design. Their performance depends on catalytic system, reaction type and it was found that every reactor system has pros and cons. POM performance of different types of reactors employed for POM is given in **Table 2.1**. Where FBR: fixed bed reactor; FlBR: fluidized bed reactor; MR: Membrane reactor; FBMR: fixed bed micro reactor; HFMR: hollow fibre membrane reactor; MoR: monolith reactor.

Table 2.1 Effect of reactor type on catalytic performance of POM

Catalyst	**Reactor**	**Temp (°C)**	**XCH_4 (%)**	**H_2/CO**	**Remarks**	**Ref.**
Rh-Ni-Al_2O_3	FBR	750	88	2.5	Catalysts prepared with solid state reaction showed higher performance than those prepared by impregnation method in FBR. Alumina supported catalysts exhibited higher activity than ceria, zirconia and magnesia supports.	[80]
Ni/3HL-ZrO_2-SiO_2	FBR (quartz tube)	800	92	2.8-3	The honey comb like structured catalyst showed higher performance than traditional SiO_2 supported catalyst and avoided Ni aggregation in FBR.	[81]
NiO/$CeO_{2-\delta}$-YSZ yttria stabilized zirconia (YSZ)	FBR	800	98	-	These advanced type bimodal mesoporous catalysts showed high activity with high Ce^{+3} concentration and optimal Ni species ratio in FBR with stability of 72 h TOS.	[82]
Ni/SDC ($Sm_{0.2}Ce_{0.8}O_{2-\delta}$)	MR ($La_{0.6}Sr_{0.4}Co_{0.2}Fe_{0.8}O_{3-\delta}$ (LSCF))	750	86	2.6	Ni/SDC catalyst in MR exhibited higher performance than alumina supported Ni catalyst due to higher absorbed active oxygen species in SDC supported catalyst.	[83]
Pt/$MgAl_2O_4$	FBMR	900	99	1.94	The catalyst have stable spinel structure at surface as well as in bulk which showed high performance for 500 h TOS in FlBR.	[84]
Ni/$LaNiO_3$/γ-Al_2O_3	HFMR ($La_{0.8}Ca_{0.2}Fe_{0.95}Ag_{0.05}O_{3-\delta}$ (LCF-Ag))	900	99	2	This ceramic reactor with hollow fibre membrane showed high tolerance for harsh conditions of acidic or reducing gases. It was stable for 200 h TOS.	[85]
20% Co/Mg-Al	FBR (quartz tube)	800	91.3	2	Hydrotalcite type cobalt catalyst showed good performance in FBR in harsh reaction conditions. Performance was highly dependent on Co loading and Mg/Al ratios.	[86]

NiO-CeO_2-Al_2O_3/Ni-foam	MoR	700	86.4	-	Ni catalyst with ceria tested in MoR showed higher performance than magnesia containing sample due to high carbon resistance of ceria by formation of $CeAlO_3$.	[87]
Ni/γ-Al_2O_3	FlBR	800	92	-	Catalyst showed high activity and prevented carbon formation in FlBR. All the phases were stable in 100 h TOS.	[62]
NiO/$NiAl_2O_4$	FlBR	850	90	2	The FlBR showed stable performance for POM with isothermal profile. Catalyst showed high activity which can be optimized by preventing catalyst to enter in cold zone of reactor.	[88]
Rh	FlBR	800	85.7	-	Catalysts showed very less carbon formation in FlBR with high catalytic performance. Although carbon formation is removed by gasification with O_2 but proper CH_4/O_2 ratio is key factor to limit carbon formation.	[89]
Pt			83.4	-		[89]
Pd			75.5	-		[89]

2.4.2 Catalyst Systems for POM

Catalyst play key role in syngas production process from POM. Generally, catalysts employed in POM are of two types (1) noble metal based catalysts (2) non-noble metal based catalysts. Noble metal based catalysts consists of Rh- [90], Ru- [91], Ir-[92], Pt- [93] and Pd- [94] noble metals, On the other hand, non-noble metal based catalysts used in POM consists of Ni, Co and Cu based catalysts [95]. In the next section, overview of these catalytic systems employed in POM is given.

Different type of noble metal catalysts has been investigated for syngas production in POM. An overview of noble metal based catalysts for POM is given below.

2.4.2.1 Noble Metal Based Catalysts

Noble metal based catalysts have been proved as highly active and stable for POM reaction with high coke formation resistance. Nevertheless, high cost and rareness of noble metals limit their commercial application. Besides high price of noble metals, these catalysts are widely used because of their excellent catalytic

performance. In their research work, Green and co-workers found that excellent CH_4 conversion and high selectivity of H_2 and CO can be obtained on almost all noble metal catalysts [96]. They obtained high 94% CH_4 conversion with H_2 and CO selectivity's of 99% and 97% respectively in POM at pressure of 1 bar and 1050 K temperature [97]. No carbon deposition or hot spot formation was reported in their work. In another work on noble metals Calridge et al. found carbon deposition trend in order of Pd >> Rh, Ru, Ir, Pt [98]. From noble metals Ru has low cost and high catalytic performance. In their study Majid and co-workers made an extensive research study on noble metal (Rh, Ru, Ir, Pt, Pd) catalysts supported on alumina stabilized magnesia [99]. The catalytic performance of different noble metal based catalysts employed in POM is presented in **Table 2.2**. It was observed from various studies that, except Pd noble metal, all other noble metals showed good catalytic performance.

Table 2.2 Catalytic performance of noble metal based catalysts in POM

Catalyst	**Temp / Catalyst loading / GHSV**	**XCH_4 (%)**	**H_2/CO**	**Remarks**	**Ref.**
Rh	700 ℃ / 150mg / 16,000 ml(h g_{cat})$^{-1}$	74.08	1.89	All catalysts showed high stability for 50 h TOS with no change in CH_4 conversion Rh and Ru showed better activity carbon deposition was not observed Sintering occurred for some metals particularly for Pd	[99]
Ru		73.12	1.92		[99]
Ir		72.11	1.86		[99]
Pt		68.37	1.93		[99]
Pd		59.01	1.94		[99]
Rh/CeO_2	700 ℃ / 250 mg / 280 ml min^{-1} (CH_4,O_2,He)	77	2	All catalysts samples tested for 12 h TOS Ir/CeO_2 showed better and stable activity than others because of small particle size (3nm) Carbon deposition and agglomeration cause lowest activity of Pd/CeO_2	[100]
Ru/CeO_2		78	2.1		[100]
Ir/CeO_2		85	2		[100]
Pt/CeO_2		83	2		[100]
Pd/CeO_2		61	2		[100]
Ir-Ni/CeO_2	700 ℃ / 100mg / 280 sccm (CH_4,O_2,He)	87	-	Ir nanoparticles remains on surface depicted by EDX Ni active sites are stable for more than 25 h TOS test performed, because Ir removes carbon deposited Ir-Ni promising catalyst to avoid carbon deposition	[101]
Pt/ZrO_2	400 ℃/ 1.45 g / 2 NL min^{-1}, 80,000 h^{-1}	79	-	Reactions in SO_2 environment Pt/ZrO_2 conversion decreased to 39 % after 60 h Highly oxidized state of Pt/ZrO_2 was stabilised by Ir and	[102]
Ir-Pt/ZrO_2		85	-		[102]

				deactivation was supressed upto 60 h.	
0.5%Rh/ZrO_2	750 °C / - / 100 000 h^{-1},2750 ml min^{-1}	80	-	0.5%Rh/CeO_2-ZrO_2 stabilized its activity value earlier than 0.5%Rh/ZrO_2. Addition of ceria increased activity of Rh/ZrO_2. Syngas selectivity is greater for richer CH_4 value but absolute value of syngas is higher for richer O_2. Results support combustion reforming mechanism.	[103]
0.5%Rh/CeO_2-ZrO_2		95	-		[103]
3.8% Rh/m-ZrO_2 (m: monoclinic)	750 °C / 10 mg / 9×10^5 NL $kg_{cat}^{-1}h^{-1}$	37	-	Rh/t-ZrO_2 has higher activity than Rh/t-ZrO_2 for 6 h TOS. Higher activity of Rh/t-ZrO_2 is due to high dispersion of Rh on tetragonal ZrO_2.	[104]
3.8%Rh/t-ZrO_2 (t:tetragonal)		95	-		[104]
3.7%Ru/Al_2O_3	600 °C / 15 mg / 30 ml min^{-1}	82.8	1.9	Higher Ru-O bond strength than Rh-O makes POM reaction of Ru/Al_2O_3 at higher temperature. Ru/Al_2O_3 reduction is difficult than Rh/Al_2O_3. Results supports combustion reforming mechanism.	[105]
3%Rh/Al_2O_3		84.1	1.9		[105]

2.4.2.2 Non-Noble Metal Based Catalysts

The most commonly used non-noble metal based catalysts employed in POM consists of Ni, Co, Cu and Fe based catalysts. Among them, Ni based catalysts have excellent catalytic performance comparable to noble metal based catalysts and have been investigated extensively [106]. Other non-noble metal catalysts also have been proved as effective catalysts in POM [107-109]. An overview of these non-noble metal catalysts is given in the next section.

Melting point of Co metal is higher than Ni and its activity for methanation reaction from syngas is lower [110]. Owing to these properties Co catalysts can emerge as promising catalysts [111]. However, lower stabilities and activities are major drawbacks of Co catalysts as, Co is easily oxidized in POM and its reducibility is low [112]. Choudhary et al. firstly investigated cobalt based catalysts in POM. He made an extensive study by using rare earth oxides (Nd_2O_2, CeO_2, Yb_2O_3, Sm_2O_3) as support material [113, 114]. He claimed a well-controlled CO and H_2 formation. Afterwards, researchers found that these claims were most likely inadequate according to the

temperature measurements and another mechanism called as combustion-reforming was suggested [115].

Figen et al. investigated Co based catalysts for POM in a tubular reactor at 600-850 ℃ with a total flow rate of 450 ml min^{-1} [107]. He studied effect of Ni and Ru addition on catalytic activity of Co catalyst and investigated hydrogen production efficiency. Co, Co-Ni, Co-Ru and Co-Ni-Ru were prepared by modified sol-gel impregnation method. Between different temperature limits it was found that at 600-650 ℃ combustion reaction was the dominant one and above 700 ℃ POM reaction was the dominant one. He came to this conclusion that Co-Ni-Ru was the best catalyst from all of the above with hydrogen production efficiency of 95.89% and only 2.13% CO_2 at 850 ℃. In another study of Co based catalysts A. Moral et al. investigated POM over Co/Mg and Co/Mg-Al oxide catalysts in a fixed bed tubular quartz reactor with CH_4/O_2 ratio of 2 at 800 ℃ [116]. Catalysts with different cobalt loadings and Mg/Al molar ratios were employed. Very poor stability was observed for 10% cobalt loading though with 20% Co loading stability was enhanced significantly. Best catalytic performance with 91.3% CH_4 conversion was yielded from 20% Co loaded Co/Mg-Al catalyst with 63 wt. % MgO and Mg/Al molar ratio of 2.2. The poor performance of Co/MgO was due to sintering and oxidation of Co/MgO, revealed through characterization of the sample. It was concluded that Co loading, support material, calcination and activation temperature plays crucial role for good catalytic performance. Wang et al. in his study of Co catalyst over alkaline earth metal oxide sports reported that MgO proved to be only suitable support [117]. In his study it was also reported that Co loading, support material and calcination temperature plays crucial role in catalytic performance. The 24 wt% Co/MgO catalyst calcined at 800 ℃ showed high activity and good stability; while those calcined below or above 800 ℃ showed a lower stability. Some of the Co based catalysts employed in POM are given in **Table 2.3.** The results from literature revealed that Co based catalysts are not as active as compared to Ni based catalysts. It was also found that preparation method and reaction condition have strong influence upon catalytic activity.

Table 2.3 Catalytic performance of Co based catalysts in POM

Catalyst	Temp / Catalyst loading / GHSV	XCH_4 (%)	H_2/CO	Remarks	Ref.
Co/Al_2O_3	650 °C / 50 mg / 15 Nl CH_4/(g h)	74	-	Modifying cobalt with another metal has no effect on activity. A metal which remains unreduced or makes oxide with Co at POM conditions can poison Co catalyst. Fe presence causes carbon deposit.	[118]
$Co-Ni/Al_2O_3$		73	-		[118]
$Co-Cr/Al_2O_3$		74	-		[118]
$Co-Mn/Al_2O_3$		74	-		[118]
$Co-Fe/Al_2O_3$		57	-		[118]
Co/Al_2O_3	650 °C / 200 mg / 15 Nl CH_4 g_{cat}^{-1} h^{-1}	75	-	Cobalt catalyst was compared with Ni based catalysts. Ni based catalyst showed high conversion at lower temperature due to high reducibility but carbon formation in those was more than Co based catalyst.	[119]
Co	800 °C / / 1×10^4 h^{-1}	94	2.03	Combustion reaction was dominant till 650 °C, above 700 °C POM was dominant. There was no considerable increase in CH4 conversion after 800 °C so this is considered optimum temperature.	[107]
Co-Ni		85	2.05		[107]
Co-Ru		94.3	2.1		[107]
Co-Ni-Ru		93.9	2		[107]
Ni		81.4	2.04		[107]
MgAl-Co	750 °C / 100 mg / -	50	-	The hydrotalcite type catalysts showed approximately similar conversion while promoters increased the carbon resistance and CO selectivity.	[120]
MgAl-LaCo		47	-		[120]
MgAl-CeCo		45	-		[120]
$CoNi_2@SiO_2$	700 °C / 0.05 g / 72,000 cm^3 h^{-1} g^{-1}	82.7	1.86	Suitable alloy of Co and Ni nanoparticles on encapsulated silica can reduce carbon deposition. Microcapsule like catalyst structure increases activity and avoids sintering at high temperature.	[108]
10%$Co/Ce_{0.5}Zr_{0.5}O_2$	800 °C / 150 mg / 9,000 h^{-1}	56	-	Results showed that higher Co loading results in higher CH_4 conversion. Co oxide is easy to reduce over $Ce_{0.5}Zr_{0.5}O_2$ into metallic Co which leads to high activity.	[121]
20%$Co/Ce_{0.5}Zr_{0.5}O_2$		65	-		[121]
30%$Co/Ce_{0.5}Zr_{0.5}O_2$		71	-		[121]
6%Co/Al	750 °C / 150 mg / 21600 mL g^{-1} h^{-1}	26	-	Addition of alkaline earth metals in Co catalyst increased carbon deposition resistance and Co_3O_4 dispersion. Sr was proved best among Mg, Ca, and Ba in terms of overall catalytic performance.	[122]
6%Co-6%Mg/Al		29	-		[122]
6%Co-6%Ca/Al		28	-		[122]
6%Co-6%Sr/Al		33	-		[122]

6%Co-6%Ba/Al		35	-		[122]
$6\%Co/Al_2O_3$	750 °C / / 12,000 ml g^{-1} h^{-1}	32	-	Ca added catalyst has high dispersion and easily reduced. Modification with Ca decreased particle size of Co metal and avoids re-oxidation of Co.	[123]
$6\%Co-6\%Ca/Al_2O_3$		88	-		[123]
$NdCaCoO_4$	915-920 °C / 0.1 g / 20–22 L g^{-1} h^{-1}	82		High activity of catalyst was due to formation of highly dispersed Co particles and promoter Nd_2O_3. Carbon formed has porous structure which have no significance influence on activity.	[124]

Nickel based catalysts are most commonly employed catalysts in POM due to their high catalytic activity comparable with noble metals and low cost [125-127]. However, conventional Ni based catalysts are deactivated by sintering and coking problem that is the major issue associated with these catalytic systems [128-130]. To tackle these issues associated with Ni based catalysts different strategies were applied, such as increasing dispersion of metallic particles, size reduction of the nanoparticles and enhancing oxygen vacancies through adding some supports and promoters[131-136]. In next section, these different types of developed Ni catalysts are discussed.

The most commonly employed and most easily synthesized catalysts in POM are supported Ni based catalysts. Different types of support material used for these catalytic systems are Al_2O_3 [137], CeO_2 [138], ZrO_2 [139], SiO_2 [140], La_2O_3 [141], Y_2O_3 [142], CaO [143], SiC [144], MgO [145] etc. Al_2O_3 is the most commonly employed support due to its large surface area, less price and high stability [146, 147].

Ding et al. investigated the effect of calcination temperature on Ni/Al_2O_3 catalyst by analysing physiochemical properties and testing catalytic performance in POM at 550 °C [148]. Catalyst was prepared by sol-gel method and multiple samples were prepared at various calcination temperature ranging 400-800 °C. Raising the calcination temperature resulted in decrease of surface area and pore volume. It was observed that at high calcination temperature metal support interaction significantly improves but due to strong metal support interaction reduction of catalyst becomes more difficult. It was concluded that catalyst prepared at 600 °C had larger surface area, lower reduction temperature and excellent catalytic performance with resistance to carbon deposition and sintering. Effect of metal support interaction on catalytic

performance of Ni/CeO_2 was investigated in a study by Kumar Singha et al. for POM [58]. Catalyst was prepared by novel two step method. It was found that Ni deposition method on support material CeO_2 played vital role for metal support interaction and formation of Ni species of various sizes. Morphology of Ni species was strongly influenced by cetyltrimethylammonium bromide (CTAB) and particle size was controlled by polyvinylpyrrolidone (PVP). Methane was activated at 400 °C and the main driving force behind this was the synergistic effect between CeO_2 nanoparticles and smaller Ni species. The catalyst with 5% Ni loading showed best catalytic performance with methane conversion above 98% at 800 ℃ for 90 h time on stream with 1.98 average H_2/CO ratio. Metal support interaction and size of Ni particles controls whether graphitic carbon or carbon nanotubes are deposited on catalyst surface. It was concluded that better metal support interaction in smaller Ni particles is resistant to carbon deposition. Performance of supported Ni based catalysts employed in POM is presented in **Table 2.4**.

Table 2.4 Catalytic performance of conventional Ni based catalysts in POM

Catalyst	**Temp / Catalyst loading / GHSV**	**XCH_4 (%)**	**H_2/CO**	**Remarks**	**Ref.**
$Ni/Ce_{0.75}Zr_{0.25}O_2$	700 ℃ / 300 mg / 1,49,000 h^{-1}	89	-	No change in CH_4 conversion for 7 h test shows good stability due to strong metal support interaction. High H_2 and CO selectivity showed, there is no carbon deposition.	[149]
$Ni/Ce_{0.5}Zr_{0.5}O_2$		86	-		[149]
$Ni/Ce_{0.25}Zr_{0.75}O_2$		84	-		[149]
1.7%Ni/ZrO_2	800 ℃ / 50 mg / 1.8 × 10^5 NL $kgcat^{-1}$ h^{-1}	78	-	Catalyst sample activated with 10%H_2/N_2 (red) has oscillating activity while sample reduced with 5%O_2/N_2 and 10%H_2/N_2 environment (ox-red) has non-oscillating activity.	[150]
4.8%Ni/ZrO_2		87	-		
2.5%Ni/CeO_2	800 ℃ / 60 mg / 80,000 ml g^{-1} h^{-1}	97	1.98	Catalyst with 2.5% and 5% Ni loading have equal activity but 5% Ni has higher rate of CO formation. High stability for 90 h of 5% Ni loaded catalyst is due to better metal support interaction between small size Ni and CeO_2 particles which avoids coking.	[151]
5%Ni/CeO_2		98	1.98		[151]
10%Ni/CeO_2		93	1.93		[151]
2.5%Ni/Al_2O_3		78.33	2.22		[152]
5%Ni/Al_2O_3		85.46	2.17		[152]

7.5%Ni/Al_2O_3	700 °C / 100 mg / 90,000 mL $(g_{cat}. h)^{-1}$	82.89	2.16	CH_4 conversion increased by increasing Ni loading up to 5 %, afterwards it decreased. Decrease in CH4 conversion above 5% Ni content is due to large Ni particle size and low dispersion. Catalyst was stable up to 48 h with no decrease in conversion.	[152]
4%Ni/CeO_2-Al_2O_3	750 °C / 150 mg / 12000 mL h^{-1} g^{-1}	73	-	Larger surface area of 8%Ni/CeO_2-Al_2O_3 (108 m^2 g^{-1}) and good reducibility of catalyst yielded high conversion and high stability up to 45 h TOS.	[153]
8%Ni/CeO_2-Al_2O_3		86	-		[153]
12%Ni/CeO_2-Al_2O_3		80	-		[153]
Ni/ZrO_2	750 °C / 100 mg / 107.5 mL min^{-1}	50	0.95	CH_4 conversion increased with increasing Mg content. Carbon formation rate also increased by increasing Mg content. Catalyst with 20 mol% Mg content has high catalytic activity with low carbon deposition.	[154]
Ni/4Mg-ZrO_2		56	1.10		[154]
Ni/20Mg-ZrO_2		81	1.70		[154]
Ni/40Mg-ZrO_2		79	1.55		[154]
Ni/MgO		91	1.62		[154]
PrO_2/ZrO_2	750 °C / 100 mg / 107 mL h^{-1}	20	-	The results revealed that catalyst with high Ni content have high activity due to high metallic dispersion. The catalyst NiO/ZrO_2 without PrO_2 promoter has lower activity.	[155]
15%NiO/ZrO_2		75	2.4		[155]
5%NiO/PrO_2/ZrO_2		48	2.8		[155]
10%NiO/PrO_2/ZrO_2		62	2.6		[155]
15%NiO/PrO_2/ZrO_2		80	2.2		[155]
Ni/SiO_2	600 °C / 100 mg / 60,000 mL g^{-1} h^{-1}	85	2.2	NiCe/SiO_2 showed good activity only if feed is supplied starting from 550 °C, starting below this temperature causes Ni re-oxidation. Catalyst containing Ce has better carbon removal because of high oxygen mobility.	[156]
NiCe/SiO_2		88	2.4		[156]
Ni/SiC	800 °C / 120 mg / 23,000 h^{-1}	90	-	Performance of catalyst was strongly influenced by nitridizing treatment, 1 h treatment resulted in best performance. Catalyst activity stable up to 200 h.	[157]
Ni/SiC-N(1) (N(1): treatment with flowing H_2/N_2 for 1 h)		93	-		[157]
1.39wt%Ni/La_2O_3	700 °C / 200 mg / -	90	2.04	Catalytic activity highly depends upon Ni reducibility. Ni in metallic form has better reducibility than NiO. At low temperature and low contact time reaction proceeds via direct mechanism while at higher values indirect mechanism is involved.	[158]
Ni/γ-Al_2O_3		79	-		[159]

Ni/Y_2O_3	700 °C / 0.1 g / 1,50,000 h^{-1}	82	-	Results of Y_2O_3 and Al_2O_3 supports revealed that Y_2O_3 is basic support while γ-Al_2O_3 was acidic one. Y_2O_3 supported Ni catalyst has higher catalytic activity and stability than Al_2O_3 supported one due to good reducibility of Y_2O_3. Ni/Y_2O_3 stable up to 550 h and only 2.2 wt% carbon was deposited.	[159]
$10\%NiO/Ce_{0.5}Ti_{0.5}O_2$	750 °C / 100 mg / 55,200 mL h^{-1} g_{cat}^{-1}	93%		The catalyst sample was highly active and stable for 100 h TOS Cerium addition increased oxygen mobility in Ti^{+4} solution consequently increasing coke removal property and thus stability.	[160]

Perovskites, applied as catalyst precursors, generally represented by ABO_3 are such types of structure where homogeneously dispersed catalyst could be developed [161]. Here, A and B are said to be cations and perovskites structure is substituted either on both A and B or upon one of them. Perovskite type precursors improves metal particle dispersion and produce nano-size crystals of metallic particles after reduction which consequently enhances the coking resistance and avoids sintering of catalyst [131, 162]. Moreover, their thermal stability and catalytic activity can be tuned by partial substitution of A or B cations [163]. Mobility of lattice oxygen is enhanced by substitution on A-site while catalytic properties are improved by B-site substitution [164].

Duan et al. investigated Ni based catalyst derived from $LaNiO_3$ perovskites in POM at 300-800 °C [131]. The mesoporous $LaNiO_3$ perovskite was prepared by modified nanocasting method developing high order mesoporous structure. Catalytic performance of catalyst prepared by modified nanocasting method was compared with its conventional counterpart prepared by citrate method. The novel catalyst resulted in higher methane conversion of 96% at 800 °C than 82% conversion by conventional catalyst at the same conditions. The excellent catalytic performance was attributed to highly order mesoporous structure with large surface area and homogeneously dispersed small size Ni particles. In another study of perovskite catalysts Santana Santos et al. investigated the effect of partial substitution of Ni with Co and pre-

treatment of catalyst ($LaNi_{1-x}Co_xO_3$) with H_2 environment [163]. It was found that pre-reduction, in absence of H_2 environment results in spinel phase while reducing the catalyst in presence of H_2 no spinel phase was detected. Physiochemical analysis indicated that pre-reduction with H2 smaller nano-size crystal of Ni was formed on La_2O_3. It was also found from catalytic activity results that pre-reduction favours stoichiometric H_2/CO ratio of 2 while without H_2 pre-treatment it was 1.6 indicating the presence of parallel reactions occurring during POM. Composite with partial substitution of Co ($Ni_{0.8}Co_{0.2}/La_2O_3$) showed higher H_2/CO ratio of 2.2. After 24 h time on stream test graphitic carbon was formed on surface of all samples while it was lower in case of $Ni_{0.8}Co_{0.2}/La_2O_3$ composite. Some more perovskite catalysts are presented in **Table 2.5**. It was observed from literature that perovskites based Ni catalysts are highly active and stable. Ni-Co based perovskites catalysts are widely investigated in POM and found to be highly active and stable one. Perovskites structure has high mobility of oxygen inside their structure which reacts with carbon species before deposition which consequently avoids deactivation of catalyst.

Table 2.5 Catalytic performance of Ni based perovskites catalysts in POM

Catalyst	**Temp / Catalyst loading / GHSV**	**XCH_4 (%)**	**H_2/CO**	**Remarks**	**Ref.**
$LaNiO_3$ (conventional)	700 °C / 0.5 g / GHSV = 21 .6 L h^{-1} g^{-1}	73	2.1	Higher conversion under mesoporous $LaNiO_3$ was due to fine dispersion of Ni although small amount of carbon formation occurred evidenced by TGA and XRD. H_2/CO ratio slightly larger than stoichiometric value may be due to water gas shift reaction.	[165]
$LaNiO_3$ (mesoporous)		87	2.1		[165]
$LaCoO_3$	800 °C / 50 mg / -	60	2.1	The partial addition of Co upon Ni based perovskite, reduced coke formation and it was stable for 24 h TOS. STEM-EDX results revealed formation of Ni-Co nanocrystals which is considered main factor for best performance of $LaNi_{0.8}Co_{0.2}O_3$.	[166]
$LaNiO_3$		73	2.1		[166]
$LaNi_{0.5}Co_{0.5}O_3$		70	2.1		[166]
$LaNi_{0.8}Co_{0.2}O_3$		74	2.2		[166]
20Ni/80Co-$Gd_{0.1}Ti_{0.1}Zr_{0.1}Ce_{0.7}O_2$	925 °C / - / -	65	2	The sample with 80Ni/20Co ratio has best activity and stability for POM. Because finely dispersed Ni particles are difficult to deactivate and cause high conversion, moreover, Co presence removes carbon formed through oxidation and purifies catalyst.	[167]
50Ni/50Co-$Gd_{0.1}Ti_{0.1}Zr_{0.1}Ce_{0.7}O_2$		80	2.1		[167]
80Ni/20Co-$Gd_{0.1}Ti_{0.1}Zr_{0.1}Ce_{0.7}O_2$		96	2		[167]

$LaNiO_3$	500-580 °C / 50 mg / 60,000 ml g^{-1} h^{-1}	20	-	CeO_2 addition increased CH_4 conversion and prevented catalyst from deactivation due to cerium redox properties. Sample with CeO_2 was stable for 18 h low temperature stability test ($LaNiO_3$ at 580 °C and $LaNiO_3$-CeO_2 at 500 °C) while without CeO_2 it deactivated in just 1 h.	[168]
$LaNiO_3$-CeO_2		60	-		[168]
$Ni_{0.2}/SrTiO_3$	800 °C / 150 mg / -	94.4	-	The reaction follows combustion reforming mechanism. High resistance to coking is might due to high activity of reforming reaction boosted by active oxygen on perovskite structure. Finely dispersed Ni on perovskite caused high and stable activity.	[169]
$Ni_{0.2}/BaTiO_3$		93.9	-		[169]
$Ni_{0.2}/CaTiO_3$		93.8	-		[169]
$La_2Ni_{0.5}Zr_{0.5}O_6$	750 °C / 10 mg / 3×10^6 L Kg^{-1} h^{-1}	27	-	La_2NiZrO_6 showed high stability for POM and avoided carbon deposition. Crystallinity of catalyst can be increased by calcining at high temperature and activity could be improved.	[170]
$La_2Ni_{0.7}Zr_{0.3}O_6$		32	-		[170]
La_2NiO_6		43	-		[170]
$NiMn_2O_4$ (calcined at 750 °C)	700 °C / 0.2 g / 52 900 l kg^{-1} h^{-1}	51	-	Catalyst calcined at 900 °C has good dispersion of Ni and stable structure, therefore high CH_4 conversion. Sample calcined at 750 °C has high selectivity for CO_2 due to formation of $NiMnO_3$ which has high affinity for complete oxidation.	[171]
$NiMn_2O_4$ (calcined at 900 °C)		80	-		[171]
NiO/MgO	700 °C / 0.5 g / -	82.2	6	Air was used instead of expensive O_2 and catalyst performed effectively. Addition of Cr_2O_3 increased reducibility of NiO which has less reducibility in NiO-MgO due to strong Ni-O bond in NiO-MgO.	[172]
NiO-Cr_2O_3/MgO		92.7	2.4		[172]
$LaGa_{0.65}Mg_{0.15}Ni_{0.20}O_{3-\delta}$	900 °C / / 55 mL min^{-1} g^{-1}	81.2	-	Catalyst showed high syngas selectivity and stability of 210 h TOS which is due to high mobility of oxygen inside perovskite structure, this active oxygen react with carbon before its deposition on catalyst surface.	[173]
Ni(Co)–$Gd_{0.1}Ti_{0.1}Zr_{0.1}Ce_{0.7}O_2$	960 °C / 0.2 g / 10 L^{-1} g^{-1} h^{-1}	90	2	Ni-Co based catalyst with cerium is found to be highly active and stable for POM. Cerium addition increased oxygen mobility which reacts with carbon and prevents carbon deposition.	[174]

It is found from literature that crystallite size and dispersion of Ni on catalyst surface plays vital role for catalytic performance. Then one can speculate that if some certain type of precursor could be developed where Ni particles are homogeneously distributed and it remains stable even at high reaction temperature of POM then this could be used as an effective catalyst system in POM applications. Hydrotalcites are

such type of precursors where nanocrystals of Ni particles are finely distributed over catalyst surface.

Hydrotalcite-like compounds have exhibited various practical application as catalyst precursors or catalysts [175, 176]. Particularly, hydrotalcites compounds make way to catalysts with small crystal sizes, high surface area, good activity, and allowing fine dispersion of Ni inside their structure. Ni based hydrotalcites compounds have been tested as suitable precursors of Ni catalysts that exhibits high thermal stability at higher reaction temperatures and resistant to carbon deposition [177, 178]. Consequently, these interesting properties of hydrotalcites improves resistance to sintering and carbon formation in Ni based catalysts [179]. However, industrial processes require better degree of performance than provided by these hydrotalcites. Various material promoters can be added with hydrotalcites to enhance their catalytic performance. In literature, CeO_2 has been studied as one of the most effective promoter for hydrotalcite based catalysts which improves their performance by increasing catalytic activity and lowering coke deposition due to some characteristics properties of cerium for oxidation reactions [180-182]. Cerium can store and release different levels of bulk and surface oxygen vacancies due to its ability to exist in different oxidation states which makes it very attractive for use in oxidation reactions [183, 184]. During POM reaction, presence of activated oxygen molecules absorbed on the surface of catalyst removes coke by forming CO [154]. Alessandra et al. [185] investigated the performance of cerium promoted hydrotalcite based catalyst in POM, he found that presence of cerium on catalyst surface enhance the resistance of catalyst to coke formation because cerium favours the absorption of oxygen on catalyst surface. In carbon formation related reactions of hydrocarbons, catalytic performance is enhanced due to these properties achieved by promotion effect of cerium. Catalytic performance of recently employed Ni based hydrotalcite catalysts in POM is presented in **Table 2.6**. It was observed from literature that Ni based hydrotalcites have high activity and stability for POM reaction. In these type of structures, high activity of Ni based catalysts is possible applying lower Ni loadings due to fine and homogeneous dispersion of Ni inside their structure [186]. Mg/Al molar ratio, Ni content, preparation method and calcination temperature are some of the most influential parameters affecting performance of catalysts.

Table 2.6 Catalytic performance of Ni based hydrotalcites catalysts in POM

Catalyst	**Temp / Catalyst loading / GHSV**	**XCH_4 (%)**	**H_2/CO**	**Remarks**	**Ref.**
NiMgAlO	780 ℃ / 0.3 g / -	96	-	Both catalysts showed high CH_4 conversion but fluorine modified catalyst exhibited higher syngas selectivity. NiMgAlO deactivated after 60 h while NiMgAlO-F maintained its stability for 120 h due to enhanced reducibility and basicity by F^- promotion effect.	[187]
NiMgAlO-F		95	-		[187]
Ni/Al_2O_3	700 ℃ / 50 mg / 2,40,000 $cm^3\ g^{-1}\ h^{-1}$	83	1.8	Ni/Al_2O_3 catalyst started to deactivate after 13 h while $Ni_{0.5}Mg_{2.5}Al$ and $Ni_{0.5}Ca_{2.5}Al$ exhibited stable performance for 20 h TOS with high CH_4 conversion and stoichiometric H_2/CO ratio of 2.	[188]
$Ni_{0.5}Mg_{2.5}Al$		85	2		[188]
$Ni_{0.5}Ca_{2.5}Al$		85	2		[188]
NiMgAl/La (OML-1)	780 ℃ / 100 mg / -	98	-	NiMgAl hydrotalcite promoted with less than 6.5 mol% of La exhibited high activity. OML-2 with 6.5 mol % La exhibited 84 h TOS stability due to fine dispersion of Ni and increased basicity due to La^{+3}, While OML-1 deactivated after 60 h. Note:OML-1 has lower La content than OML-2.	[189]
NiMgAl/6.5La (OML-2)		99	-		[189]
NiMgAl-1 (Mg/Ni=1)	750 ℃ / - / $6.4 \times 10^5\ cm^3\ h^{-1}g^{-1}$	95	2.1	Hydrotalcite samples with higher Ni content showed higher activity and stability than lower Ni content samples. Synergic effect by combination of Ni and Rh enhanced the catalytic activity and stability up to 30 h TOS due to increase in Ni reducibility.	[190]
NiMgAl-15 (Mg/Ni=15)		63	1.8		[190]
NiMgAl-25 (Mg/Ni=25)		54	1.3		[190]
0.6%Rh/NiMgAl-25		88	2		[190]
Ni/Al_2O_3	700 ℃/ 40 mg / 1,57,500 l $kg^{-1}h^{-1}$	75	2.15	H_2/CO ratio was decreased continuously by increasing Mg content due to RWGS reaction. $Ni/Mg_{2.5}AlO$ showed least carbon deposition and better activity.	[191]
$Ni/MgO/Al_2O_3$		77	2.1		[191]
$Ni/Mg_{2.5}AlO$		82	2		[191]
NiMgAl	900 ℃ / 0.2 g / -	89	-	Ni based hydrotalcite exhibited high conversion	[192]
NiMgAl/Co		28	-		[192]

				while Co addition suppressed conversion and caused carbon deposition due to presence of oxidative cobalt oxide.	
$(Ni_{0.1}Mg_{0.9})Al_{0.5}$	750 °C / 200 mg / -	24	3.4	Addition of Cu increased the reducibility of NiO by transferring the reduction peaks at lower temperature and consequently enhanced the CH_4 conversion. Fe addition boosted CO_2 selectivity due to full oxidation.	[193]
$(Ni_{0.05}Fe_{0.05}Mg_{0.9})Al_{0.5}$		16	9.4		[193]
$(Ni_{0.05}Cu_{0.05}Mg_{0.9})Al_{0.5}$		88	1.3		[193]
Ni/Mg/Al (1:11:4)	750 °C / 60 mg / 1,20,000 h^{-1}	87.2	-	Increase in Mg/Al molar ratio increased reducibility and same is the case for increase in Ni loading. Ni loading of 8-15.5 % was optimum loading for these catalysts.	[186]
Ni/Mg/Al (1:11:3)		87.5	-		[186]
Ni/Mg/Al (1:11:2.4)		88.1	-		[186]
Ni/Mg/Al (0.4:11:2.4)		12.3	-		[186]
Ni/Mg/Al (1.9:11:2.4)		88.4	-		[186]
NiMgAl	750 °C / 100 mg / -	53	-	All the catalyst samples showed about similar results. High oxygen mobility by promotion with La or Ce increased the selectivity of CO and decreased carbon deposition.	[194]
NiMgAl/La		51	-		[194]
NiMgAl/Ce		50	-		[194]

Ni and Co based catalysts are most commonly employed catalysts in POM. In addition to Ni and Co, Copper (Cu) and iron (Fe) based catalysts have been reported in literature. Mostly, Cu and Fe catalysts are employed in form of zeolites in POM. Cu-exchanged zeolites attracted the researchers in 1986 due to high NO decomposition activity [195]. Their high activity for POM attracted the attention of researchers in 2005 [196]. In selective catalytic reduction, these are used as catalysts for diesel emissions control [197, 198].

Karoshi and co-workers employed Cu catalyst using eggshell as support material in POM at 650 °C and atmospheric pressure [199]. It was observed that Cu loading affects the product selectivity yielding various products at different loadings. 2% Cu loading activated pathway towards syngas production in POM while 5% and 10% Cu loading led to higher order hydrocarbons due to oxidative coupling of methane. It was found that oxygenated products were produced mostly from CuO and CaO active sites while higher order hydrocarbons were mostly generated from CaO active sites. Methane conversion and product selectivity was observed to vary with flow rate and

CH_4/O_2 ratio while increase in temperature increased the H_2O and CO_2 production without any effect on methane conversion rate. It was concluded that catalyst can be reactivated for four cycles and conversion was observed to be increased for successive cycles possibly due to exposure of multiple active sites for different cycles. In another study Karoshi and co-workers investigated iron (Fe) catalyst using recycled eggshell as precursor [200]. A decrease in methane conversion was observed from data when Fe loading exceeds 5 wt%. An increase in temperature resulted in full oxidation thus CO_2 production was increased. Besides, decrease in O_2 concentration increased methane conversion and significant drop in CO_2 production. It was concluded that the catalyst can be reactivated and can be used efficiently for four reaction cycles. Non-conventional non-noble metal based catalysts employed in POM are listed in **Table 2.7**. It was found from literature that, in POM, Cu based catalysts could rarely show high CH_4 conversion and syngas selectivity with some suitable promoter while Fe based catalysts have very low CH_4 conversion and syngas selectivity.

Table 2.7 Catalytic performance of non-conventional catalysts in POM

Catalyst	**Temp / Catalyst loading / GHSV**	**XCH_4 (%)**	**H_2/CO**	**Remarks**	**Ref.**
$2CuO\text{-}CeO_2$	750 °C / 100 mg / 8500 mL g^{-1} h^{-1}	90	2	Activity of his catalyst prepared by intermetallic route is much higher than its counterpart prepared by Sol-gel method. High activity is due to unusual interaction between Cu and Ce which prevents deactivation.	[201]
$Fe/La\text{-}Al_2O_3$	900 / 100 mg / -	30	1.9	Fe catalysts exhibited low activity, these are active for full oxidation. They might be useful to avoid methanation reaction in low temperature zone of FlBR.	[202]
Fe/Oxidized diamond	600 °C / 60 mg / 30,000 $h^{-1}mLg^{-1}cat^{-1}$	4	-	The catalyst showed very low CH4 conversion and syngas was not produced.	[203]
$Cu/Gd\text{-}CeO_2$	500 °C / 100 mg / -	30	-	Cu with $Gd\text{-}CeO_2$ showed very poor activity while combining $Cu/Gd\text{-}CeO_2$ and $Ni/Gd\text{-}CeO_2$ increased CH_4 conversion in dual bed reactor. $Cu/Gd\text{-}CeO_2$ boosted WGS reaction which increased H_2 yield.	[204]
$Ni/Gd\text{-}CeO_2$		79.77	-		[204]
$Cu/Gd\text{-}CeO_2$ + $Ni/Gd\text{-}CeO_2$		81.18	-		[204]
Calcined eggshell	750 °C / 10 g / -	28	-	Calcined eggshell produced higher hydrocarbons and syngas was not produced.	[205]

$Ca_3Al_2(SiO_4)_{0.8}(OH)_{8.8}$:Mayenite	800 °C / 100 mg / 1.8×10^4 h^{-1}	20	-	Substitution of Cr-, Co-, Cu-, Fe, on mayenite increased methane conversion slightly while Ni-substitution enhanced methane conversion to a high value which is might due to Ni ability to effectively catalyze combustion reforming mechanism for indirect syngas production	[206]
CaCr-Mayenite		24	-		[206]
CaCo-Mayenite		26	-		[206]
CaCu-Mayenite		25.5	-		[206]
CaFe-Mayenite		25	-		[206]
CaNi-Mayenite		93	-		[206]

Summary

Synthesis gas a mixture of H_2 and CO has vast application for production of valuable chemical products and fuels. Steam reforming, dry reforming, partial oxidation, auto-thermal reforming and tri-reforming are the major reforming techniques employed for methane conversion to syngas. Steam reforming of methane is applied on industrial scale for syngas production while some disadvantages associated with this technique are, H_2/CO ratio higher than 3 which is not suitable for Fischer-Tropsch synthesis, endothermic nature of reaction makes it energy intensive and complicated reactor design results in capital cost intensive technique. Partial oxidation of methane has some advantages over other reforming technique. In POM H_2/CO ratio of 2 makes it suitable for Fischer-Tropsch process, exothermic nature of reaction makes it energy saving and another main advantage is simple reactor design. However, major problem associated with POM are hot spot formation, pure oxygen supply and catalyst stability at higher temperature of reaction. To prevent from hot spot formation different reactor technologies have been investigated like fixed bed reactor, fluidized bed reactor, membrane reactor, fixed bed micro reactor, hollow fibre membrane reactor, monolith reactor etc. Membrane reactors use air instead of expensive pure oxygen. To enhance the catalytic stability researchers are investigating different catalysts. Two types of catalytic systems employed for POM are noble metal based catalysts and non-noble metal based catalysts. Noble metal based catalysts have high activity and stability but high cost of noble metals limit their commercial application. Non-noble metal catalysts that are generally employed in POM consists of Ni, Co, Cu and Fe based catalysts. Among them, Ni based catalysts have comparable

activity with noble metals but sintering and coking of Ni based catalysts is major issue. To enhance coking resistance of Ni catalysts for stability purpose different support and promoter materials are added with these catalysts. Some advanced materials used as catalysts or catalyst support of Ni based catalysts are hydrotalcites and perovskites catalysts which have good catalytic performance.

References

1. Speight, J.G., Natural gas: a basic handbook. 2018: Gulf Professional Publishing.

2. Wood, D.A., C. Nwaoha, and B.F. Towler, Gas-to-liquids (GTL): A review of an industry offering several routes for monetizing natural gas. Journal of Natural Gas Science and Engineering, 2012. 9: p. 196-208.

3. Khirsariya, P. and R.K. Mewada, Single Step Oxidation of Methane to Methanol–Towards Better Understanding. Procedia Engineering, 2013. 51: p. 409-415.

4. Christian Enger, B., R. Lødeng, and A. Holmen, A review of catalytic partial oxidation of methane to synthesis gas with emphasis on reaction mechanisms over transition metal catalysts. Applied Catalysis A: General, 2008. 346(1-2): p. 1-27.

5. Singha, R.K., et al., Partial oxidation of methane to synthesis gas over Ni-supported ceria catalyst. 2014.

6. Allen, D.T., et al., Methane emissions from process equipment at natural gas production sites in the United States: pneumatic controllers. Environ Sci Technol, 2015. 49(1): p. 633-40.

7. Abdulrasheed, A., et al., A review on catalyst development for dry reforming of methane to syngas: Recent advances. Renewable and Sustainable Energy Reviews, 2019. 108: p. 175-193.

8. Horn, R. and R. Schlögl, Methane Activation by Heterogeneous Catalysis. Catalysis Letters, 2014. 145(1): p. 23-39.

9. McFarland, E., Chemistry. Unconventional chemistry for unconventional natural gas. Science, 2012. 338(6105): p. 340-2.

10. Galadima, A. and O. Muraza, Revisiting the oxidative coupling of methane to ethylene in the golden period of shale gas: A review. Journal of Industrial and Engineering Chemistry, 2016. 37: p. 1-13.

11. Guo, X., et al., Direct, nonoxidative conversion of methane to ethylene, aromatics, and hydrogen. Science, 2014. 344(6184): p. 616-9.

12. Hammond, C., S. Conrad, and I. Hermans, Oxidative methane upgrading. ChemSusChem, 2012. 5(9): p. 1668-86.

13. York, A.P., T. Xiao, and M.L. Green, Brief overview of the partial oxidation of methane to synthesis gas. Topics in Catalysis, 2003. 22(3-4): p. 345-358.

14. Khoja, A.H., et al., Thermal dry reforming of methane over La_2O_3 co-supported $Ni/MgAl_2O_4$ catalyst for hydrogen-rich syngas production. Research on Chemical Intermediates, 2020.

15. Mazhar, A., et al., Performance Analysis of TiO_2-Modified $Co/MgAl_2O_4$ Catalyst for Dry Reforming of Methane in a Fixed Bed Reactor for Syngas (H_2, CO) Production. Energies, 2021. 14(11): p. 3347.

16. Lisboa, J.S., et al., Investigation of $Ni/Ce–ZrO_2$ catalysts in the autothermal reforming of methane. Fuel Processing Technology, 2011. 92(10): p. 2075-2082.

17. Zhang, M., et al., Effect of Ni(111) surface alloying by Pt on partial oxidation of methane to syngas: A DFT study. Surface Science, 2014. 630: p. 236-243.

18. Krenzke, P.T., et al., Synthesis gas production via the solar partial oxidation of methane-ceria redox cycle: Conversion, selectivity, and efficiency. International Journal of Hydrogen Energy, 2016. 41(30): p. 12799-12811.

19. Song, L., Y. Kong, and X. Li, Hydrogen production from partial oxidation of methane over dielectric barrier discharge plasma and NiO/γ-Al2O3 catalyst. International Journal of Hydrogen Energy, 2017. 42(31): p. 19869-19876.

20. Cecere, D., E. Giacomazzi, and A. Ingenito, A review on hydrogen industrial aerospace applications. International Journal of Hydrogen Energy, 2014. 39(20): p. 10731-10747.

21. Bailera, M., et al., Future applications of hydrogen production and CO_2 utilization for energy storage: Hybrid Power to Gas-Oxycombustion power plants. International Journal of Hydrogen Energy, 2017. 42(19): p. 13625-13632.

22. Abdul Mujeebu, M., Hydrogen and syngas production by superadiabatic combustion – A review. Applied Energy, 2016. 173: p. 210-224.

23. Dedov, A.G., et al., High-selectivity partial oxidation of methane into synthesis gas: the role of the red-ox transformations of rare earth — alkali earth cobaltate-based catalyst components. Fuel Processing Technology, 2016. 148: p. 128-137.

24. Roslan, N.A., et al., A review on glycerol reforming processes over Ni-based catalyst for hydrogen and syngas productions. International Journal of Hydrogen Energy, 2020. 45(36): p. 18466-18489.

25. Xie, Y., et al., A comprehensive review on laminar spherically premixed flame propagation of syngas. Fuel Processing Technology, 2018. 181: p. 97-114.

26. Figen, H.E. and S.Z. Baykara, Effect of ruthenium addition on molybdenum catalysts for syngas production via catalytic partial oxidation of methane in a

monolithic reactor. International Journal of Hydrogen Energy, 2018. 43(2): p. 1129-1138.

27. Barelli, L., et al., Hydrogen production through sorption-enhanced steam methane reforming and membrane technology: a review. Energy, 2008. 33(4): p. 554-570.

28. De Coninck, H., et al., The acceptability of CO2 capture and storage (CCS) in Europe: An assessment of the key determining factors: Part 1. Scientific, technical and economic dimensions. International Journal of Greenhouse Gas Control, 2009. 3(3): p. 333-343.

29. Aramouni, N.A.K., et al., Catalyst design for dry reforming of methane: Analysis review. Renewable and Sustainable Energy Reviews, 2018. 82: p. 2570-2585.

30. Change, I.C., Mitigation of climate change. Contribution of Working Group III to the Fifth Assessment Report of the Intergovernmental Panel on Climate Change, 2014. 1454.

31. Challiwala, M.S., et al., A combined thermo-kinetic analysis of various methane reforming technologies: Comparison with dry reforming. Journal of CO2 Utilization, 2017. 17: p. 99-111.

32. Jang, W.-J., et al., A review on dry reforming of methane in aspect of catalytic properties. Catalysis Today, 2019. 324: p. 15-26.

33. Li, X., et al., Dry reforming of methane over Ni/La_2O_3 nanorod catalysts with stabilized Ni nanoparticles. Applied Catalysis B: Environmental, 2017. 202: p. 683-694.

34. Han, J.W., et al., Uncoupling the size and support effects of Ni catalysts for dry reforming of methane. Applied Catalysis B: Environmental, 2017. 203: p. 625-632.

35. Wang, Y., et al., Low-Temperature Catalytic CO_2 Dry Reforming of Methane on Ni-Si/ZrO_2 Catalyst. ACS Catalysis, 2018. 8(7): p. 6495-6506.

36. Khoja, A.H., M. Tahir, and N.A.S. Amin, Recent developments in non-thermal catalytic DBD plasma reactor for dry reforming of methane. Energy Conversion and Management, 2019. 183: p. 529-560.

37. le Saché, E., et al., Ni stabilised on inorganic complex structures: superior catalysts for chemical CO_2 recycling via dry reforming of methane. Applied Catalysis B: Environmental, 2018. 236: p. 458-465.

38. Löfberg, A., et al., Ni/CeO_2 based catalysts as oxygen vectors for the chemical looping dry reforming of methane for syngas production. Applied Catalysis B: Environmental, 2017. 212: p. 159-174.

39. Snoeck, J.-W., G. Froment, and M. Fowles, Steam/CO2 reforming of methane. Carbon filament formation by the Boudouard reaction and gasification by CO2, by H2, and by steam: kinetic study. Industrial & engineering chemistry research, 2002. 41(17): p. 4252-4265.

40. Wang, Y., et al., Effect of Pr addition on the properties of Ni/Al2O3 catalysts with an application in the autothermal reforming of methane. International journal of hydrogen energy, 2014. 39(2): p. 778-787.

41. Araújo, P.M., K.M. da Costa, and F.B. Passos, Hydrogen production from methane autothermal reforming over $CaTiO_3$, $BaTiO_3$ and $SrTiO_3$ supported nickel catalysts. International Journal of Hydrogen Energy, 2021. 46(47): p. 24107-24116.

42. Mosayebi, Z., et al., Autothermal reforming of methane over nickel catalysts supported on nanocrystalline MgAl 2 O 4 with high surface area. International Journal of Hydrogen Energy, 2012. 37(2): p. 1236-1242.

43. Ismagilov, I.Z., et al., Hydrogen production by autothermal reforming of methane over NiPd catalysts: Effect of support composition and preparation mode. International Journal of Hydrogen Energy, 2014. 39(36): p. 20992-21006.

44. Majewski, A.J. and J. Wood, Tri-reforming of methane over Ni@SiO 2 catalyst. International Journal of Hydrogen Energy, 2014. 39(24): p. 12578-12585.

45. Song, C. and W. Pan, Tri-reforming of methane: a novel concept for catalytic production of industrially useful synthesis gas with desired H2/CO ratios. Catalysis Today, 2004. 98(4): p. 463-484.

46. Singha, R.K., et al., Energy efficient methane tri-reforming for synthesis gas production over highly coke resistant nanocrystalline Ni–ZrO_2 catalyst. Applied Energy, 2016. 178: p. 110-125.

47. Kumar, R., et al., Effect of support materials on the performance of Ni-based catalysts in tri-reforming of methane. Fuel Processing Technology, 2019. 186: p. 40-52.

48. Liander, H., The utilisation of natural gases for the ammonia process. Transactions of the Faraday Society, 1929. 25: p. 462-472.

49. Ma, Z., et al., Thermodynamically unconstrained forced concentration cycling of methane catalytic partial oxidation over CeO_2 FeCralloy catalysts. Chemical Engineering Journal, 2020. 380: p. 122470.

50. Mosayebi, A., Kinetic modeling of catalytic partial oxidation of methane over Ni-Rh/γ-Al_2O_3 catalyst for syngas formation. Journal of the Taiwan Institute of Chemical Engineers, 2020. 114: p. 36-46.

51. Chaubey, R., et al., A review on development of industrial processes and emerging techniques for production of hydrogen from renewable and sustainable sources. Renewable and Sustainable Energy Reviews, 2013. 23: p. 443-462.

52. Sengodan, S., et al., Advances in reforming and partial oxidation of hydrocarbons for hydrogen production and fuel cell applications. Renewable and Sustainable Energy Reviews, 2018. 82: p. 761-780.

53. Al-Sayari, S.A., Recent developments in the partial oxidation of methane to syngas. The Open Catalysis Journal, 2013. 6(1).

54. Chen, W.-H., et al., Thermodynamic analysis of hydrogen production from methane via autothermal reforming and partial oxidation followed by water gas shift reaction. international journal of hydrogen energy, 2010. 35(21): p. 11787-11797.

55. Nikoo, M.K. and N. Amin, Thermodynamic analysis of carbon dioxide reforming of methane in view of solid carbon formation. Fuel Processing Technology, 2011. 92(3): p. 678-691.

56. Nourbakhsh, H., et al., A thermodynamic analysis of biogas partial oxidation to synthesis gas with emphasis on soot formation. International Journal of Hydrogen Energy, 2018. 43(33): p. 15703-15719.

57. Wang, H., et al., Thermodynamic analysis of hydrogen production from glycerol autothermal reforming. International Journal of Hydrogen Energy, 2009. 34(14): p. 5683-5690.

58. Singha, R.K., et al., Effect of metal-support interaction on activity and stability of Ni-CeO2 catalyst for partial oxidation of methane. Applied Catalysis B: Environmental, 2017. 202: p. 473-488.

59. Kumar Singha, R., et al., Synthesis effects on activity and stability of Pt-CeO $_2$ catalysts for partial oxidation of methane. Molecular Catalysis, 2017. 432: p. 131-143.

60. Luo, H., et al., Performance of a ceramic membrane reactor with high oxygen flux Ta-containing perovskite for the partial oxidation of methane to syngas. Journal of Membrane Science, 2010. 350(1-2): p. 154-160.

61. Hafeez, S., et al., Catalytic Conversion and Chemical Recovery, in Plastics to Energy, S.M. Al-Salem, Editor. 2019, William Andrew Publishing. p. 147-172.

62. Ji, Y., et al., Catalytic partial oxidation of methane to synthesis gas over Ni/γ-Al_2O_3 catalyst in a fluidized-bed. Applied Catalysis A: General, 2001. 213(1): p. 25-31.

63. Gunjal, P.R. and V.V. Ranade, Catalytic Reaction Engineering, in Industrial Catalytic Processes for Fine and Specialty Chemicals, S.S. Joshi and V.V. Ranade, Editors. 2016, Elsevier: Amsterdam. p. 263-314.

64. Ostrowski, T., et al., Comparative study of the catalytic partial oxidation of methane to synthesis gas in fixed-bed and fluidized-bed membrane reactors. Catalysis Today, 1998. 40(2-3): p. 181-190.

65. Bizzi, M., et al., Modeling the partial oxidation of methane in a fixed bed with detailed chemistry. AIChE journal, 2004. 50(6): p. 1289-1299.

66. Veeramani, M., S. Narasimhan, and N. Bhatt, Identification of Reaction Systems using Spectroscopic Measurements and Micro-reactors, in 13th International Symposium on Process Systems Engineering (PSE 2018), M.R. Eden, M.G. Ierapetritou, and G.P. Towler, Editors. 2018, Elsevier. p. 931-936.

67. Moghtaderi, B., Effect of enhanced mixing on partial oxidation of methane in a novel micro-reactor. Fuel, 2007. 86(4): p. 469-476.

68. Cao, D.S., et al., Development of a cordierite monolith reactor coated with CeO_2-supported BaSrCo-based perovskite for chemical looping steam methane reforming. Fuel Processing Technology, 2021. 220: p. 106889.

69. Stutz, M.J. and D. Poulikakos, Optimum washcoat thickness of a monolith reactor for syngas production by partial oxidation of methane. Chemical Engineering Science, 2008. 63(7): p. 1761-1770.

70. Makarshin, L., et al., Syngas production by partial oxidation of methane in a microchannel reactor over a Ni–Pt/La0. 2Zr0. 4Ce0. 4Ox catalyst. Fuel Processing Technology, 2015. 131: p. 21-28.

71. Arevalo, R.L., et al., Tuning methane decomposition on stepped Ni surface: The role of subsurface atoms in catalyst design. Sci Rep, 2017. 7(1): p. 13963.

72. Bhavsar, S. and G. Veser, Chemical looping beyond combustion: production of synthesis gas via chemical looping partial oxidation of methane. Rsc Advances, 2014. 4(88): p. 47254-47267.

73. Elbadawi, A.H., et al., Catalytic partial oxidation of methane to syngas: review of perovskite catalysts and membrane reactors. Catalysis Reviews, 2020. 63(1): p. 1-67.

74. Shelepova, E., et al., Theoretical and experimental study of methane partial oxidation to syngas in catalytic membrane reactor with asymmetric oxygen-permeable membrane. Catalysis Today, 2016. 268: p. 103-110.

75. Wang, Z.G., et al., Highly Efficient NO Decomposition via Dual-Functional Catalytic Perovskite Hollow Fiber Membrane Reactor Coupled with Partial

Oxidation of Methane at Medium-Low Temperature. Environmental Science & Technology, 2019. 53(16): p. 9937-9946.

76. Zhang, K., et al., Research progress and materials selection guidelines on mixed conducting perovskite-type ceramic membranes for oxygen production. RSC advances, 2011. 1(9): p. 1661-1676.

77. Sutthiumporn, K., et al., CO_2 dry-reforming of methane over La0. 8Sr0. 2Ni0. 8M0. $2O_3$ perovskite (M= Bi, Co, Cr, Cu, Fe): Roles of lattice oxygen on C–H activation and carbon suppression. International Journal of Hydrogen Energy, 2012. 37(15): p. 11195-11207.

78. Tan, X., et al., Catalytic perovskite hollow fibre membrane reactors for methane oxidative coupling. Journal of Membrane Science, 2007. 302(1-2): p. 109-114.

79. Wang, Z., et al., Low temperature partial oxidation of methane via BaBi 0.05 Co 0.8 Nb 0.15 O 3−δ -Ni phyllosilicate catalytic hollow fiber membrane reactor. Chemical Engineering Journal, 2017. 315: p. 315-323.

80. Alvarez-Galvan, C., et al., Partial Oxidation of Methane to Syngas Over Nickel-Based Catalysts: Influence of Support Type, Addition of Rhodium, and Preparation Method. Front Chem, 2019. 7(104): p. 104.

81. Guo, S.S., et al., Confining Ni nanoparticles in honeycomb-like silica for coking and sintering resistant partial oxidation of methane. International Journal of Hydrogen Energy, 2018. 43(13): p. 6603-6613.

82. Somacescu, S., et al., Bimodal mesoporous NiO/CeO_2-δ-YSZ with enhanced carbon tolerance in catalytic partial oxidation of methane—Potential IT-SOFCs anode. Applied Catalysis B: Environmental, 2019. 241: p. 393-406.

83. Elbadawi, A.H., et al., RETRACTED: Partial oxidation of methane to syngas in catalytic membrane reactor: Role of catalyst oxygen vacancies. Chemical Engineering Journal, 2020. 392: p. 123739.

84. Wang, F., et al., Crucial support effect on the durability of Pt/$MgAl_2O_4$ for partial oxidation of methane to syngas. Applied Catalysis B-Environmental, 2018. 231: p. 292-298.

85. Zhang, S., et al., One stone two birds: Simultaneous realization of partial oxidation of methane to syngas and N_2 purification via robust ceramic oxygen-permeable membrane reactors. Chemical Engineering Journal, 2021. 419: p. 129462.

86. Moral, A., et al., Partial oxidation of methane to syngas using Co/Mg and Co/Mg-Al oxide supported catalysts. Catalysis Today, 2019. 333: p. 259-267.

87. Chai, R., et al., Ni-foam-structured NiO-MO x -Al 2 O 3 (M = Ce or Mg) nanocomposite catalyst for high throughput catalytic partial oxidation of methane to syngas. Microporous and Mesoporous Materials, 2017. 253: p. 123-128.

88. Santos, A., M. Menéndez, and J. Santaríana, Partial oxidation of methane to carbon monoxide and hydrogen in a fluidized bed reactor. Catalysis Today, 1994. 21(2-3): p. 481-488.

89. Ji, Y., et al., A Study of Carbon Deposition on Catalysts During the Catalytic Partial Oxidation of Methane to Syngas in a Fluidized bed. Reaction Kinetics and Catalysis Letters, 2001. 73(1): p. 27-32.

90. Kondratenko, V.A., C. Berger-Karin, and E.V. Kondratenko, Partial Oxidation of Methane to Syngas Over γ-Al2O3-Supported Rh Nanoparticles: Kinetic and Mechanistic Origins of Size Effect on Selectivity and Activity. ACS Catalysis, 2014. 4(9): p. 3136-3144.

91. Velasco, J.A., et al., Catalytic partial oxidation of methane over nickel and ruthenium based catalysts under low O_2 /CH_4 ratios and with addition of steam. Fuel, 2015. 153: p. 192-201.

92. Nakagawa, K., et al., Partial oxidation of methane to synthesis gas over supported iridium catalysts. Applied Catalysis A: General, 1998. 169(2): p. 281-290.

93. Wang, F., et al., Crucial support effect on the durability of $Pt/MgAl_2O_4$ for partial oxidation of methane to syngas. Applied Catalysis B: Environmental, 2018. 231: p. 292-298.

94. Li, B., et al., Synthesis gas production from partial oxidation of methane over highly dispersed Pd/SiO_2 catalyst. Fuel, 2013. 103: p. 1032-1038.

95. Vella, L., et al., Catalytic partial oxidation of CH_4 with nickel–lanthanum-based catalysts. Catalysis today, 2011. 171(1): p. 84-96.

96. Tsang, S., J. Claridge, and M. Green, Recent advances in the conversion of methane to synthesis gas. Catalysis today, 1995. 23(1): p. 3-15.

97. Ashcroft, A., et al., Selective oxidation of methane to synthesis gas using transition metal catalysts. Nature, 1990. 344(6264): p. 319-321.

98. Claridge, J.B., et al., A study of carbon deposition on catalysts during the partial oxidation of methane to synthesis gas. Catalysis Letters, 1993. 22(4): p. 299-305.

99. Khajenoori, M., M. Rezaei, and B. Nematollahi, Preparation of noble metal nanocatalysts and their applications in catalytic partial oxidation of methane. Journal of Industrial and Engineering Chemistry, 2013. 19(3): p. 981-986.

100. Ahn, K., et al., A comparative study of catalytic partial oxidation of methane over CeO_2 supported metallic catalysts. J Nanosci Nanotechnol, 2011. 11(7): p. 6414-9.

101. Ahn, K., et al., Enhanced carbon tolerance of Ir alloyed Ni-Based metal for methane partial oxidation. Heliyon, 2018. 4(6): p. e00652.

102. Ohtsuka, H., The Oxidation of Methane at Low Temperatures Over Zirconia-Supported Pd, Ir and Pt Catalysts and Deactivation by Sulfur Poisoning. Catalysis Letters, 2011. 141(3): p. 413-419.

103. Scarabello, A., et al., Partial oxidation of methane on Rh/ZrO_2 and $Rh/Ce–ZrO_2$ on monoliths: Catalyst restructuring at reaction conditions. Applied Catalysis B: Environmental, 2015. 174-175: p. 308-322.

104. Campa, M.C., et al., Rhodium supported on tetragonal or monoclinic ZrO_2 as catalyst for the partial oxidation of methane. Applied Catalysis B: Environmental, 2013. 142-143: p. 423-431.

105. Liu, Y., et al., In situ Raman study on the partial oxidation of methane to synthesis gas over Rh/Al_2O_3 and Ru/Al_2O_3 catalysts. Journal of Catalysis, 2008. 256(2): p. 192-203.

106. Requies, J., et al., Nickel/alumina catalysts modified by basic oxides for the production of synthesis gas by methane partial oxidation. Catalysis Today, 2006. 116(3): p. 304-312.

107. Figen, H.E. and S.Z. Baykara, Hydrogen production by partial oxidation of methane over Co based, Ni and Ru monolithic catalysts. International Journal of Hydrogen Energy, 2015. 40(24): p. 7439-7451.

108. Li, L., et al., Silica-encapsulated bimetallic Co–Ni nanoparticles as novel catalysts for partial oxidation of methane to syngas. Catalysis Communications, 2012. 26: p. 72-77.

109. Dinh, K.T., et al., Viewpoint on the partial oxidation of methane to methanol using Cu-and Fe-exchanged zeolites. 2018, ACS Publications.

110. Slagtern, Å., et al., Catalytic partial oxidation of methane over Ni-, Co- and Fe-based catalysts. Catalysis Today, 1998. 46(2-3): p. 107-115.

111. York, A.P.E., Brief overview of the partial oxidation of methane to synthesis gas. Topics in Catalysis, 2003. 22(3/4): p. 345-358.

112. Choudhary, V.R., et al., Partial oxidation of methane to CO and H_2 over nickel and/or cobalt containing ZrO_2, ThO_2, UO_2, TiO_2 and SiO_2 catalysts. Fuel, 1998. 77(15): p. 1803-1807.

113. Choudhary, V., A. Rajput, and V. Rane, Low temperature oxidative conversion of methane to synthesis gas over Co/rare earth oxide catalysts. Catalysis letters, 1992. 16(3): p. 269-272.

114. Choudhary, V., V.H. Rane, and A. Rajput, Selective oxidation of methane to CO and H 2 over unreduced NiO-rare earth oxide catalysts. Catalysis letters, 1993. 22(4): p. 289-297.

115. Chang, Y.-F. and H. Heinemann, Partial oxidation of methane to syngas over Co/MgO catalysts. Is it low temperature? Catalysis letters, 1993. 21(3): p. 215-224.

116. Moral, A., et al., Partial oxidation of methane to syngas using Co/Mg and Co/Mg-Al oxide supported catalysts. Catalysis Today, 2019. 333: p. 259-267.

117. Wang, H.Y. and E. Ruckenstein, Partial Oxidation of Methane to Synthesis Gas over Alkaline Earth Metal Oxide Supported Cobalt Catalysts. Journal of Catalysis, 2001. 199(2): p. 309-317.

118. Enger, B.C., R. Lødeng, and A. Holmen, Modified cobalt catalysts in the partial oxidation of methane at moderate temperatures. Journal of Catalysis, 2009. 262(2): p. 188-198.

119. Lødeng, R., et al., Catalytic partial oxidation of CH_4 to H_2 over cobalt catalysts at moderate temperatures. Applied Catalysis A: General, 2007. 333(1): p. 11-23.

120. Lucrédio, A.F., G. Jerkiewicz, and E.M. Assaf, Cobalt catalysts promoted with cerium and lanthanum applied to partial oxidation of methane reactions. Applied Catalysis B: Environmental, 2008. 84(1-2): p. 106-111.

121. Yu, C.-l., et al., Preparation of $Co/Ce0.5Zr0.5O_2$ catalysts and their catalytic performance in methane partial oxidation to produce synthesis gas. Journal of Fuel Chemistry and Technology, 2012. 40(4): p. 418-423.

122. Yu, C., et al., Additive effects of alkaline-earth metals and nickel on the performance of $Co/\gamma\text{-}Al_2O_3$ in methane catalytic partial oxidation. Journal of Natural Gas Chemistry, 2011. 20(2): p. 135-139.

123. Gao, X.X., et al., Partial oxidation of methane to synthesis gas over $Co/Ca/Al_2O_3$ catalysts. Catalysis Today, 2008. 131(1-4): p. 211-218.

124. Dedov, A.G., et al., Partial oxidation of methane to produce syngas over a neodymium–calcium cobaltate-based catalyst. Applied Catalysis A: General, 2015. 489: p. 140-146.

125. Larimi, A. and S. Alavi, Ceria-Zirconia supported Ni catalysts for partial oxidation of methane to synthesis gas. Fuel, 2012. 102: p. 366-371.

126. Larimi, A.S. and S.M. Alavi, Ceria-Zirconia supported Ni catalysts for partial oxidation of methane to synthesis gas. Fuel, 2012. 102: p. 366-371.

127. Vella, L.D., et al., Catalytic partial oxidation of CH4 with nickel–lanthanum-based catalysts. Catalysis Today, 2011. 171(1): p. 84-96.

128. Dai, C., et al., Hollow zeolite encapsulated Ni–Pt bimetals for sintering and coking resistant dry reforming of methane. Journal of Materials Chemistry A, 2015. 3(32): p. 16461-16468.

129. Watanabe, R., et al., High tolerance to coke deposition in methane steam reforming for yttria-stabilized zirconia catalyst-supported nickel by electroless plating. Chemistry Letters, 2015. 44(1): p. 82-84.

130. Du, X., et al., Coke-and sintering-resistant monolithic catalysts derived from in situ supported hydrotalcite-like films on Al wires for dry reforming of methane. Nanoscale, 2013. 5(7): p. 2659-2663.

131. Duan, Q., et al., Partial oxidation of methane over Ni based catalyst derived from order mesoporous $LaNiO_3$ perovskite prepared by modified nanocasting method. Fuel, 2017. 193: p. 112-118.

132. Du, X., et al., Morphology Dependence of Catalytic Properties of Ni/CeO_2 Nanostructures for Carbon Dioxide Reforming of Methane. The Journal of Physical Chemistry C, 2012. 116(18): p. 10009-10016.

133. Xie, T., et al., Ni nanoparticles immobilized Ce-modified mesoporous silica via a novel sublimation-deposition strategy for catalytic reforming of methane with carbon dioxide. International Journal of Hydrogen Energy, 2015. 40(31): p. 9685-9695.

134. Oemar, U., et al., CO_2 reforming of methane over highly active La-promoted Ni supported on SBA-15 catalysts: mechanism and kinetic modelling. Catalysis Science & Technology, 2016. 6(4): p. 1173-1186.

135. Du, X., et al., Design of modular catalysts derived from NiMgAl-LDH@ m-SiO_2 with dual confinement effects for dry reforming of methane. Chemical Communications, 2013. 49(60): p. 6770-6772.

136. Yang, W., et al., Properties of yolk–shell structured Ni@ SiO_2 nanocatalyst and its catalytic performance in carbon dioxide reforming of methane to syngas. Catalysis Today, 2016. 259: p. 438-445.

137. Horiguchi, J., et al., Mesoporous $NiO–Al_2O_3$ catalyst for high pressure partial oxidation of methane to syngas. Applied Catalysis A: General, 2011. 392(1-2): p. 86-92.

138. Löfberg, A., et al., Ni/CeO2 based catalysts as oxygen vectors for the chemical looping dry reforming of methane for syngas production. Applied Catalysis B: Environmental, 2017. 212: p. 159-174.

139. Song, Y.-Q., H.-M. Liu, and D.-H. He, Effects of hydrothermal conditions of ZrO_2 on catalyst properties and catalytic performances of Ni/ZrO_2 in the partial oxidation of methane. Energy & fuels, 2010. 24(5): p. 2817-2824.

140. Xia, W.-S., et al., Partial oxidation of methane into syngas (H2+ CO) over effective high-dispersed Ni/SiO2 catalysts synthesized by a sol–gel method. International journal of hydrogen energy, 2012. 37(10): p. 8343-8353.

141. Requies, J., et al., Partial oxidation of methane to syngas over Ni/MgO and Ni/La_2O_3 catalysts. Applied Catalysis A: General, 2005. 289(2): p. 214-223.

142. WANG, Y.-L., et al., Catalytic Behaviors and Stability of Y_2O_3-Modified Ni/SiO_2 for Partial Oxidation of Methane into Synthesis Gas. Acta Physico-Chimica Sinica, 2016. 32(11): p. 2776-2784.

143. Qiu, Y., J. Chen, and J. Zhang, Effect of CeO_2 and CaO promoters on ignition performance for partial oxidation of methane over Ni/MgO-Al2O3 catalyst. Journal of natural gas chemistry, 2007. 16(2): p. 148-154.

144. Leroi, P., et al., Ni/SiC: a stable and active catalyst for catalytic partial oxidation of methane. Catalysis today, 2004. 91: p. 53-58.

145. Asencios, Y.J. and E.M. Assaf, Combination of dry reforming and partial oxidation of methane on $NiO–MgO–ZrO_2$ catalyst: Effect of nickel content. Fuel Processing Technology, 2013. 106: p. 247-252.

146. Kobayashi, Y., et al., Effect of NiO content in mesoporous $NiO–Al_2O_3$ catalysts for high pressure partial oxidation of methane to syngas. Applied Catalysis A: General, 2011. 395(1-2): p. 129-137.

147. Kim, H.W., K.M. Kang, and H.-Y. Kwak, Preparation of supported Ni catalysts with a core/shell structure and their catalytic tests of partial oxidation of methane. International journal of hydrogen energy, 2009. 34(8): p. 3351-3359.

148. Ding, C., et al., One step synthesis of mesoporous $NiO–Al_2O_3$ catalyst for partial oxidation of methane to syngas: The role of calcination temperature. Fuel, 2015. 162: p. 148-154.

149. Larimi, A. and S. Alavi, Partial oxidation of methane over $Ni/CeZrO_2$ mixed oxide solid solution catalysts. Int. J. Chem. Eng. Appl, 2012. 3: p. 6-9.

150. Pietrogiacomi, D., et al., Oscillatory Behaviour of Ni Supported on ZrO_2 in the Catalytic Partial Oxidation of Methane as Determined by Activation Procedure. Materials 2021, 14, 2495. 2021, s Note: MDPI stays neutral with regard to jurisdictional claims in published ….

151. Singha, R.K., et al., Effect of metal-support interaction on activity and stability of Ni-CeO_2 catalyst for partial oxidation of methane. Applied Catalysis B: Environmental, 2017. 202: p. 473-488.

152. Peymani, M., S.M. Alavi, and M. Rezaei, Synthesis gas production by catalytic partial oxidation of methane, ethane and propane on mesoporous nanocrystalline Ni/Al2O3 catalysts. International Journal of Hydrogen Energy, 2016. 41(42): p. 19057-19069.

153. Yu, C., et al., Novel Ni/CeO_2-Al_2O_3 composite catalysts synthesized by one-step citric acid complex and their performance in catalytic partial oxidation of methane. Journal of energy chemistry, 2014. 23(2): p. 235-243.

154. Asencios, Y.J., P.A. Nascente, and E.M. Assaf, Partial oxidation of methane on NiO–MgO–ZrO_2 catalysts. Fuel, 2012. 97: p. 630-637.

155. Asencios, Y., et al., Oxidative-reforming of methane and partial oxidation of methane reactions over NiO/PrO_2/ZrO_2 catalysts: effect of nickel content. Brazilian Journal of Chemical Engineering, 2016. 33: p. 627-636.

156. Emamdoust, A., et al., Partial oxidation of methane over SiO_2 supported Ni and NiCe catalysts. Journal of Energy Chemistry, 2020. 47: p. 1-9.

157. Shang, R., et al., Partial oxidation of methane over nickel catalysts supported on nitrogen-doped SiC. Catalysis Communications, 2009. 10(11): p. 1502-1505.

158. Fleys, M., et al., Investigation of the reaction of partial oxidation of methane over Ni/La_2O_3 catalyst. Energy & fuels, 2006. 20(6): p. 2321-2329.

159. Liu, H. and D. He, Properties of Ni/Y_2O_3 and its catalytic performance in methane conversion to syngas. International journal of hydrogen energy, 2011. 36(22): p. 14447-14454.

160. Zhang, Y., et al., Partial oxidation of methane over Ni/Ce-Ti-O catalysts. Chemical Engineering Journal, 2006. 121(2-3): p. 115-123.

161. Silva, C.R.B., et al., Partial oxidation of methane over Ni–Co perovskite catalysts. Catalysis Communications, 2011. 12(7): p. 665-668.

162. Nair, M.M., S. Kaliaguine, and F. Kleitz, Nanocast $LaNiO_3$ perovskites as precursors for the preparation of coke-resistant dry reforming catalysts. Acs Catalysis, 2014. 4(11): p. 3837-3846.

163. Santos, M.d.S., et al., Perovskite as catalyst precursors in the partial oxidation of methane: The effect of cobalt, nickel and pretreatment. Catalysis Today, 2018. 299: p. 229-241.

164. Enger, B.C., R. Lødeng, and A. Holmen, A review of catalytic partial oxidation of methane to synthesis gas with emphasis on reaction mechanisms over

transition metal catalysts. Applied Catalysis A: General, 2008. 346(1-2): p. 1-27.

165. Fonseca, H.C., et al., Partial oxidation of methane over lanthana-supported catalysts derived from perovskites. Catalysis Today, 2020. 344: p. 212-226.

166. Santos, M.D., et al., Perovskite as catalyst precursors in the partial oxidation of methane: The effect of cobalt, nickel and pretreatment. Catalysis Today, 2018. 299: p. 229-241.

167. Zagaynov, I.V., et al., Influence of the Ni/Co ratio in bimetallic NiCo catalysts on methane conversion into synthesis gas. Mendeleev Communications, 2017. 27(5): p. 509-511.

168. La Parola, V., et al., Plain and CeO_2 – Supported La_xNiO_y catalysts for partial oxidation of CH_4. Catalysis Today, 2018. 307: p. 189-196.

169. Takehira, K., T. Shishido, and M. Kondo, Partial Oxidation of CH_4 over $Ni/SrTiO_3$ Catalysts Prepared by a Solid-Phase Crystallization Method. Journal of Catalysis, 2002. 207(2): p. 307-316.

170. Ma, Y.Y., et al., Highly stable nanofibrous La_2NiZrO_6 catalysts for fast methane partial oxidation. Fuel, 2020. 265: p. 116861.

171. Hadj-Sadok Ouaguenouni, M., et al., Preparation and catalytic activity of nickel–manganese oxide catalysts in the reaction of partial oxidation of methane. Comptes Rendus Chimie, 2009. 12(6-7): p. 740-747.

172. Nakayama, O., et al., Production of Synthesis Gas from Methane Using Lattice Oxygen of $NiO{-}Cr_2O_3{-}MgO$ Complex Oxide. Industrial & Engineering Chemistry Research, 2009. 49(2): p. 526-534.

173. Meng, B., et al., A novel $LaGa_{0.65}Mg_{0.15}Ni_{0.20}O_{3-\delta}$ perovskite catalyst with high performance for the partial oxidation of methane to syngas. Catalysis Today, 2016. 259: p. 388-392.

174. Zagaynov, I.V., et al., Ni(Co)–Gd 0.1 Ti 0.1 Zr 0.1 Ce 0.7 O 2 mesoporous materials in partial oxidation and dry reforming of methane into synthesis gas. Chemical Engineering Journal, 2016. 290: p. 193-200.

175. Cesar, D.V., et al., Stability of Ni and Rh–Ni catalysts derived from hydrotalcite-like precursors for the partial oxidation of methane. international journal of hydrogen energy, 2013. 38(14): p. 5616-5626.

176. Dedov, A., et al., Catalytic Materials Based on Hydrotalcite-Like Aluminum, Magnesium, Nickel, and Cobalt Hydroxides for Partial Oxidation and Dry Reforming of Methane to Synthesis Gas. Petroleum Chemistry, 2018. 58(5): p. 418-426.

177. Ozdemir, H., M.A.F. Oksuzomer, and M.A. Gurkaynak, Effect of the calcination temperature on $Ni/MgAl_2O_4$ catalyst structure and catalytic properties for partial oxidation of methane. Fuel, 2014. 116: p. 63-70.

178. Bepari, S., et al., Steam reforming of ethanol over cerium-promoted Ni-Mg-Al hydrotalcite catalysts. Catalysis Today, 2017. 291: p. 47-57.

179. Serrano-Lotina, A., et al., Dry reforming of methane to syngas over La-promoted hydrotalcite clay-derived catalysts. International Journal of Hydrogen Energy, 2012. 37(17): p. 12342-12350.

180. Fan, M.S., A.Z. Abdullah, and S. Bhatia, Catalytic technology for carbon dioxide reforming of methane to synthesis gas. ChemCatChem, 2009. 1(2): p. 192-208.

181. Requies, J., et al., Effect of redox additives over Ni/Al_2O_3 catalysts on syngas production via methane catalytic partial oxidation. Fuel, 2008. 87(15-16): p. 3223-3231.

182. Daza, C.E., et al., High stability of Ce-promoted Ni/Mg–Al catalysts derived from hydrotalcites in dry reforming of methane. Fuel, 2010. 89(3): p. 592-603.

183. Li, B., X. Xu, and S. Zhang, Synthesis gas production in the combined CO_2 reforming with partial oxidation of methane over Ce-promoted Ni/SiO_2 catalysts. International journal of hydrogen energy, 2013. 38(2): p. 890-900.

184. Peymani, M., S.M. Alavi, and M. Rezaei, Preparation of highly active and stable nanostructured Ni/CeO_2 catalysts for syngas production by partial oxidation of methane. International journal of hydrogen energy, 2016. 41(15): p. 6316-6325.

185. Lucrédio, A.F., G. Jerkiewickz, and E.M. Assaf, Nickel catalysts promoted with cerium and lanthanum to reduce carbon formation in partial oxidation of methane reactions. Applied Catalysis A: General, 2007. 333(1): p. 90-95.

186. Jiang, Z., et al., Catalytic Partial Oxidation of Methane over Ni-Based Catalysts Derived from Ni−Mg/Al Ternary Hydrotalcites. Energy & Fuels, 2009. 23(3): p. 1634-1639.

187. Zhang, J., W. Wei, and Y. Sun, Fluorine-Modified Mesoporous Ni–Mg–Al Mixed Oxides for Partial Oxidation of Methane. Catalysis Letters, 2010. 135(3-4): p. 321-329.

188. Song, H.S., et al., Synthesis Gas Production via Partial Oxidation, CO_2 Reforming, and Oxidative CO_2 Reforming of CH_4 over a Ni/Mg-Al Hydrotalcite-type Catalyst. Clean Technology, 2014. 20(2): p. 189-201.

189. Zhang, J., et al., Partial oxidation of methane over Ni/Mg/Al/La mixed oxides prepared from layered double hydrotalcites. International Journal of Hydrogen Energy, 2010. 35(21): p. 11776-11786.

190. Cesar, D.V., et al., Stability of Ni and Rh–Ni catalysts derived from hydrotalcite-like precursors for the partial oxidation of methane. International Journal of Hydrogen Energy, 2013. 38(14): p. 5616-5626.

191. Özdemir, H., M.A. Faruk Öksüzömer, and M. Ali Gürkaynak, Preparation and characterization of Ni based catalysts for the catalytic partial oxidation of methane: Effect of support basicity on H_2/CO ratio and carbon deposition. International Journal of Hydrogen Energy, 2010. 35(22): p. 12147-12160.

192. Dedov, A.G., et al., Catalytic Materials Based on Hydrotalcite-Like Aluminum, Magnesium, Nickel, and Cobalt Hydroxides for Partial Oxidation and Dry Reforming of Methane to Synthesis Gas. Petroleum Chemistry, 2018. 58(5): p. 418-426.

193. Kaddeche, D., A. Djaidja, and A. Barama, Partial oxidation of methane on co-precipitated Ni–Mg/Al catalysts modified with copper or iron. International Journal of Hydrogen Energy, 2017. 42(22): p. 15002-15009.

194. Lucredio, A.F., G. Jerkiewickz, and E.M. Assaf, Nickel catalysts promoted with cerium and lanthanum to reduce carbon formation in partial oxidation of methane reactions. Applied Catalysis a-General, 2007. 333(1): p. 90-95.

195. Iwamoto, M., et al., Copper (II) ion-exchanged ZSM-5 zeolites as highly active catalysts for direct and continuous decomposition of nitrogen monoxide. Journal of the Chemical Society, Chemical Communications, 1986(16): p. 1272-1273.

196. Groothaert, M.H., et al., Selective oxidation of methane by the bis(mu-oxo)dicopper core stabilized on ZSM-5 and mordenite zeolites. J Am Chem Soc, 2005. 127(5): p. 1394-5.

197. Beale, A.M., et al., Recent advances in automotive catalysis for NO x emission control by small-pore microporous materials. Chemical Society Reviews, 2015. 44(20): p. 7371-7405.

198. Deka, U., et al., Local environment and nature of Cu active sites in zeolite-based catalysts for the selective catalytic reduction of NO x. ACS catalysis, 2013. 3(3): p. 413-427.

199. Karoshi, G., et al., Valorization of Eggshell Waste into Supported Copper Catalysts for Partial Oxidation of Methane. International Journal of Environmental Research, 2019. 14(1): p. 61-70.

200. Karoshi, G., et al., Recycled eggshells as precursors for iron-impregnated calcium oxide catalysts for partial oxidation of methane. Bioresources and Bioprocessing, 2020. 7(1): p. 48.

201. Ferreira, A.C., et al., Partial oxidation of methane over bimetallic copper–cerium oxide catalysts. Journal of Molecular Catalysis A: Chemical, 2010. 320(1-2): p. 47-55.

202. Slagtern, Å., et al., Catalytic partial oxidation of methane over Ni-, Co-and Fe-based catalysts. Catalysis Today, 1998. 46(2-3): p. 107-115.

203. Nakagawa, K., et al., Synthesis gas production from methane using oxidized-diamond-supported group VIII metal catalysts. Energy & fuels, 2003. 17(4): p. 971-976.

204. Rungsri, P., et al., Catalytic Activities of Ni and Cu Supported over Gd-CeO_2 toward Partial Oxidation of Methane. Journal of Sustainable Energy & Environment, 2018. 9: p. 47-50.

205. Karoshi, G., et al., Calcined eggshell as an inexpensive catalyst for partial oxidation of methane. Journal of the Taiwan Institute of Chemical Engineers, 2015. 57: p. 123-128.

206. Sato, K., et al., High performance of Ni-substituted calcium aluminosilicate for partial oxidation of methane into syngas. Catalysis Communications, 2007. 8(11): p. 1735-1738.

Chapter 3: Materials and Methods

Firstly, Mg-Ni-Al hydrotalcite was synthesized by co-precipitation method followed by CeO_2 impregnation via wet impregnation method. The samples were characterized to determine the physiochemical properties employing XRD, SEM, TGA, FTIR and BET techniques. These samples were then tested for syngas production via POM in fixed bed reactor. Flow diagram for experimental methodology is shown in **Fig. 3.1**.

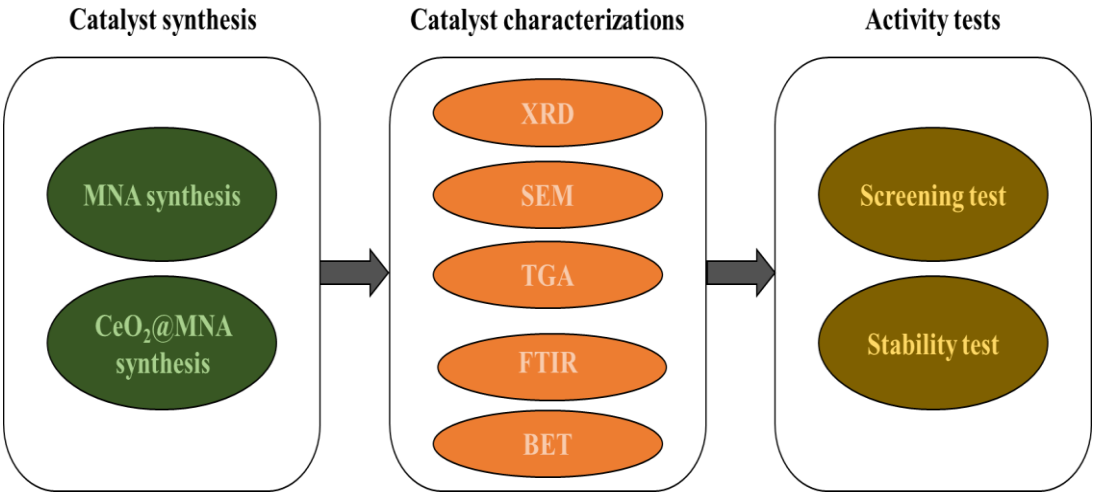

Figure 3.1 Block flow diagram for experimental methodology

3.1 Synthesis of Catalyst

Catalyst preparation methods are influential in catalytic performance of the catalyst. As the preparation techniques of the catalyst include certain steps such as precursors, solvent concentration, calcination temperature, PH and aging time which directly affect the properties of the final prepared catalyst [1]. The performance of the catalyst depends upon the properties of the catalyst. Catalyst is prepared by various methods but the most common methods include impregnation method, precipitation and co-precipitation method, hydrothermal method, sol-gel method, surfactant-assisted methods and advanced preparation methods.

Magnesium nitrate hexahydrate ($Mg(NO_3)_2.6H_2O$), aluminium nitrate nonahydrate ($Al(NO_3)_3.9H_2O$), nickel nitrate hexahydrate ($Ni(NO_3)_2.6H_2O$), sodium

carbonate (Na_2CO_3) and CeO_2 materials were purchased from Sigma Aldrich Ltd. Deionized water was used for different molarity solutions preparation of these materials. In this research work all materials used were of analytical purity and no further purification process was performed before using.

3.1.1 Material Synthesis

Magnesium nitrate hexahydrate ($Mg(NO_3)_2.6H_2O$), aluminium nitrate nonahydrate ($Al(NO_3)_3.9H_2O$), nickel nitrate hexahydrate ($Ni(NO_3)_2.6H_2O$), CeO_2 material and sodium carbonate (Na_2CO_3) were sourced from Sigma Aldrich Ltd. DI water was utilized for the preparation of molarity of solutions. In this research work all materials used for catalyst synthesis were of analytical purity and no further purification process was performed before using.

3.1.2 Preparation of CeO_2@MNA

Composite material CeO_2@MNA was synthesized in two steps process. Initially, MNA was prepared via co-precipitation technique. Nitrate solutions consisting of Al^{+3}, Mg^{+2}, and Ni^{+2} and ions of molarity 0.75, 0.75 and 0.25 were prepared respectively. The solutions were mixed in appropriate ratios in a magnetic stirrer [2]. Afterwards, the mixture was titrated dropwise into a certain amount of 0.5 M vigorously stirred solution of precipitating agent Na_2CO_3 at 70 ℃ in a three-necked flask. During the mixing process, the slurry was kept at pH=10 by dropwise addition of 1M NaOH solution.

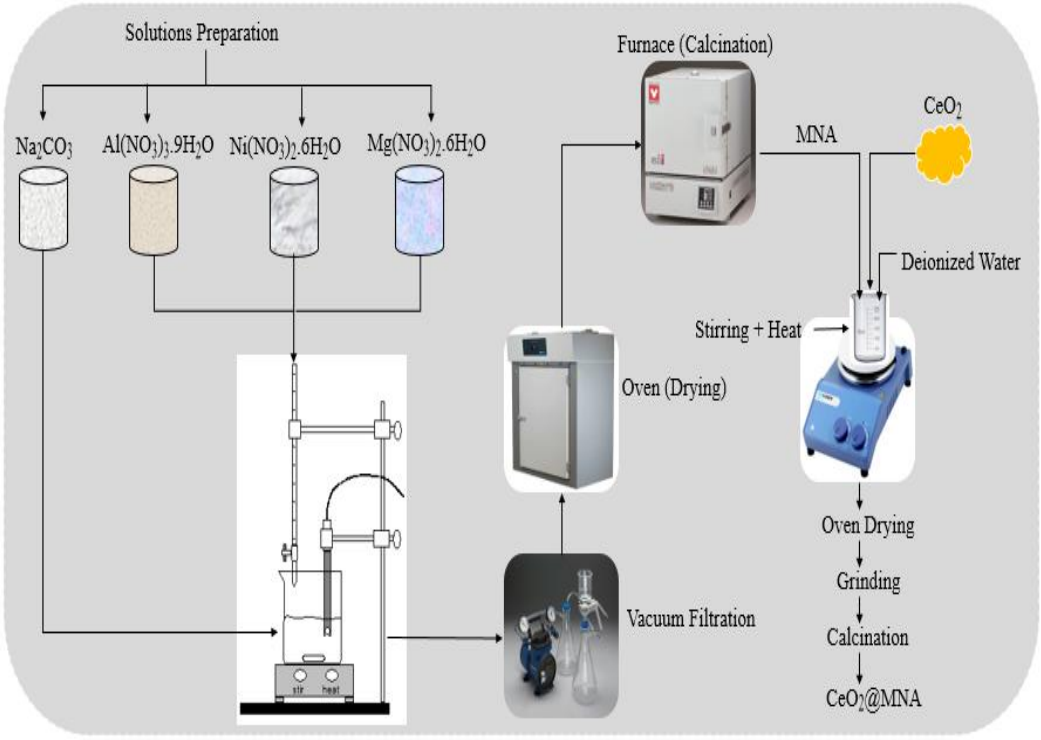

Figure 3.2 Step by step schematic of catalyst preparation

The precipitates were washed and filtered five times with deionized water through vacuum filtration to remove any sodium ions from the precipitates. After filtration, to remove entrapped H_2O the precipitates were kept in the oven for overnight at 110 ℃. Afterwards, to synthesize the double-layered hydroxide, the dry out solid was finely crushed to powder form and calcined for 5 hours at 850 ℃ with 10 ℃ min^{-1} heating rate under static air muffle furnace. The CeO_2 synthesis method is reported elsewhere [3]. For the preparation of CeO_2@MNA, 0-15 wt% loadings of CeO_2 in MNA were prepared via wetness impregnation technique. CeO_2 and MNA in calculated amounts were added in continuously stirred deionized water placed on hot plate at 110 ℃ for 5 h. This mixture solution was oven dried for overnight at 110 ℃ and calcined for 5 h at 850 ℃ with 10 ℃ min^{-1} heating rate under static air.

3.2 Catalyst Characterizations

The prepared catalysts were then brought to different characterisation techniques to determine the physiochemical properties of the material which are explained in the below sections.

3.2.1 X-Ray Diffraction (XRD)

To analyse the crystalline structure and phase transitions of the prepared samples, XRD was used. The calcined and well grinded samples were brought to Bruker D8 advanced X-ray diffractometer as shown in **Fig. 3.3** with specifications of 1.5418 Å irradiation wavelength at 40 kV and 40 mA set conditions to identify their diffraction peaks. Additionally, diffraction angles range was set at 5°–90° and 0.05°-2θ step size was used to analyse XRD patterns. Also the size of crystallite was obtained using Scherrer equation[4].

Figure 3.3 Advanced X-ray Diffractometer

3.2.2 Scanning Electron Microscopy (SEM)

The morphology of the both fresh and spent samples were visualized by SEM. The SEM images were obtained using SEM Model JSM-6490A JEOL (Japan) as shown in **Fig. 3.4** and micro level images with different resolutions of 5 µm, 1 µm and 500nm were obtained additionally with EDS images at 10 µm resolution. The microscope resolution was set at 3nm and 30 kV operation parameter.

Figure 3.4 Scanning Electron Microscope

3.2.3 Thermogravimetric Analysis (TGA)

To observe the deposited carbon associated with fresh and spent samples and to seek their respective thermal stability and weight losses with respect to temperature changes, TGA was used. TGA analysis was performed using TGA 5500, TA Instruments (USA) as shown in **Fig. 3.5**. 10mg sample was used for TGA analysis while the nitrogen flow was maintained at 25 mL min^{-1} and maximum temperature of 900℃ with 10 °C min^{-1} heating rate was used.

Figure 3.5 Thermogravimertric Analyser

3.2.4 Fourier Transform Infrared Spectroscopy (FTIR)

To check out the corresponding functional groups present in the sample, FTIR was used. FTIR analysis was done using Cary 630 FTIR (Agilent Technologies, USA) as shown in **Fig. 3.6** and wavenumber were set in the range 4000 cm^{-1} to 650 cm^{-1}.

Figure 3.6 Fourier Transform Infrared Spectroscopy

3.2.5 Brunauer-Emmett-Teller (BET) Analysis

Textural properties (specific surface area, pore radius, pore volume) of the samples were calculated from nitrogen adsorption-desorption isotherms obtained at nitrogen temperature of -196 ℃ (Quantachrome instruments, Model: NOVA 2200e, USA) shown in **Fig. 3.7**. Specific surface area was measured applying Brunauer-Emmett-Teller (BET) method and average pore radius was calculated from Barret-Joyner-Halenda (BJH) method. Prior to analysis, all the specimens were degassed at 300 ℃ under vacuum.

Figure 3.7 Brunauer-Emmett-Teller analyser

3.3 Experimental Setup

The schematic of experimental setup for POM is shown in **Fig. 3.8**. The testing was performed in a downward flow fixed bed cylindrical reactor (SS-316) of PARR (Model LSP-2.38-0-32-1C-2335EEE, Moline USA). The reactor consists of stainless-steel tube having 76 cm length, 12 mm inner and 14 mm outer diameter placed inside a furnace. 0.3 g catalyst sample sandwiched between quartz wool was loaded at the centre of the reactor tube. Temperature of reaction was under control by PARR 4871 series process controller connected by a K-type thermocouple located at outlet of the catalyst bed of reactor. Before the activity test, catalyst reduction was performed with H_2 flow rate of 40 mL/min at 850 °C for 1 h. The reaction occurred at fixed temperature 850 °C and atmospheric pressure with feed gases mixture flow rate 30 mL/min (ratios: $CH_4/O_2 = 2$). Feed gases CH_4 and O_2 supply were regulated by digital mass flow controllers. The product gases (H_2, CO_2, CH_4, CO) after passing through the condenser were analysed by gas chromatography (GC-2010 Plus, SHIMADZU Japan) provided with TCD column [3]. GC column temperature was set at 200 °C with peak retention time of 10 min.

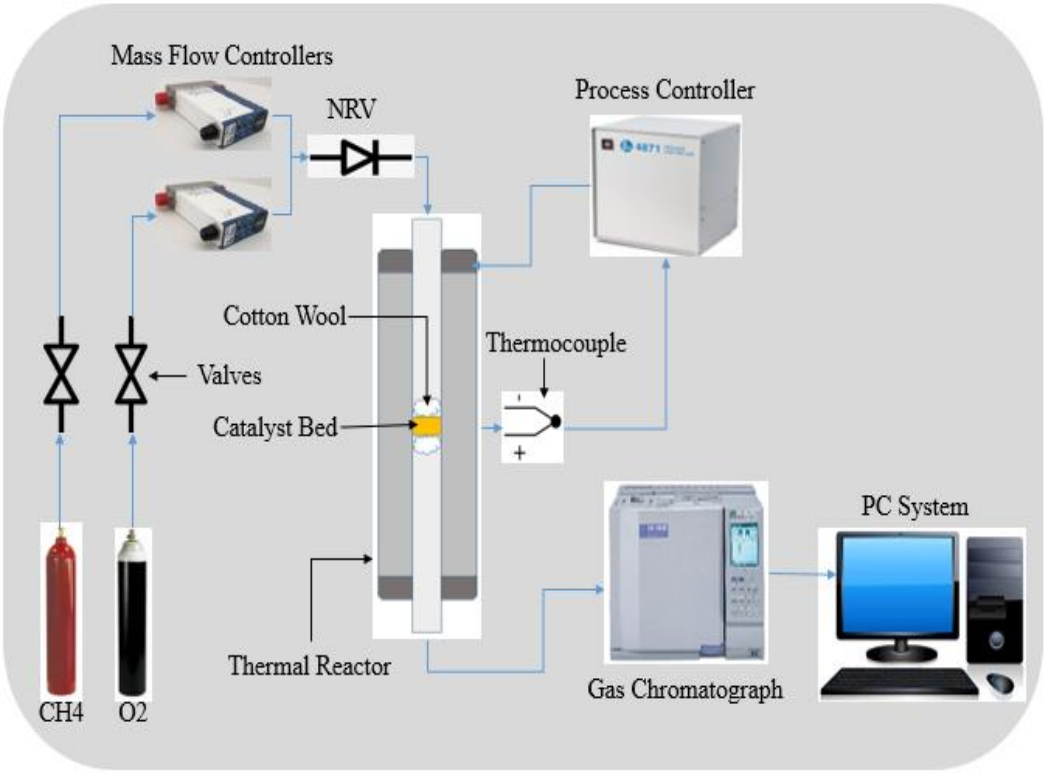

Figure 3.8 Experimental setup for POM reaction

3.4 Catalytic Activity

The activity of MNA, CeO_2 and 10% CeO_2@MNA catalysts over POM were examined through CH_4 conversion, CO, H_2 selectivity and H_2/CO ratio using equations (E1-E4). The experiments were standardised and analysed the activity using standard calculating using error bars of ±5%.

$$CH_4 \text{conversion}\left(X_{CH_4}\right)\% = \left[\frac{(CH_4)_{\text{converted}}}{(CH_4)_{\text{feed}}} \times 100\right] \quad \text{(E1)}$$

$$H_2 \text{ selectivity } (S_{H_2})\% = \left[\frac{(H_2)_{\text{produced}}}{2 \times (CH_4)_{\text{converted}}} \times 100\right] \quad \text{(E2)}$$

$$\text{CO selectivity}\left(S_{CO}\right)\% = \left[\frac{(CO)_{\text{produced}}}{(CO)_{\text{produced}} + (CO_2)_{\text{produced}}} \times 100\right] \quad \text{(E3)}$$

$$H_2/\text{CO ratio} = \left[\frac{\text{selectivity}(S_{H_2})}{\text{selectivity}(S_{CO})}\right] \quad \text{(E4)}$$

References

1. Pereira, A.L.C., et al., A comparison between the precipitation and impregnation methods for water gas shift catalysts. Journal of Molecular Catalysis A: Chemical, 2008. 281(1-2): p. 66-72.

2. Sikander, U., S. Sufian, and M.A. Salam, Synthesis and structural analysis of double layered Ni-Mg-Al hydrotalcite like catalyst. Procedia engineering, 2016. 148: p. 261-267.

3. Raza, J., et al., Methane decomposition for hydrogen production over biomass fly ash-based CeO_2 nanowires promoted cobalt catalyst. Journal of Environmental Chemical Engineering, 2021. 9(5): p. 105816.

4. Charisiou, N., et al., Syngas production via the biogas dry reforming reaction over nickel supported on modified with CeO2 and/or La2O3 alumina catalysts. Journal of Natural Gas Science and Engineering, 2016. 31: p. 164-183.

Chapter 4: Results and Discussion

4.1 Characterizations of Fresh Catalyst

The prepared fresh catalyst was characterized using various characterisations like XRD, SEM, TGA, FTIR and BET in order to identify structures of constituents present in catalyst, its morphology, its behaviour with temperature change effect and to figure out the type of functional groups associated with catalyst.

4.1.1 XRD Analysis

The XRD patterns to determine crystallography and phase identification of calcined samples ((a) CeO_2 (b) MNA (c) 10%CeO_2@MNA) are shown in **Fig. 4.1**. As evident MNA was prepared through the calcination of hydrotalcites precursors, therefore, highly stable mixed metallic oxides were detected as widely reported in the literature [1, 2]. The diffraction peaks for cubic $NiAl_2O_4$ (JCPDS# 10-0339) with hkl indices were identified with a 2θ value at 19.07° (111), 31.4° (220), 37.0° (311), 44.9° (400), 59.6° (511) and 65.5° (440) respectively [3]. The cubical $NiAl_2O_4$ illustrates the space group fd-3m (227). Diffraction peaks for cubical structure CeO_2 (JCPDS# 43-1002), space group Fm-3m (225) were detected including hkl indices with 2θ value at 28.6° (111), 33.1° (200), 47.5° (220) and 56.3° (311) [4]. The presence of CeO_2 were reflected as sharp peaks as in parent cerium in 10%CeO_2@MNA due to the neat preparation of composite. The formation of cubical $MgAl_2O_4$ (JCPDS# 21-1152) with space group Fd-3m (227) is noticed in 2θ= 19.0° (111), 31.27° (227), 36.65° (311), 44.8° (400), 59.3 (511) and 65.2 (440) respectively [5, 6]. The cubical NiO (JCPDS# 44-1159) of space group Fd-3m (225) has diffraction peaks with hkl indices at 2θ= 37.2° (101), 43.3° (012) and 63.0° (110) [7]. Diffraction peaks with hkl indices for cubical MgO (JCPDS# 45-0946) at 2θ are detected at 36.9° (111), 42.9° (200) and 62.3° (220) respectively [8, 9]. Peaks of cubical $MgNiO_2$ (24-0712) space group Fm-3m (223) has been detected at 2θ (hkl) = 37.1° (111), 43.1° (200) and 62.5° (220) [10-12]. As observed cubic spinel phases of $MgAl_2O_4$ appeared in both MNA and 10%CeO_2@MNA. These spinel phases are expected to inhibit the deposition of coke, leading to enhanced stability of catalyst during reaction [13]. The better interaction of

Ni with Mg and Al is evident in the composite. Structural phases of all catalyst compounds are presented in **Table 4.1**.

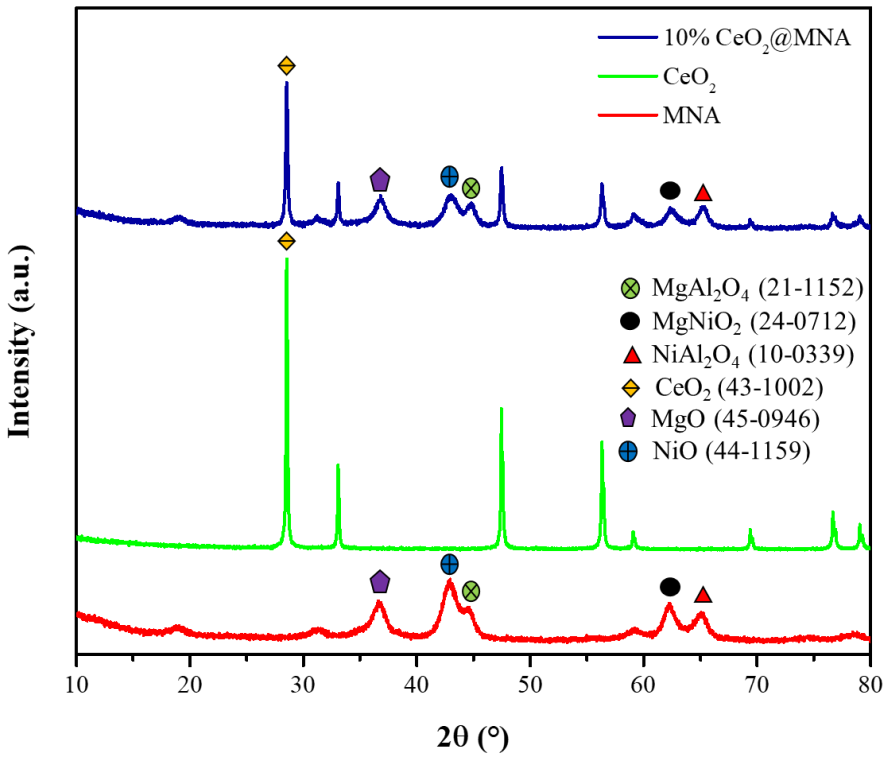

Figure 4.1 XRD analysis of prepared (a) MNA (b) CeO_2 (c) 10%CeO_2@MNA

Table 4.1 XRD analysis of fresh catalyst

Compounds	**Structure**	**PDF #**	**2θ (°)**	**Phase (hkl)**
$NiAl_2O_4$	Cubic	10-0339	19.07 31.4 37 44.9 59.6 65.5	111 220 311 400 511 440
CeO_2	Cubic	43-1002	28.6 33.1 47.5 56.3	111 200 220 311
$MgAl_2O_4$	Cubical	21-1152	19 31.27 36.65 44.8 59.3 65.2	111 227 311 400 511 440

NiO	Cubical	44-1159	37.2 43.3 63	101 012 110
MgO	Cubical	45-0946	36.9 42.9 62.3	111 200 220
$MgNiO_2$	Cubical	24-0712	37.1 43.1 62.5	111 200 220

4.1.2 FTIR Analysis

FTIR spectra of the catalysts are presented in **Fig. 4.2**. This shows appearance of vibrational bands for MNA, CeO_2 and 10% CeO_2@MNA. Major peaks observed in a range of 3400-3460 cm^{-1} represents OH stretching mode in MNA, CeO_2 and 10% CeO_2@MNA samples. CeO_2 addition reduced the O—H vibration in 10% CeO_2@MNA. In the sample of MNA and 10% CeO_2@MNA, sharp peak at 1635 cm^{-1} signifies the stretching vibrations of C—O and C==O [14]. A shoulder at 1650 cm^{-1} might be due to interlayer H_2O molecules bending [15]. Anti-symmetric stretching band at 1386 cm^{-1} reveals the presence of trace amounts of residual NO_3^{-1}/CO_3^{2-} anions [16]. At 1490 cm^{-1}, a splits occurred in sample without CeO_2 upon lowering in symmetry [14]. Peaks in a range of 850-600 cm^{-1} are inferred as lattice vibrations of metal and oxygen (Mg-O, Ni-O, Al-O) [17]. These peaks are overlapped in 10% CeO_2@MNA because of the presence of Ce—O stretching band below 700 cm^{-1}.

In **Fig. 4.2 (b)** transmittance peaks of CeO_2 are shown. The band at 562 cm^{-1} are credited to the stretching of Ce—O vibration [18]. The asymmetric stretching vibrations of CO_2 and bending vibrations of CO_3^{2-} are observed in range of 700-1000 cm^{-1} [19]. In addition, a broad band at 1630 cm^{-1} is the O—C—O stretching overlapping with H—O—H bending [20].

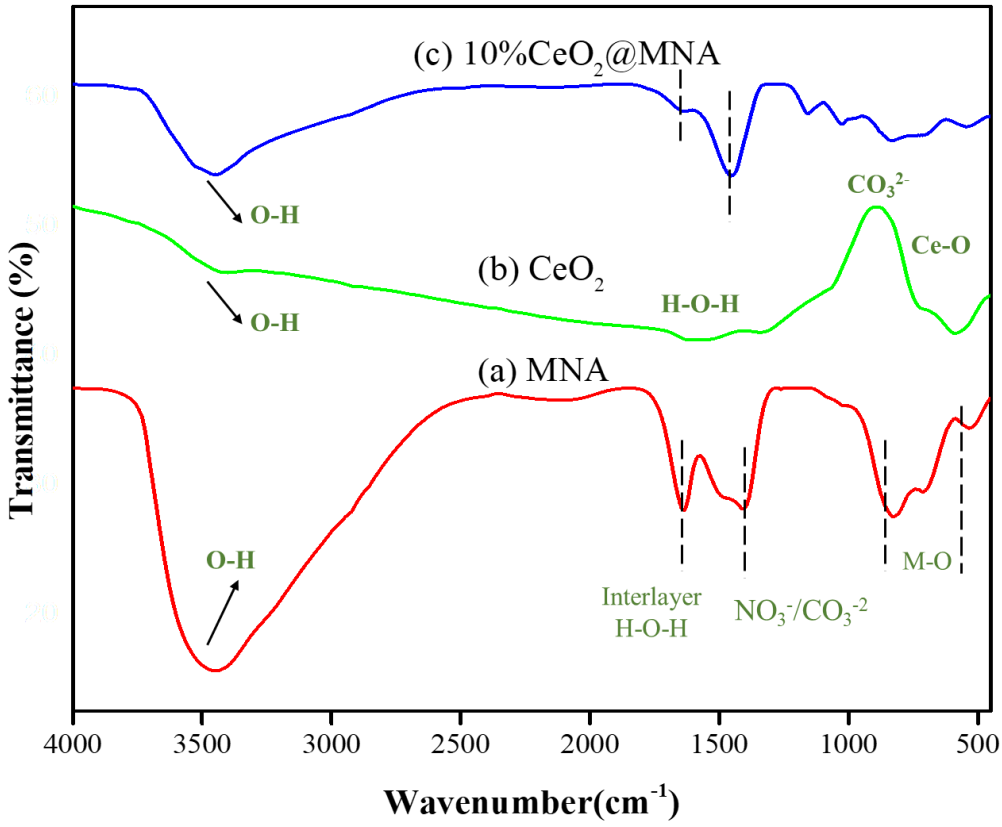

Figure 4.2 FTIR analysis of samples (a) MNA (b) CeO_2 (c) 10% CeO_2@MNA

4.1.3 TGA Analysis

The weight loss over increasing temperature of samples was analysed TGA curves presented in **Fig. 4.3**. Each of layered double hydrotalcite structure undergoes two stage thermal decomposition. In **Fig. 4.3(a)**, up to 230 ℃ temperature, the MNA hydrotalcite undergoes a weight loss of approximately 4% due to removal of physiosorbed water, decarbonisation and release of structural water [21, 22]. Between 230 and 650 °C dihydroxylation of layered structure of hydrotalcite and the decomposition of interlayer anions takes place with a weight loss of approximately 9% [23]. **Fig. 4.3(b)** shows about 5% total weight loss in CeO_2 sample. This shows that CeO_2 is highly stable showing overall weight loss of 5%. Up to 230 ℃, the weight loss may be owing to the adsorbed water and surface acetate groups. While the weight loss in temperature range of 300 - 600 ℃ implies the formation of some complexes with cerium ($Ce_2O_2CO_3$), (CH_3COO), and Ce(OH)). These complex formations have been reported in literature [24].

In case of of CeO_2@MNA **(Fig. 4.3(c))**, the weight loss is about 7% occurs up to 600°C. Thermal stability is enhanced with changed morphology and composition of sample as less weight loss is observed as compared to MNA. By addition of CeO_2, base to acid ratio is changed in the sample which increased the thermally stability of the sample.

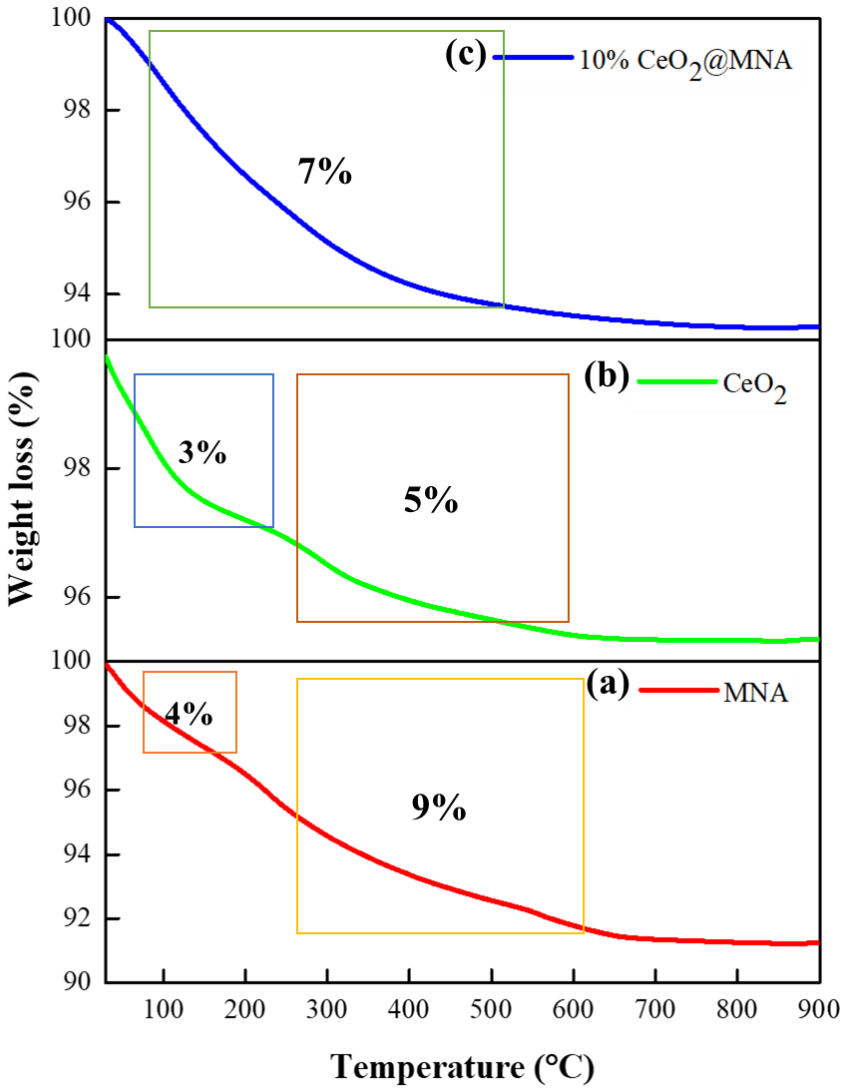

Figure 4.3 TGA analysis of (a) MNA (b) CeO_2 (c) 10% CeO_2@MNA

4.1.4 SEM Analysis

The morphologies of the synthesized material recorded by SEM are displayed in **Fig. 4.4**. The SEM micrograph in **Fig. 4.4(a-b)** reveals a highly porous spinel layered structure of HT like precursor prepared by co-precipitation method as typically reported in the literature [25]. A highly porous coral-like structure was observed due to the presence of divalent and trivalent cations (Mg^{+2}, Ni^{+2}, and Al^{+3}) in the outer layer of hydrotalcite. **Fig. 4.4(c-d)** show the SEM images of CeO_2, exhibiting two types of morphologies including rod-like and particle structure as reported in the literature [26-28]. Incorporation of CeO_2@MNA as in **Fig. 4.4(e-f)** maintained the coral-like structure but with CeO_2 particles of uniformly distributed irregular rod and spherical shapes [29]. It was observed that sample containing CeO_2 appears to be coated over coral surfaces of MNA [30]. It is evident that the particle structure of CeO_2 self-assembled with the rod structure of CeO_2 on the surface of MNA. This analysis is also supported by literature [27].

EDS analysis of 10% CeO_2@MNA is shown in **Fig. 4.5**. Elemental presence of CeO_2 in the sample with various elements of hydrotalcites (Ni, Mg, Al) were observed in the synthesized samples. The presence of O element is due to the formation of metallic oxides by calcination of precipitates from hydrotalcite type precursors [27].

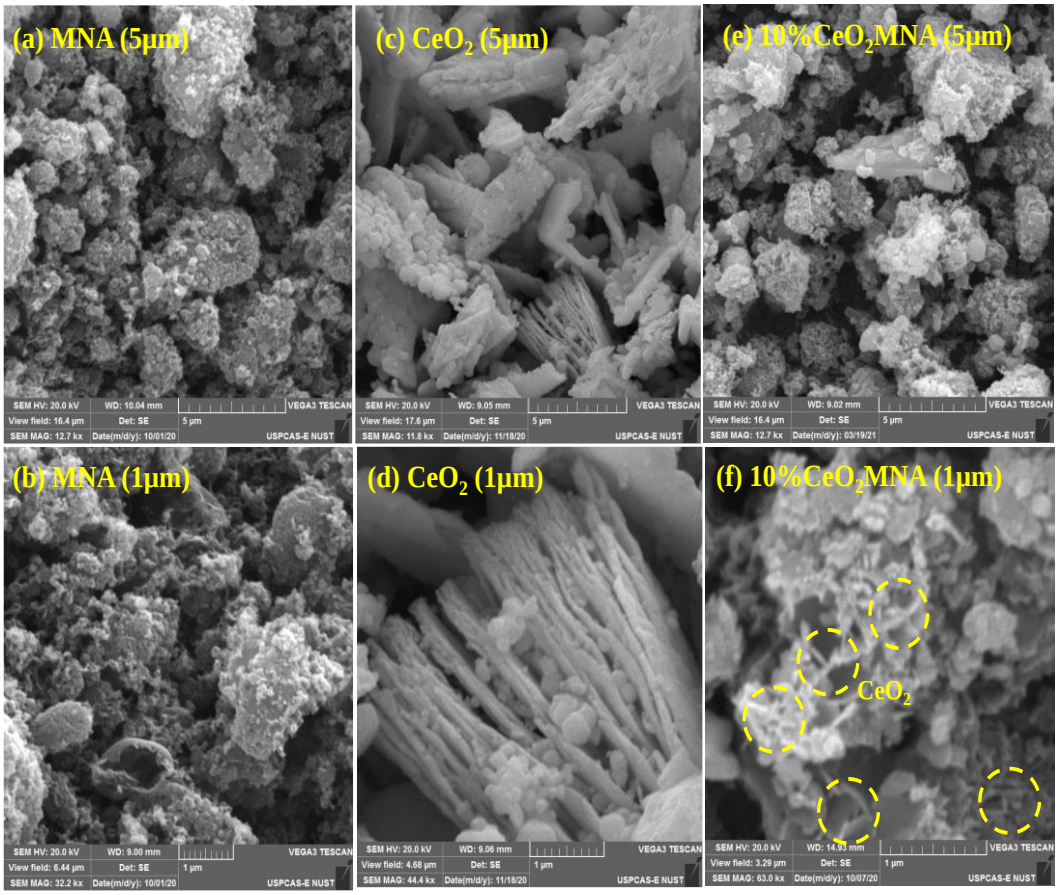

Figure 4.4 SEM micrograph images of (a,b) MNA, (c,d) CeO_2, (e,f) 10% CeO_2@MNA

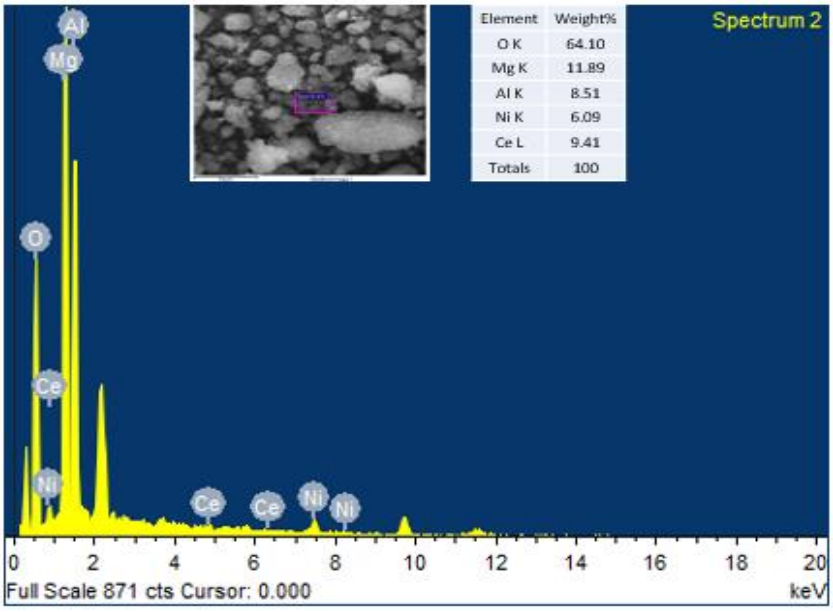

Figure 4.5 EDS analysis of fresh 10%CeO_2@MNA

4.1.5 BET Analysis

The specific surface area of MNA and 10%CeO_2@MNA was calculated by the BET surface area analyser. The analysis is presented in **Table 4.2**. MNA exhibited a surface area and pore volume of 47.1 m^2/g and 0.12 cm^3/g that decreased to 41.2 m^2/g and 0.086 cm^3/g, respectively, on CeO_2 addition probably because of the location of CeO_2 species into the pores of MNA as presented in **Fig. 4.4(a,b)** [31-33]. **Fig. 4.6(a)** presents the nitrogen adsorption-desorption isotherms of samples showing type IV isotherms with mesoporous structure and hysteresis loop of H2 type with strong interaction [34]. For MNA, the loop is noticed at higher quantity adsorbed (cm^3/g) values, indicating more surface area as compared to 10%CeO_2@MNA as confirmed in Table 4.1. Reduction in surface area in case of 10%CeO_2@MNA could also be due to CeO_2 introduction in MNA after calcination, where the structure of MNA was already built. For this reason, the hysteresis shape of MNA and 10%CeO_2@MNA is the same in literature [35]. Moreover, pore size distributions of samples are presented in **Fig. 4.6(b)** ranging in 2-20 nm. Pore size distribution (BJH) manifested pore radius decrease from 8.5 to 1.8 nm on CeO_2 incorporation in MNA. Furthermore, CeO_2 addition moved the pore size distribution to a smaller size as evident in **Fig. 4.6(b)**.

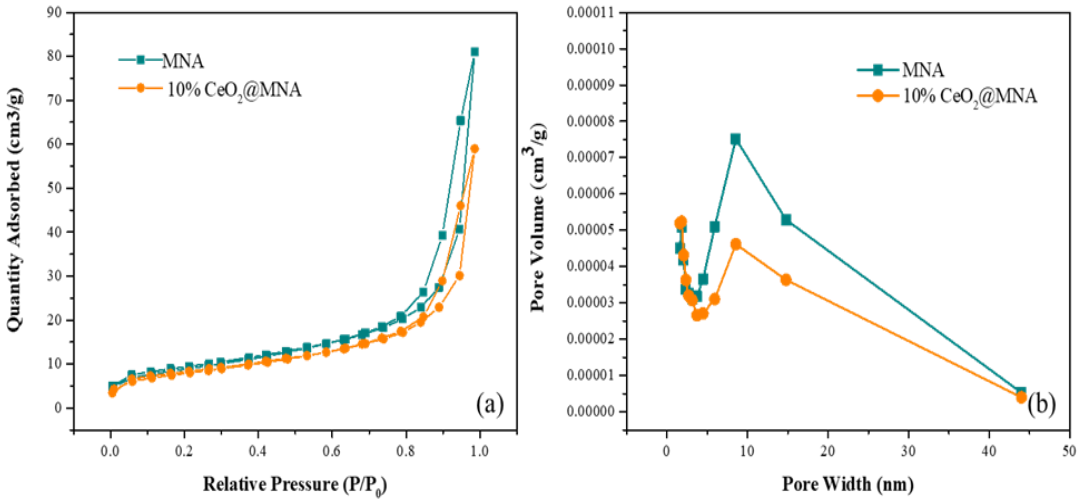

Figure 4.6 (a) N2 adsorption-desorption isotherms of MNA and 10% CeO_2@MNA (b) Pore size distribution (BJH) of MNA and 10% CeO_2@MNA

Table 4.2 Surface properties of MNA and 10% CeO_2@MNA

Sample name	**S_{BET} (m^2/g)**	**V_P (cm^3/g)**	**r_p (nm)**
MNA	47.1	0.12	8.5
10%CeO_2 @MNA	41.2	0.096	5.8

4.2 Catalyst Activity Tests

The catalysts so prepared were introduced into the fixed bed reactor for the POM reaction to check out the catalytic activity and stability results with the conditions of reactor temperature at 850℃, catalyst loading of 0.3g, total feed flow rate set at 30mLmin^{-1} and the feed gas ratio of CH_4/O_2=2.

4.2.1 Catalyst Screening

Catalyst activity tests results for MNA, CeO_2, 5% CeO_2@MNA, 10% CeO_2@MNA, 15% CeO_2@MNA are shown in **Fig. 4.7(a-d)**. All catalysts were screened for 10 h time on stream (TOS) at 850 ℃, CH_4/O_2=2 and GHSV = 6000 mL/h-g_{cat} to get the uniform results. Under the adopted conditions for POM the major products known by GC are H_2, CO, CO_2, and unreacted CH_4. Initially, MNA and CeO_2 were tested for catalytic POM, followed by 5-15%CeO_2 incorporated MNA. **Fig. 4.7(a)** presents the comparison of CH_4 conversions for all catalysts. It was observed that CH_4 conversion was greatly affected by the addition of CeO_2 in MNA during POM. CH_4 conversions increased on CeO_2 incorporation from 52% in MNA to 70%, 95% and 90% for 5% CeO_2@MNA, 10% CeO_2@MNA and 15% CeO_2@MNA, respectively. The increase in activity on CeO_2 addition might be due to strong interaction between CeO_2 and NiO that is formed as a result of calcination of hydrotalcite precursors and detected in XRD. This analysis is supported by the literature [36] that reported stronger NiO and CeO_2 interaction increases the oxygen mobility, providing favourable conditions for carbon removal in the form of CO. Another reason for improved catalytic performance in CeO_2 promoted samples might be due to improved Ni dispersion and reducibility due to CeO_2 [21]. However, 15% CeO_2@MNA exhibited less CH_4 conversion as compared to 10% CeO_2@MNA.

Reduction in CH_4 conversion beyond 10% CeO_2 might be due to the clustering of CeO_2 particles that can block the active sites during reaction [33]. A similar pattern was observed in the case of H_2 selectivity and H_2/CO ratio. This suggests that further incorporation of CeO_2 than 10% caused a slight reduction of activity of the catalyst system [37]. 10% CeO_2@MNA showed best performance with 95% CH_4 conversion, 47% H_2 selectivity, 17% CO selectivity and H_2/CO ratio of 2.7, suggesting better CeO_2 dispersion in the porous support of MNA. As evident from the results of BET, the surface area decreased and PSD moved to a smaller size on CeO_2 addition. This increased dispersion role was also confirmed from the literature [37] and XRD of present study, as it generated smaller crystals size of composite as compared to MNA.

Fig. 4.8 illustrates the CH_4 conversion and H_2/CO overall catalysts during a TOS of 10 hours. As mentioned earlier, CH_4 conversions increased on the addition of CeO_2 in MNA to a certain value as in **Fig. 4.8(a)**. However, stable results were obtained throughout the screeing. Initially, CH_4 conversion for 10% CeO_2@MNA was 92%, which further increased to 95% after 4 hours. **Fig. 4.8(b)** exhibited a similar pattern with 10% CeO_2@MNA exhibiting maximum H_2/CO ratio. The key reason of varying ratios of H_2/CO between the catalysts was the addition of CeO_2 that increased the basic character of MNA by promoting the adsorption of CO_2 on the catalyst surface [38]. Literature suggests that the addition of rare earth oxides with basic properties can increase the basicity of hydrotalcites [39]. Therefore, addition of CeO_2 in MNA increased the H_2/CO ratio to a certain value. A maximum H_2/CO ratio of 2.7 was exhibited by 10% CeO_2@MNA, therefore giving the least CO selectivity. H_2/CO ratio greater than 2.0 have been reported in the literature with much higher values than equilibrium at lower temperatures. However, the selectivities of H_2 and CO are found close to equilibrium at temperatures around 800 ℃ [40]. This suggests 10%

CeO_2@MNA could be promising for higher syngas production. Therefore, this catalyst was furthur tested for stability analysis.

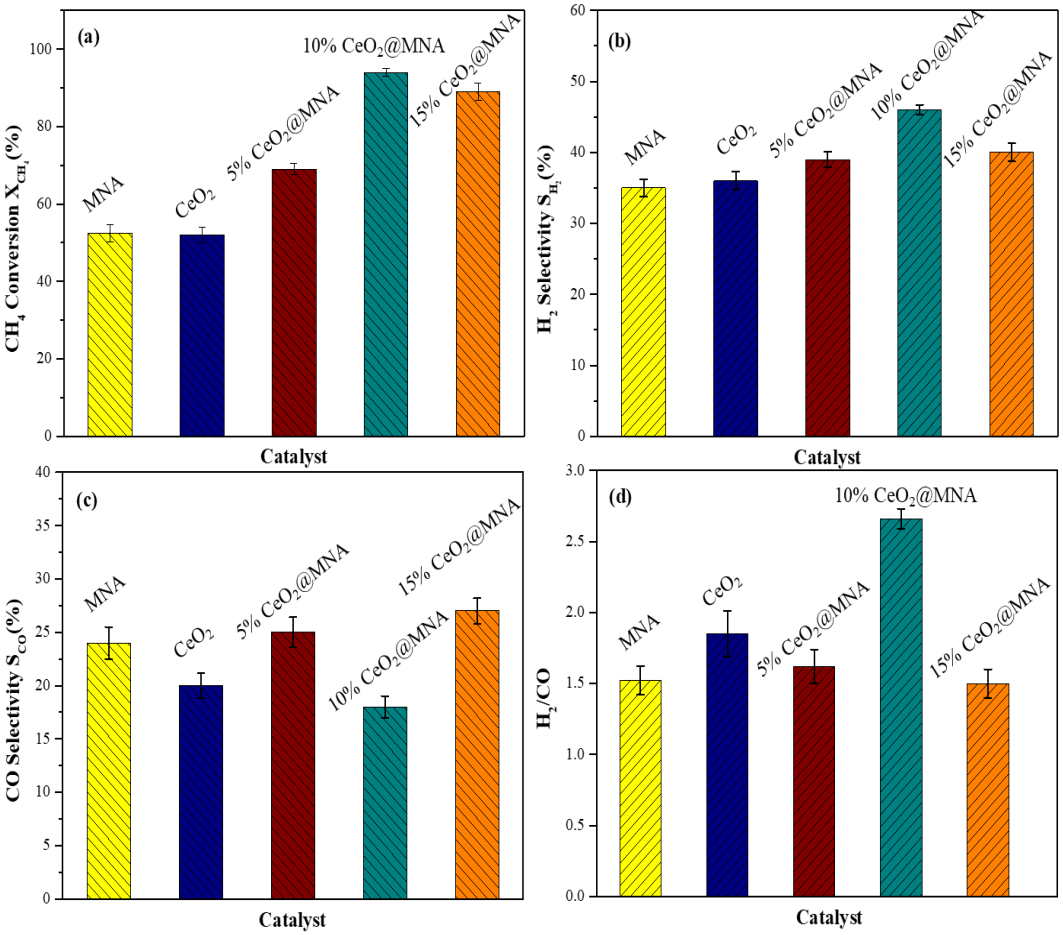

Figure 4.7 Catalyst activity tests at 850 °C, CH_4/O_2=2, 8 h (a) CH_4 Conversion (b) H_2 selectivity (c) CO Selectivity (d) H_2/CO ratio, GHSV= 6000 mL/h-gcat

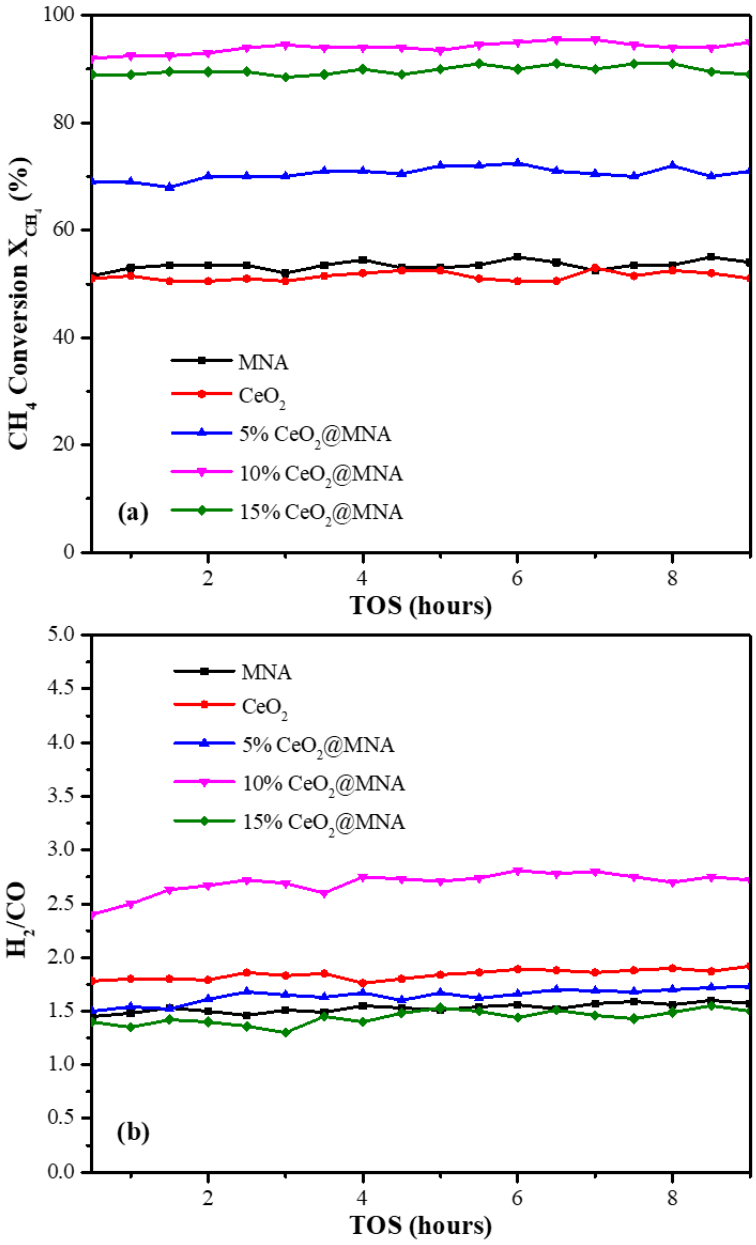

Figure 4.8 Screening test for TOS of 10 hours over catalysts (a) CH_4 Conversion (b) H_2/CO ratio Conditions: catalyst loading = 0.3 g, temperature 850 °C, feed ratio CH_4/O_2=20/10 mL, GHSV= 6000 mL/h-gcat

4.2.2 Stability Analysis for 10% CeO_2@MNA

The stability test performed for 10% CeO_2@MNA is presented in **Fig. 4.9**. The catalyst was tested for POM over the same reaction conditions for 35 hours. Initially, 92% CH_4 conversion was observed that was stabilized to 95% after some time.

However, H_2/CO ratio was found to be in a range of 2-3. Moreover, no decrease in CH_4 conversion rate was observed during this 35 h stability test that shows high resistance of composite to deactivation [41]. As evident in **Fig. 4.9**, CH_4 conversion increased after some time during the reaction, implying an activation process to achieve high catalytic performance for the catalyst. This activation process is because, after the reduction of catalyst, the surface of Ni active site becomes smooth. During the reaction, the activity increased because of the redox process that roughed the active site surface [37]. The excellent catalytic performance and resistance to deactivation is ascribed to the $NiAl_2O_4$ formation in metallic oxides on the catalyst surface, which after reduction leads to Ni particle formation resulting in resistance to catalyst deactivation at enhanced temperatures [41]. According to the literature [42-44], during the pretreatment reduction process increased level of oxygen vacancies are developed around particles of metal by the addition of CeO_2. Due to increase in number of exposed vacancy sites, oxygen transfer from cerium to metal particles takes place, hence the carbon cleaning capacity of catalyst is increased. Consequently, catalytic

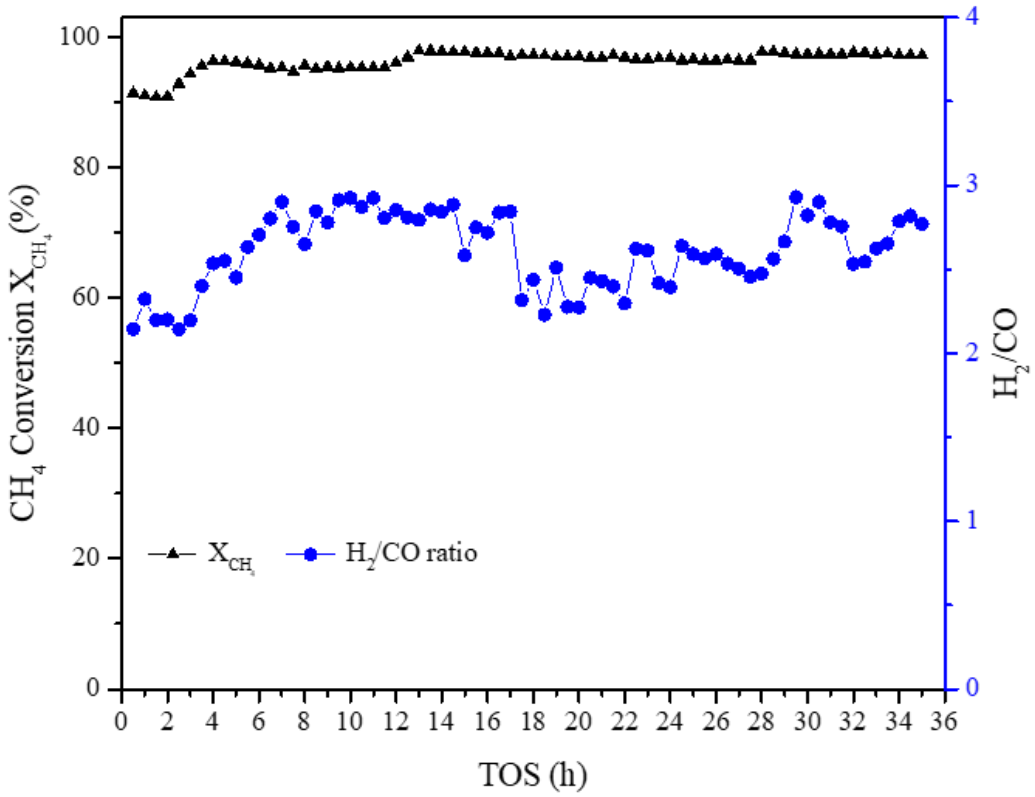

Figure 4.9 Catalyst stability test for 10% CeO_2@MNA in POM reaction.

Experimental conditions: 850 °C, CH_4/O_2=2, TOS = 35 h, GHSV= 6000 mL/h-gcat

stability is greatly enhanced due to higher capacity of oxygen transfer of CeO_2 promoter. The metal surface remains free of inactive carbon due higher exchange rate of oxygen.

To validate the catalytic performance of CeO_2@MNA, a comparison study of recently investigated catalysts for POM is given in **Table 4.3**. From the compared reports, it is manifest that the studied catalyst has comparatively exhibited competitive catalytic performance compared to other recently studied catalysts. The reported catalysts also resulted in high CH_4 conversion and H_2/CO ratio, although a direct comparison is not possible due to different reaction conditions. However, CeO_2 incorporation in the present support resulted in enhancing the thermal stability and catalytic performance of the MNA as evident from TGA and screening tests of CeO_2@MNA. The catalyst exhibited a high conversion of 95% and H_2/CO ratio of 2.7 revealing excellent catalytic activity due to the influential basic properties of CeO_2.

Table 4.3 Catalytic performance of recently employed catalysts for POM

Catalyst	**CH_4 conversion (%)**	**H_2/CO ratio**	**Reaction conditions**	**Ref.**
10%CeO_2@MNA	95	2.7	T=850 °C, Catalyst loading=0.3g GHSV=6000 ml CH_4 g^1h^{-1}	Present study
$NiAl_2O_4$ (Ni/Al=0.25)	81	2.3	T=700 °C, Catalyst loading=0.125g GHSV=38400 ml CH_4 g^1h^{-1}	[45]
Ni/3HL-ZrO_2-SiO_2	92	2.8-3	T=800 °C, Catalyst loading=0.5g GHSV=25200 ml CH_4 g^1h^{-1}	[46]
(27.5%NiO/52.5% Al/20% Al_2O_3)	96	2.5	T=900 °C, GHSV= 860h^{-1}	[47]
Ni/SDC($Sm_{0.2}Ce_{0.8}O_{2-\delta}$)	86	-	T=750 °C	[48]
5% Co/Al_2O_3-ZrO_2	84	2.2-2.3	T=800 °C, Catalyst loading=0.15g, GHSV= 6000 ml CH_4 g^1h^{-1}	[49]

4.3 Characterizations of Spent Catalyst

SEM micrographs of spent catalyst 10% CeO_2@MNA are shown in **Fig. 4.10**. The POM reaction was conducted in a fixed bed reactor at 850°C for 35 hours. The morphology of the catalyst is slightly changed, and a small amount of carbon is deposited on the catalyst surface seen from SEM micrograph. The less carbon formation in CeO_2 promoted samples is also reported, which stated comparatively less carbon formation as compared to unpromoted CeO_2 catalysts [50] EDS analysis is illustrated in **Fig. 4.10(c)** exhibiting a very small carbon peak, indicating less carbon formation on the catalyst surface. Less carbon formation in the spent catalyst is also attributed to the formation of NiO and MgO in the mixed metallic oxides that make strong interaction between support and active phase [51], these oxides were also

reflected in FTIR in the low-frequency region. Thus, SEM-EDS analysis of spent catalyst shows high resistance of catalyst towards coke deposition that in turn increases catalyst stability.

TGA analysis of the spent 10% CeO_2@MNA is demonstrated in **Fig. 4.11**. TGA was performed to observe the coke deposition on the catalyst surface after the reaction. A 16% weight loss above 600-700 °C is attributed to the oxidation of reactive (α-C) carbon [52].

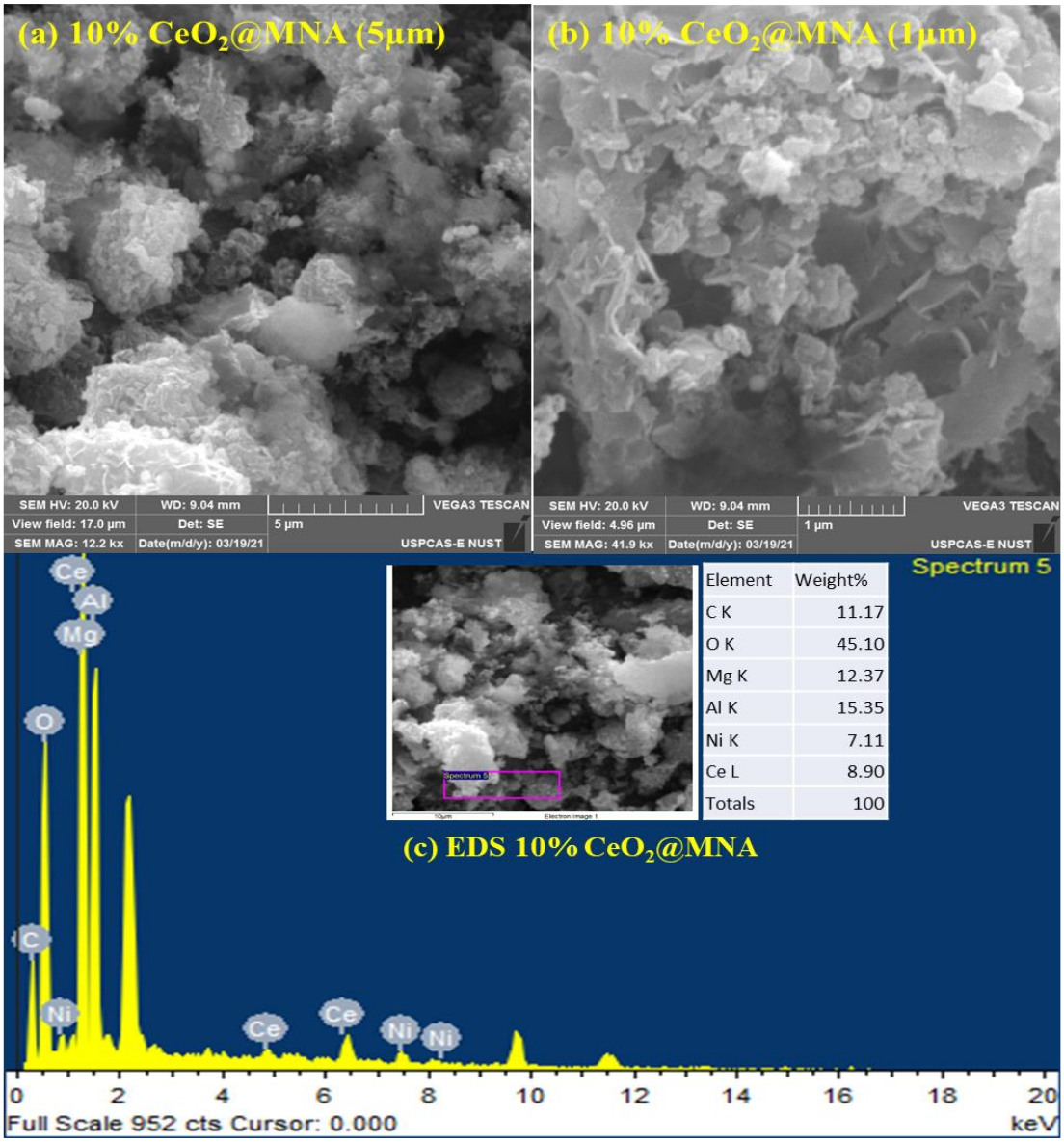

Figure 4.10 SEM and EDS analysis of spent catalyst 10% CeO_2@MNA

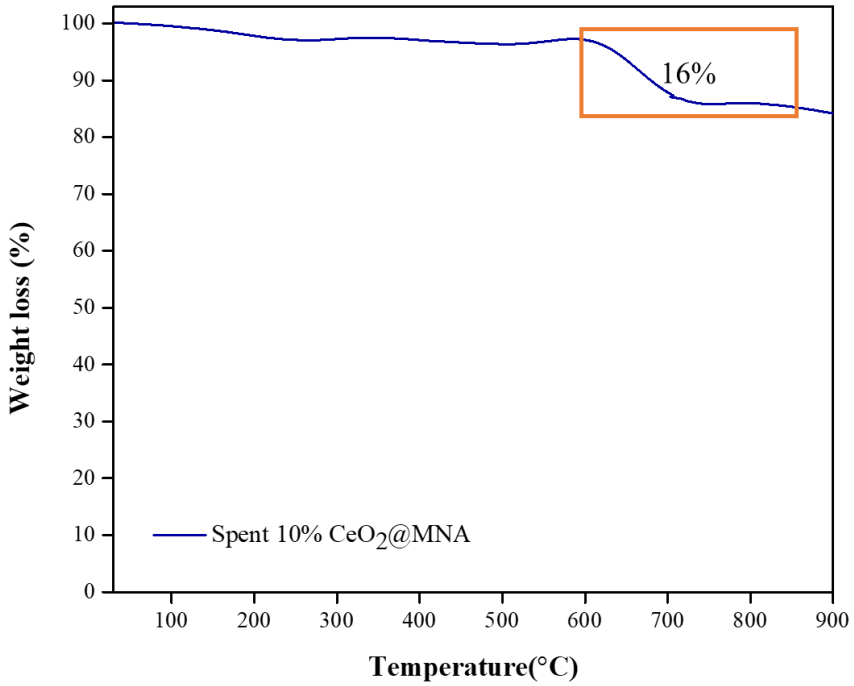

Figure 4.11 TGA analysis of spent 10% CeO_2@MNA

Spent 10% CeO_2@MNA catalyst after 35 h stability test was analysed through XRD to check the reaction parameters effect on structural phases of catalyst **Fig 4.12**. Most of the species of fresh catalyst were detected in spent XRD analysis, like cubical NiO (JCPDS# 44-1159) with space group R-3m (166) and diffraction peaks at 2θ (hkl) = 37.2° (101), 43.3° (012) and 63.0° (110) respectively [53], cubical CeO_2 (JCPDS# 43-1002) space group Fm-3m (225) at 2θ (hkl) = 28.6° (111), 33.1° (200), 47.5° (220) [54], cubical $MgNiO_2$ (JCPDS# 24-0712) with space group Fm-3m (223) at 2θ (hkl) = 37.1° (111), 43.1° (200) and 62.5° (220) [55] [56]. Moreover, cubical $NiAl_2O_4$ (JCPDS# 10-0339) at 2θ (hkl) =19.07° (111), 31.4° (220), 37.0° (311) and 44.9° (400) respectively [57]. The unchanged structural phases of cubic CeO_2 and other components were detected that shows thermal stability and sintering resistance of catalyst [58]. Additionally, peaks of cubical $CeAlO_3$ (JCPDS# 28-0260) were detected at 2θ (hkl) = 23.5° (100), 23.3° (110) and 41.4° (111), that is formed during the high temperature reduction process [59-61]. In pre-reduction environment of H_2, CeO_2 promoter causes reduction of $NiAl_2O_4$ and $CeAlO_3$ which has good thermal stability at the high reaction temperature of POM and retains active Ni particles [62]. $CeAlO_3$

produces activated surface oxygen by capturing O_2 and is converted into CeO_2 and Al_2O_3, then CeO_2 rehabilitates to $CeAlO_3$ by reduction with carbon species [63]. Moreover, graphitic carbon (JCPDS# 41-1487) peak was detected at phase angle 2θ (hkl) = 26.6° (002) [64, 65] supporting the arguments of carbon formation from EDS **(Fig. 4.10)** and TGA analysis of spent catalyst **(Fig. 4.11)**.

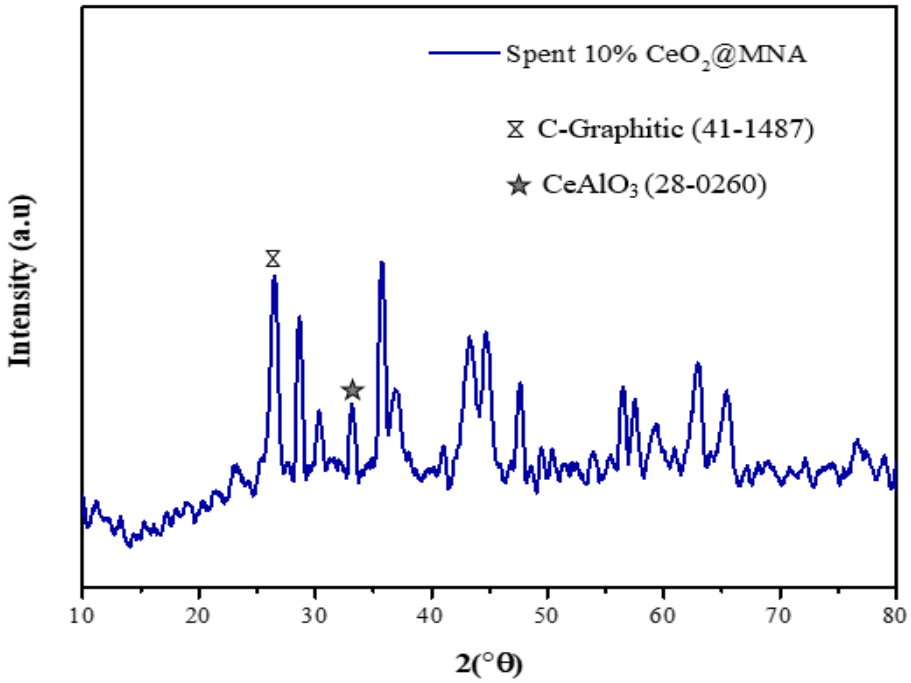

Figure 4.12 XRD analysis of spent 10% CeO_2@MNA

4.4 Reaction Mechanism

Concrete understanding of mechanism of a system that is its reaction equilibria and effects of variables (temperature and pressure) is essential to have a sound cognizance of such system. Basics understandings of reaction mechanism is necessary for results interpretation and therefore, detailed POM system analysis has been published [66, 67].

Two possible reaction mechanisms are reported for POM process. First one is the direct route in which CH_4 and O_2 are directly converted into H_2 and CO (R-(3)). While second one is the indirect route in which CH_4 and O_2 first form H_2O and CO_2 (R-(9)) followed by SRM (R-(1)) and DRM (R-(2)) process to synthesize H_2 and CO, this is also called combustion reforming mechanism [68]

Direct route

$$CH_4 + 0.5O_2 \rightarrow CO + 2H_2 \qquad \Delta H°_{298K} = -36\ KJ/mol \qquad R\text{-}(3)$$

Indirect route

$$CH_4 + 2O_2 \rightarrow CO_2 + 2H_2O \qquad \Delta H°_{298K} = -801\ KJ/mol \qquad R\text{-}(9)$$

$$CH_4 + H_2O \rightarrow CO + 3H_2 \qquad \Delta H°_{298K} = 206\ KJ/mol \qquad R\text{-}(1)$$

$$CH_4 + CO_2 \rightarrow 2CO + 2H_2 \qquad \Delta H°_{298K} = 247\ KJ/mol \qquad R\text{-}(2)$$

Elements in catalytic bed before start of reaction and after reaction of POM process are shown in **Fig. 4.13**.

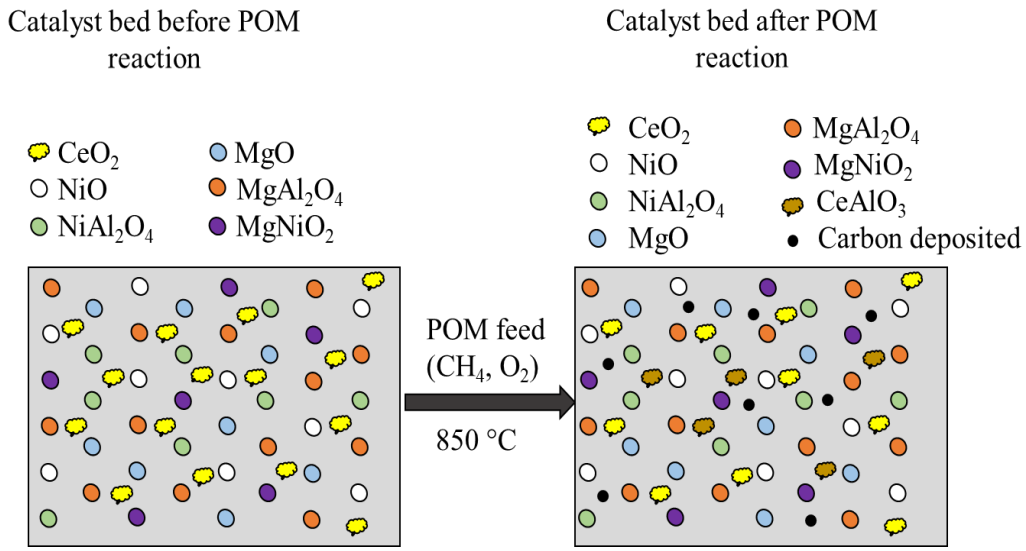

Figure 4.13 POM reaction mechanism

Summary

Samples of CeO_2, MNA and nano-composite CeO_2@MNA were subjected to characterization techniques XRD, SEM, TGA, FTIR and BET to determine the physiochemical properties of the catalyst. The XRD exhibited various diffraction peaks for CeO_2, $MgAl_2O_4$, $NiAl_2O_4$, NiO, MgO and $MgNiO_2$. In MNA sample highly porous coral-like structure was observed due to presence of divalent and trivalent

cations (Mg^{+2}, Ni^{+2}, and Al^{+3}) in the outer layer. Two types of morphologies including rod-like and particle structure were revealed in CeO_2 SEM images. It was observed that, in CeO_2@MNA, CeO_2 particles self-assembled with CeO_2 rod like structure were uniformly distributed over surface of coral like MNA. TGA analysis of nano-composite sample revealed good stability up to 900 ℃ that makes it suitable for high temperature applications like in POM. Surface area and pore size distribution of composite material CeO_2@MNA were observed to be less than MNA, which is probably because of CeO_2 location inside the pores of MNA. Samples were tested for syngas production in fixed bed reactor for POM. Nano-composite CeO_2@MNA showed much better performance after impregnation of CeO_2 upon MNA hydrotalcite. However, nano-composite showed best performance for 10% CeO_2 loading, further increase in CeO_2 loading resulted in reduction of CH_4 conversion that is due to blockage of active sites by clustering of ceria particles. Stability test for best composite material 10% CeO_2@MNA was performed, starting from 92% CH_4 conversion the nano-composite maintained stable 95% CH_4 conversion up to 35 h. Characterization of spent catalyst 10% CeO_2@MNA revealed thermally stable structure with presence of parent compounds, that indicates good stability.

References

1. García-Sancho, C., et al., Hydrogen production by methane decomposition: A comparative study of supported and bulk ex-hydrotalcite mixed oxide catalysts with Ni, Mg and Al. International Journal of Hydrogen Energy, 2018. 43(20): p. 9607-9621.

2. Shi, Z., et al., Characterization and catalytic behavior of hydrotalcite-derived Ni–Al catalysts for methane decomposition. International Journal of Hydrogen Energy, 2020. 45(35): p. 17299-17310.

3. Rodrigues, L.M., et al., Partial oxidation of methane on Ni and Pd catalysts: Influence of active phase and CeO_2 modification. Catalysis today, 2012. 197(1): p. 137-143.

4. Miao, J.-J., et al., Ultrasonic-induced synthesis of CeO_2 nanotubes. Journal of Crystal Growth, 2005. 281(2-4): p. 525-529.

5. Raj, S.S., et al., $MgAl_2O_4$ spinel: Synthesis, carbon incorporation and defect-induced luminescence. Journal of Molecular Structure, 2015. 1089: p. 81-85.

6. Naghizadeh, R., H. Rezaie, and F. Golestani-Fard, Effect of TiO_2 on phase evolution and microstructure of $MgAl_2O_4$ spinel in different atmospheres. Ceramics international, 2011. 37(1): p. 349-354.

7. Pudukudy, M., Z. Yaakob, and M.S. Takriff, Methane decomposition over Pd promoted Ni/$MgAl_2O_4$ catalysts for the production of COx free hydrogen and multiwalled carbon nanotubes. Applied Surface Science, 2015. 356: p. 1320-1326.

8. Penkova, A., et al., Hydrogen production by methanol steam reforming on NiSn/MgO–Al_2O_3 catalysts: The role of MgO addition. Applied Catalysis A: General, 2011. 392(1-2): p. 184-191.

9. Gh, A.B., M. Sabbaghan, and Z. Mirgani, A comparative study on properties of synthesized MgO with different templates. Spectrochimica Acta Part A: Molecular and Biomolecular Spectroscopy, 2015. 137: p. 1286-1291.

10. Ali, N., et al., Nanoflakes $MgNiO_2$ synthesised via a simple hydrothermal method and its catalytic roles on the hydrogen sorption performance of MgH_2. Journal of Alloys and Compounds, 2019. 796: p. 279-286.

11. Maitra, S., R. Mitra, and T. Nath, Investigation of electrochemical performance of MgNiO2 prepared by sol-gel synthesis route for aqueous-based supercapacitor application. Current Applied Physics, 2020. 20(5): p. 628-637.

12. Rodrigues, T.S., et al., Synthesis, characterization and catalytic potential of $MgNiO_2$ nanoparticles obtained from a novel [MgNi (opba)] n· $9nH_2O$ chain. Ceramics International, 2016. 42(12): p. 13635-13641.

13. Dieuzeide, M.L., M. Jobbagy, and N. Amadeo, Glycerol steam reforming over Ni/γ-Al_2O_3 catalysts, modified with Mg(II). Effect of Mg (II) content. Catalysis Today, 2013. 213: p. 50-57.

14. Das, J., D. Das, and K.M. Parida, Preparation and characterization of Mg–Al hydrotalcite-like compounds containing cerium. Journal of Colloid and Interface Science, 2006. 301(2): p. 569-574.

15. Rives, V., Layered double hydroxides: present and future. 2001: Nova Publishers.

16. Djebarri, B., et al., Promoting effect of Ce and Mg cations in Ni/Al catalysts prepared from hydrotalcites for the dry reforming of methane. Reaction Kinetics, Mechanisms and Catalysis, 2014. 111(1): p. 259-275.

17. Titulaer, M.K., J.B.H. Jansen, and J.W. Geus, The Quantity of Reduced Nickel in Synthetic Takovite: Effects of Preparation Conditions and Calcination Temperature. Clays and Clay Minerals, 1994. 42(3): p. 249-258.

18. Zhang, B., S. Zhang, and B. Liu, Effect of oxygen vacancies on ceria catalyst for selective catalytic reduction of NO with NH_3. Applied Surface Science, 2020. 529: p. 147068.

19. Syed Khadar, Y.A., et al., Synthesis, characterization and antibacterial activity of cobalt doped cerium oxide (CeO_2:Co) nanoparticles by using hydrothermal method. Journal of Materials Research and Technology, 2019. 8(1): p. 267-274.

20. Oana, L., et al., FT-IR studies of cerium oxide nanoparticles and natural zeolite mater. Bull Food Sci Technol, 2015. 72: p. 50-5.

21. Daza, C.E., et al., CO_2 reforming of methane over Ni/Mg/Al/Ce mixed oxides. Catalysis Today, 2008. 133: p. 357-366.

22. Tsyganok, A.I., et al., Rational design of Mg–Al mixed oxide-supported bimetallic catalysts for dry reforming of methane. Applied Catalysis A: General, 2005. 292: p. 328-343.

23. Tsyganok, A. and A. Sayari, Incorporation of transition metals into Mg–Al layered double hydroxides: Coprecipitation of cations vs. their pre-complexation with an anionic chelator. Journal of Solid State Chemistry, 2006. 179(6): p. 1830-1841.

24. Tok, A.I.Y., et al., Hydrothermal synthesis of CeO_2 nano-particles. Journal of Materials Processing Technology, 2007. 190(1-3): p. 217-222.

25. Jirátová, K., et al., Preparation and characterisation of activated Ni (Mn)/Mg/Al hydrotalcites for combustion catalysis. Catalysis Today, 2002. 76(1): p. 43-53.

26. Liu, W., J. Zhou, and J. Yao, Shuttle-like CeO_2/g-C_3N_4 composite combined with persulfate for the enhanced photocatalytic degradation of norfloxacin under visible light. Ecotoxicology and Environmental Safety, 2020. 190: p. 110062.

27. Zeng, S., et al., Inverse rod-like CeO_2 supported on CuO prepared by hydrothermal method for preferential oxidation of carbon monoxide. Catalysis Communications, 2012. 23: p. 62-66.

28. Zhang, D.-E., et al., Fabrication of rod-like CeO_2: Characterization, optical and electrochemical properties. Solid State Sciences, 2006. 8(11): p. 1290-1293.

29. Djebarri, B., et al., Promoting effect of Ce and Mg cations in Ni/Al catalysts prepared from hydrotalcites for the dry reforming of methane. Reaction Kinetics, Mechanisms and Catalysis, 2014. 111(1): p. 259-275.

30. Zhao, S., et al., Effect of Ce-doping on catalysts derived from hydrotalcite-like precursors for COS hydrolysis. Journal of Rare Earths, 2010. 28: p. 329-333.

31. Ashok, J. and S. Kawi, Steam reforming of toluene as a biomass tar model compound over CeO_2 promoted Ni/CaO–Al_2O_3 catalytic systems. International Journal of Hydrogen Energy, 2013. 38(32): p. 13938-13949.

32. Daza, C.E., et al., High stability of Ce-promoted Ni/Mg–Al catalysts derived from hydrotalcites in dry reforming of methane. Fuel, 2010. 89(3): p. 592-603.

33. Bepari, S., et al., Steam reforming of ethanol over cerium-promoted Ni-Mg-Al hydrotalcite catalysts. Catalysis Today, 2017. 291: p. 47-57.

34. Zhang, J., et al., Partial oxidation of methane over Ni/Mg/Al/La mixed oxides prepared from layered double hydrotalcites. International Journal of Hydrogen Energy, 2010. 35(21): p. 11776-11786.

35. Pizzolitto, C., et al., Increase of Ceria Redox Ability by Lanthanum Addition on Ni Based Catalysts for Hydrogen Production. ACS Sustainable Chemistry & Engineering, 2018. 6(11): p. 13867-13876.

36. Pantaleo, G., et al., Ni/CeO_2 catalysts for methane partial oxidation: Synthesis driven structural and catalytic effects. Applied Catalysis B: Environmental, 2016. 189: p. 233-241.

37. Ma, Y., et al., Synergistic promotion effect of MgO and CeO_2 on nanofibrous Ni/Al_2O_3 catalysts for methane partial oxidation. Fuel, 2019. 258: p. 116103.

38. Hu, Y.H. and E. Ruckenstein, Catalytic conversion of methane to synthesis gas by partial oxidation and CO_2 reforming. ChemInform, 2004. 35(49): p. no-no.

39. Angelescu, E., et al., Cyanoethylation of ethanol on Mg–Al hydrotalcites promoted by Y^{3+} and La^{3+}. Catalysis Communications, 2004. 5(10): p. 647-651.

40. Özdemir, H., M.A. Faruk Öksüzömer, and M. Ali Gürkaynak, Preparation and characterization of Ni based catalysts for the catalytic partial oxidation of methane: Effect of support basicity on H2/CO ratio and carbon deposition. International Journal of Hydrogen Energy, 2010. 35(22): p. 12147-12160.

41. Rodrigues, L.M.T.S., et al., Partial oxidation of methane on Ni and Pd catalysts: Influence of active phase and CeO_2 modification. Catalysis Today, 2012. 197(1): p. 137-143.

42. Salazar-Villalpando, M.D. and B. Reyes, Hydrogen production over Ni/ceria-supported catalysts by partial oxidation of methane. International journal of hydrogen energy, 2009. 34(24): p. 9723-9729.

43. Irankhah, A., et al., Fischer-Tropsch reaction kinetics of cobalt catalyst in supercritical phase. Journal of Natural Gas Chemistry, 2007. 16(2): p. 115-120.

44. Feio, L., et al., The effect of ceria content on the properties of $Pd/CeO_2/Al_2O_3$ catalysts for steam reforming of methane. Applied Catalysis A: General, 2007. 316(1): p. 107-116.

45. Gil-Calvo, M., et al., Effect of Ni/Al molar ratio on the performance of substoichiometric $NiAl_2O_4$ spinel-based catalysts for partial oxidation of methane. Applied Catalysis B: Environmental, 2017. 209: p. 128-138.

46. Guo, S., et al., Confining Ni nanoparticles in honeycomb-like silica for coking and sintering resistant partial oxidation of methane. International Journal of Hydrogen Energy, 2018. 43(13): p. 6603-6613.

47. Tungatarova, S.A., et al., New composite materials prepared by solution combustion synthesis for catalytic reforming of methane. Chemical Engineering Transactions, 2017. 61: p. 1921-1926.

48. Elbadawi, A.H., et al., Partial oxidation of methane to syngas in catalytic membrane reactor: Role of catalyst oxygen vacancies. Chemical Engineering Journal, 2020. 392: p. 123739.

49. Fakeeha, A.H., et al., Highly Selective Syngas/H2 Production via Partial Oxidation of CH_4 Using (Ni, Co and Ni–Co)/ZrO_2–Al_2O_3 Catalysts: Influence of Calcination Temperature. Processes, 2019. 7(144).

50. Akbari, E., S.M. Alavi, and M. Rezaei, CeO_2 Promoted Ni-MgO-Al_2O_3 nanocatalysts for carbon dioxide reforming of methane. Journal of CO_2 Utilization, 2018. 24: p. 128-138.

51. Min, J.-E., et al., Carbon dioxide reforming of methane on Ni–MgO–Al_2O_3 catalysts prepared by sol–gel method: Effects of Mg/Al ratios. Journal of Industrial and Engineering Chemistry, 2015. 26: p. 375-383.

52. Ding, M., et al., Enhancement of methanation of bio-syngas over CeO_2-modified Ni/Al_2O_3 catalysts. Biomass and Bioenergy, 2016. 85: p. 12-17.

53. Khoja, A.H., M. Tahir, and N.A.S. Amin, Evaluating the Performance of a Ni Catalyst Supported on La_2O_3-$MgAl_2O_4$ for Dry Reforming of Methane in a Packed Bed Dielectric Barrier Discharge Plasma Reactor. Energy & Fuels, 2019. 33(11): p. 11630-11647.

54. Raza, J., et al., Methane decomposition for hydrogen production over biomass fly ash-based CeO_2 nanowires promoted cobalt catalyst. Journal of Environmental Chemical Engineering, 2021. 9(5): p. 105816.

55. Li, S., et al., Co-precipitated Ni–Mg–Al catalysts for hydrogen production by supercritical water gasification of glucose. International Journal of Hydrogen Energy, 2013. 38(23): p. 9688-9700.

56. Nawfal, M., et al., Hydrogen production by methane steam reforming over Ru supported on Ni–Mg–Al mixed oxides prepared via hydrotalcite route. International Journal of Hydrogen Energy, 2015. 40(2): p. 1269-1277.

57. Khoja, A.H., et al., Kinetic study of dry reforming of methane using hybrid DBD plasma reactor over La_2O_3 co-supported $Ni/MgAl_2O_4$ catalyst. International Journal of Hydrogen Energy, 2020. 45(22): p. 12256-12271.

58. Singha, R.K., et al., Effect of metal-support interaction on activity and stability of Ni-CeO2 catalyst for partial oxidation of methane. Applied Catalysis B: Environmental, 2017. 202: p. 473-488.

59. Chein, R.Y. and W.Y. Fung, Syngas production via dry reforming of methane over CeO_2 modified Ni/Al_2O_3 catalysts. International Journal of Hydrogen Energy, 2019. 44(28): p. 14303-14315.

60. Han, J., et al., Natural gas reforming of carbon dioxide for syngas over Ni–Ce–Al catalysts. International Journal of Hydrogen Energy, 2017. 42(29): p. 18364-18374.

61. Zou, X.J., et al., Development of highly effective supported nickel catalysts for pre-reforming of liquefied petroleum gas under low steam to carbon molar ratios. International Journal of Hydrogen Energy, 2010. 35(22): p. 12191-12200.

62. Ma, Y., et al., Synergistic promotion effect of MgO and CeO_2 on nanofibrous Ni/Al_2O_3 catalysts for methane partial oxidation. Fuel, 2019. 258: p. 116103.

63. Chai, R., et al., Ni-foam-structured NiO-MO x -Al $_2$ O $_3$ (M = Ce or Mg) nanocomposite catalyst for high throughput catalytic partial oxidation of methane to syngas. Microporous and Mesoporous Materials, 2017. 253: p. 123-128.

64. Asencios, Y.J.O., P.A.P. Nascente, and E.M. Assaf, Partial oxidation of methane on NiO–MgO–ZrO_2 catalysts. Fuel, 2012. 97: p. 630-637.

65. Song, Y., et al., Partial oxidation of methane to syngas over Ni/Al2O3 catalysts prepared by a modified Sol− Gel method. Energy & Fuels, 2009. 23(4): p. 1925-1930.

66. Chen, W.-H., et al., Thermodynamic analysis of hydrogen production from methane via autothermal reforming and partial oxidation followed by water gas shift reaction. international journal of hydrogen energy, 2010. 35(21): p. 11787-11797.

67. Horn, R., et al., Methane catalytic partial oxidation on autothermal Rh and Pt foam catalysts: Oxidation and reforming zones, transport effects, and approach to thermodynamic equilibrium. Journal of Catalysis, 2007. 249(2): p. 380-393.

68. Al-Sayari, S.A., Recent developments in the partial oxidation of methane to syngas. The Open Catalysis Journal, 2013. 6(1).

Chapter 5: Conclusions and Recommendations

5.1 Conclusions

This thesis focuses on the POM process keeping in mind the basic theme of effective utilization of CH_4 which is a major component of natural gas and greenhousegases with special attention on catalyst preparation and the comprehensive analysis of the catalytic activity and the catalyst deactivation induced by the reaction conditions. The carbon deposition resulting in catalyst deactivation is the major setback of the POM reaction.

The catalytic performance of CeO_2 promoted MNA hydrotalcite based catalyst (CeO_2@MNA) synthesized by co-precipitation and wet impregnation method was comprehensively investigated for different loading of CeO_2 in MNA for POM reaction. The results revealed that the incorporation of CeO_2 to MNA significantly improved the catalytic performance to a certain loading of CeO_2, that decreased beyond 10 wt% CeO_2 in MNA due to clustering of particles. Among these catalysts, 10% CeO_2@MNA catalyst showed excellent performance and high stability for 35 h at 850 °C without any decrease in catalytic activity with 95% CH_4 conversion. Referring to the CeO_2 addition effect, the results confirmed that the cerium addition improved the H_2 and CO selectivity, CH_4 conversion and resistance to deactivation of MNA hydrotalcite in POM reaction. This effect is the special attribute of cerium to store and release different levels of oxygen vacancies due to its existence in different oxidation states. The metal surface remains free of inactive carbon due to the higher exchange rate of oxygen. Thus synthesized CeO_2@MNA catalyst tested in this work could be used efficiently for syngas production in POM for future work.

5.2 Recommendations

POM process finds promising future in the effective utilization of CH_4 for syngas production. The major challenges in the POM process are the development of the catalysts that are more resistant to deactivation and this need the usage of modern and highly developed advanced catalyst preparation methods. Also the reactor designs need to be developed with suitable reaction conditions for POM processes. Moreover, efforts should be done in order to optimize the design of catalyst to make the POM process commercially viable.

Appendix

Muhammad Anees Ul Hasnain, Asif Hussain Khoja, Faaz Ahmed Butt, Mariam Ayesha, Faisal Saleem, Muhammad Taqi Mehran, Rabia Liaquat, Majid Ali, and Zaki Ismail Zaki. "*Partial oxidation of methane over CeO_2 loaded hydrotalcite (MgNiAl) catalyst for the production of hydrogen rich syngas (H_2, CO)*." International Journal of Hydrogen Energy, 2021. 46(74): p. 36663-36677. (IF=5.8, Q1).

INTERNATIONAL JOURNAL OF HYDROGEN ENERGY 46 (2021) 36663–36677

Available online at www.sciencedirect.com

ScienceDirect

journal homepage: www.elsevier.com/locate/he

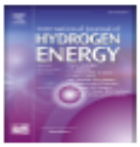

Partial oxidation of methane over CeO_2 loaded hydrotalcite (MgNiAl) catalyst for the production of hydrogen rich syngas (H_2, CO)

Muhammad Anees Ul Hasnain [a], Asif Hussain Khoja [a,*], Faaz Ahmed Butt [b], Mariam Ayesha [c], Faisal Saleem [d], Muhammad Taqi Mehran [c], Rabia Liaquat [a], Majid Ali [a], Zaki Ismail Zaki [e]

[a] U.S.-Pakistan Centre of Advanced Studies in Energy (USPCAS-E), National University of Sciences & Technology (NUST), Sector H-12, Islamabad, (44000), Pakistan
[b] Materials Engineering Department, NED University of Engineering and Technology, Karachi, 75270, Pakistan
[c] School of Chemical and Materials Engineering (SCME), National University of Sciences & Technology (NUST), Sector H-12, Islamabad, (44000), Pakistan
[d] Department of Chemical and Polymer Engineering, University of Engineering and Technology Lahore, Faisalabad Campus, Pakistan
[e] Department of Chemistry, College of Science, Taif University, P.O. Box 11099, Taif, 21944, Saudi Arabia

HIGHLIGHTS

- CeO_2@MgNiAl (MNA) hydrotalcite is synthesized for POM reaction.
- CeO_2 addition over MNA greatly improved the H_2/CO ratio.
- The catalyst is stable for more than 35 h on POM reaction.
- The spent catalyst shows no sign of graphitic carbon after 35 h.

GRAPHICAL ABSTRACT

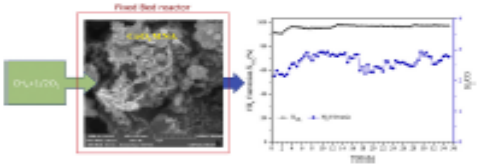

ARTICLE INFO

Article history:
Received 18 June 2021
Received in revised form
23 August 2021
Accepted 24 August 2021
Available online 11 September 2021

Keywords:
CeO_2

ABSTRACT

In this work, partial oxidation of methane (POM) was investigated using Mg-Ni-Al (MNA) hydrotalcite promoted CeO_2 catalyst in a fixed bed reactor. MNA hydrotalcite was synthesized using the co-precipitation process, while CeO_2 was incorporated via the wetness impregnation technique. The CeO_2@MNA samples were characterized by X-ray diffraction (XRD), scanning electron microscopy (SEM), energy dispersive X-ray analysis (EDS), thermal gravimetric analysis (TGA), Fourier transform infrared spectroscopy (FTIR), and Brunauer-Emmett-Teller (BET) technique. The catalytic activity of CeO_2 promoted MNA (CeO_2@MNA) for POM reaction was evaluated for various CeO_2 loading kept the feed ratio $CH_4/O_2 = 2$ at 850 °C. The catalyst containing 10 wt% cerium loading (10%CeO_2@MNA) showed 94% CH_4

* Corresponding author.
E-mail address: [redacted] (A.H. Khoja).
https://doi.org/10.1016/j.ijhydene.2021.08.169